UNIVERSITÀ
DEGLI STUDI
DI PADOVA

Sede Amministrativa: Università degli Studi di Padova

Dipartimento di *Ingegneria Industriale*

SCUOLA DI DOTTORATO DI RICERCA IN: INGEGNERIA INDUSTRIALE
INDIRIZZO: INGEGNERIA CHIMICA, DEI MATERIALI E MECCANICA
CICLO XXIX

MODELING OF SEGREGATION IN DENSE GRANULAR FLOWS

Coordinatore: Ch.mo Prof. Giovanni Meneghetti

Supervisore: Ch.mo Prof. Andrea Claudio Santomaso

Dottorando: Silvia Volpato

Contents

Sommario

I materiali granulari sono largamente utilizzati in ambito chimico, farmaceutico ed alimentare. Essi presentano comportamenti caratteristici legati al loro modo di scorrere. Durante il flusso di miscele multicomponenti, granuli con caratteristiche fisiche simili, per esempio dimensioni, densità o forma, tendono a concentrarsi all'interno della miscela separandosi dal resto. Questo fenomeno, chiamato segregazione, affligge molte operazioni industriali, come per esempio la miscelazione, lo stoccaggio di sili o anche la semplice manipolazione della miscela. La segregazione è un problema soprattutto in quei processi in cui è richiesta una elevata omogeneità del prodotto finale.

Il flusso di materiali granulari viene modellato attraverso due approcci: l'approccio continuo, che considera il materiale granulare come un mezzo continuo, a cui si possono associare campi di pressione e di velocità, oppure attraverso il cosiddetto approccio DEM, che considera il materiale granulare come un insieme di granuli distinti che vengono modellati attraverso le loro reciproche forze di interazioni. Le scale di applicazione di questi due approcci sono differenti: il primo è adatto a simulare flussi su larga scala all'interno di apparecchiature di dimensioni industriali; il secondo agisce ad una scala inferiore ed è utile per investigare meccanismi che si creano a livello granulare. Entrambi questi approcci sono utilizzati in questo studio. In questa tesi è stato utilizzato un modello continuo, che utilizza equazioni di massa, momento ed energia cinetica accoppiato ad uno capace di descrivere l'evoluzione dell'interfaccia tra aria e granulare per studiare il moto denso di materiali granulari all'interno di due apparecchiature di interesse industriale: miscelatori rotanti e sili di stoccaggio. Il modello, sviluppato da Artoni *et al.* (2009), per chiudere il sistema di equazioni utilizza delle equazioni costitutive

e un approccio fenomenologico che descrive il comportamento del granulare. Un secondo modello, capace di descrivere l'evoluzione della segregazione di miscele bi-componente attraverso una equazione di trasporto, è stato accoppiato al primo per modellare la segregazione nei sili (Bertuola *et al.*, 2016). Il modello segregativo è flessibile; infatti è possibile descrivere la velocità di segregazione utilizzando diverse relazioni a seconda dei meccanismi segregativi considerati. Come primo approccio, si è deciso di adottare una relazione ottenuta combinando due approcci trovati in Letteratura. Nonostante l'utilizzo di questa relazione abbia portato a buoni risultati, è stato fatto uno studio più approfondito basato su esperimenti e su simulazioni DEM per migliorare la descrizione della velocità di segregazione da usare nel modello segregativo.

Entrando nello specifico, il Capitolo 1 riassume brevemente lo stato dell'arte, sia in riferimento ai modelli usati per descrivere il moto di un granulare, sia per descrivere la segregazione in miscele polidisperse. Nel secondo Capitolo vengono mostrati i modelli continui utilizzati nelle simulazioni: il modello reologico con le relative condizioni al contorno, il modello utilizzato per descrivere l'evoluzione dell'interfaccia tra aria e materiale granulare, e infine le equazioni usate per modellare la segregazione. Nel Capitolo 3 il modello reologico accoppiato al modello che descrive l'interfaccia tra aria e granulare viene utilizzato per studiare la cinematica all'interno di miscelatori usati abitualmente nell'industria farmaceutica: un tamburo rotante, un miscelatore a doppio cono simmetrico e un miscelatore a doppio cono asimmetrico. Nel Capitolo 4 si è provveduto ad estendere considerazioni puramente cinematiche effettuate nel Capitolo 3 ad una miscela polidispersa mescolata all'interno di miscelatori con geometrie simili a quelle utilizzate nello studio del Capitolo 3. Lo studio si è concentrato su un particolare tipo di miscelatore, il biconico simmetrico, e si sono effettuate analisi sperimentali sul grado di miscelazione allo scarico al variare della composizione granulometrica considerata. In questo Capitolo si presenta anche il metodo d'analisi utilizzato, sviluppato ad hoc, per valutare il grado di miscelazione. Nel Capitolo

5, vengono presentati i risultati delle simulazioni ottenuto modellando il flusso e la segregazione di una miscela granulare bi-dispersa durante lo scarico di sili utilizzando un approccio numerico e i modelli continui presentati nel Capitolo 2. I risultati numerici sono stati confrontati con dati sperimentali di Letteratura. La necessità di comprendere meglio quali grandezze influenzino la segregazione, e in particolare la percolazione, ha portato allo sviluppo degli studi riportati nel Capitolo 6 e 7. Il primo è uno studio sperimentale, effettuato in una cella di "shear", che ha permesso di ottenere dati riguardanti la velocità di percolazione al variare del rapporto dei diametri e del gradiente di velocità per materiali granulari sferici e non. Questo lavoro su una geometria semplificata ha permesso lo sviluppo di un modello teorico che riesce a predire i dati sperimentali. Nel Capitolo 7 vengono presentati i risultati ottenuti con un approccio DEM. In questo caso, la velocità di percolazione è stata studiata al variare della frazione volumetrica di materiale fine nella miscela e della direzione della gravità rispetto al gradiente di velocità, due variabili difficili da controllare sperimentalmente.

Summary

Granular materials are widely used in industrial application, for example in chemical, metallurgical, pharmaceutical and food industries. They have peculiar behaviors related to their flow. During the flow of multicomponent mixtures, granules with similar physical characteristics, for example size, density, shape, tend to concentrate within the mixture separating from the bulk. This phenomenon, called segregation, plagues many industrial operations, such as mixing, filling and emptying of silos or even the simple handling of the mixture. Segregation is a problem in particular in those processes where a high homogeneity of the final product is required. The flow of granular materials is modeled through two approaches: the continuum approach, which considers the granular material as a continuous medium or through the so-called DEM approach, which considers the granular material as an assembly of granules modeled through the interaction of forces between them. The scales of application of these two approaches are different: the first is used to simulate large-scale flows within industrial full-size equipment; the second is used at a lower scale, and it is useful for investigating mechanisms that occur at a grain level. Both of these approaches are used in this study.

In this thesis, a continuum framework, composed of equations of mass, momentum and fluctuating kinetic energy, coupled to one capable of describing the evolution of the interface between air and granular material, was used to study the dense motion of granular materials within two industrially relevant equipments: mixers and silos. The model, developed by Artoni *et al.* (2009), uses the constitutive equations to close the system of equations and a phenomenological approach to describe the behavior of granular materials. A second model, capable

of describing the evolution of the segregation of a bidispersed mixtures through a transport equation, was used to model the segregation (Bertuola *et al.*, 2016). The segregation model is flexible; in fact it is possible to describe the segregation speed using different relationships depending on the segregation mechanisms. As a first approach, it was decided to adopt a relation deriving from Literature approaches. Despite the use of this relation has led to good results, a further study based on experiments and DEM simulations has been done to improve the description of the segregation velocity to be used in segregative model.

Chapter 1 briefly summarizes the state of art, taking into account the models used to describe the motion of a granular material, and those able to describe segregation in polydispersed mixtures. In the second Chapter the continuum models used in the simulations are shown: 1) the hydrodynamic model with all the boundary conditions, 2) the model used to describe the evolution of the interface between air and the granular material, and 3) the equations used to model the segregation. In Chapter 3 the rheological model coupled to the model that describes the interface between air and granular material is used to study the kinematics inside of mixers normally used in the pharmaceutical industry: a rotary drum, a symmetrical double cone mixer and a mixer asymmetrical double cone. In Chapter 4, it was decided to extend the purely kinematic considerations made in Chapter 3, and a polydisperse mixture was mixed in geometries similar to those used in the study of Chapter 3. The study focused on a particular type of mixer, the symmetrical biconical mixer, and an experimental analysis on the degree of mixing varying the size composition was done. This chapter also presents the analysis system used to assess the degree of mixing. In Chapter 5, we present the results of the simulations of a bi-dispersed granular mixture during the unloading of silos using a numerical approach and continuum models presented in Chapter 2. The numerical results were compared with experimental data of Literature. The need for better understanding which variables influence the segregation has led to the development of the studies reported in Chapter 6

and 7. The first is an experimental study, carried out in a ”shear box”, and allowed to obtain data concerning the percolation speed varying the size ratio and the shear rate for spherical and angular granules. Chapter 7 presents the results obtained with a DEM approach. In this case, the speed of percolation has been studied varying two variables which are difficult to explore experimentally, i.e. the volume fraction of fine material in the mixture, and the direction of gravity with respect to the velocity gradient.

List of Figures

List of Tables

Chapter 1

State of the art

1.1 Introduction

Granular materials are frequently met in everyday life, as sand and gravel on the beach, rice and sugar in a kitchen and abound in the world around us. After water, granular medium is the second most used type of material in industry (Andreotti *et al.*, 2013). They are encountered, for instance, in technological applications ranging from pharmaceutical, food, powders, semiconductor industries (Richard *et al.*, 2005) to geological processes, such as landslide, erosion, debris and pyroclastic flow (Jaeger *et al.*, 1996).

Granular materials are defined as collections of discrete particles whose size is typically larger than 100 μm (De Gennes, 1999). A complete description of the behavior of granular materials is still far to be complete; in fact no theoretical framework is available to describe their behaviors, even in the ideal case of a collection of identical spherical particles (Andreotti *et al.*, 2013). Granular materials present physics more complex to describe and compared to that of gases and of liquids. For example granular materials are athermal systems and it is difficult to use a statistical approach, as it is done for liquids and gases, to find a law that links the microscopic to the macroscopic behavior of the system. The description of the granular material is also made difficult by the lack of a clear scale separation between the microscopic, the grain size, and the macroscopic size, for example the

size of the flow. At the microscopic level, the description of the interactions between grains are exacting, because it involves highly non linear phenomena such as friction and inelastic shocks (Andreotti *et al.*, 2013). Another peculiar aspect of granular materials is that their kinetic energy is instantly dissipated by collision and friction between the grains at the microscopic level. All these aspects make difficult any description of the granular behavior but, despite of the complexity of granular materials, they share fundamental features. At the macroscopic level, they can behave like a solid, liquid or a gas exhibiting phenomena such as arching, avalanches and segregation. Based on these similarities, they are often classified in three different regimes (Jaeger *et al.*, 1996): a quasi-static regime in which the material interacts by frictional contacts, a gaseous regime where the flow is very rapid and dilute and the particles interact by collision and the intermediate regime in which the material flows like a liquid and the particles interact both by collision and friction (Forterre and Pouliquen, 2008).

1.2 Models for granular flow

In general, the modeling of the granular flow can be done using two approaches: continuum or discrete. At a sufficiently small scales, a granular material can be considered composed of discrete macroscopic particles and can be modeled using DEM approach. The continuum models are applied at a large industrial scale and consider the macroscopic fields as a continuum. The continuum equations are the conservation of mass, momentum and energy. To close this system of equations, it is necessary to formulate constitutive relations that are different for fluid and solids. For a granular material, the constitutive equations are often formulated on the basis of empirical phenomenological considerations and different relations have been proposed in Literature.

Granular gases have been successfully studied by using extensions of the kinetic theory of gases (Goldhirsch, 2003), that assumes that grain collisions are binary

and that the particles separate immediately after the collision (Campbell, 1990). In this description, a granular temperature is defined as the magnitude of the velocity fluctuations and hydrodynamic equations are derived. The quasi-static regime is usually described using soil mechanics and plasticity theories (Schaeffer, 1987). The behavior of dense granular materials, which is dominated by prolonged inter-particle contacts, results more difficult to model. So far no unified theory exists, but different approaches were explored. The elasto-plastic models are commonly used; the granular material is assumed to behave elastically under small stress and plastically above a stress-threshold. The relation between strain and stress is described using a yield function and the simplest is based on the Coulomb yield criterion, according to which the shear stress is proportional to the normal stress through a coefficient of friction, similar to the description of a block sliding down an inclined plane. An alternative approach, for the description of stress in granular materials, is based on the assumption that the system of equations can be closed without considering the deformation of the material. Aranson and Tsimring (2001) propose a model that describe both the solid-like and liquid-like behavior of the granular flow. The model is a sum of two parts: a newtonian viscous liquid part and a solid part. The transition between the two behaviors is modulated using a order parameter, governed by a Landau equation (Ginzburg, 1955) by analogy with the phase transitions. This model is able to describe the hysteretic phenomena that characterize a granular material and gives good results in the description of avalanches. It also gives good predictions for velocity profiles in the shear cell experiments, but fails in the description of the flow in an inclined plane (Pouliquen and Chevoir, 2002). Another way to describe the granular flow is starting from the kinetic theory of gases, used to describe the dilute flow of a granular material, and extend its validity for high volume fraction. An attempt to describe this regime using kinetic theory is made by Savage and Lun (1988) who extends the kinetic theory of granular material introducing a shear rate independent term in order to incorporate friction which becomes important

at high volume fraction. Losert *et al.* (2000) and Bocquet *et al.* (2001), always based on the kinetic theory, proposed a locally Newtonian continuum model, in which the granular material is assumed to behave as a liquid with a local granular temperature and density dependent viscosity. In this model the viscosity diverges when the density approaches the random close packing density of grains. The model quantitatively describes all the aspects of the experimental data obtained from shear flow of granular material in a Couette geometry.

The models described so far use a local rheology in the sense that the shear stress at some points depend on the local value of the shear rate at that point. There exist some models based on a non local rheology. Mills *et al.* (1999) propose a non-local expression for the stress tensor for describing the flow of granular material on inclined planes. The model describes granular material like a viscous fluid and assumes the existence of arches in the material, which transmit stresses in a non-local way, generating an inhomogeneous distribution of contact force.

A last approach to describe dense granular flow is based on activated process (Pouliquen and Chevoir, 2002). Pouliquen *et al.* (2001) propose a non-local model that is able to capture both the quasi-static and the liquid regime of the granular flow and it is based of a self-activated process. Thermal fluctuations help elements of material to yield and overcome the energy barrier in which they are trapped. The self activated model use the stress fluctuations, instead of thermal fluctuations. The material behavior remains plastic, thus there is not rate dependence on the stress. Steady granular flows on inclined plane or in a heap could not be described by this model (Pouliquen and Chevoir, 2002). Kamrin and Koval (2012) propose a non-local relation for the fluidity, the inverse of the viscosity, during the flow of the granular materials. Artoni *et al.* (2009) develop a non-local model from analogies with the theory of glassy system to simulate the dense flow based on continuum, pseudo-fluid approximation. The non locality arise from the fact that the relationship between stress and shear rate is mediated by a differential equation controlling the distribution of granular temperature in the

system and thus the viscosity of the material. This model was used in this PhD work to describe the flow of granular material in devices of industrial interest, i.e mixers, hoppers and silos. A further development of this work (Artoni and Richard, 2015) has divided the stress tensor in two components: a contact term dissipated locally and a kinetic one which contribute to a non-local balance. The model was coupled with segregation one to describe the flow and the segregation of binary mixture of granular materials.

Another way to model the flow of a granular material is to model the particle-particle interactions, and thus to use a discrete element methods (DEMs) (Cundall and Strack, 1979). A finite number of discrete particles can interact by means of contact and non contact forces and the motion of the particles is described by Newton's equations of motion.

1.3 Segregation of granular material

In the previous section, the behavior of monodisperse granular flows was described, but frequently the grains are not identical, and differ in their size, shape or mechanical properties (Andreotti *et al.*, 2013; Williams, 1963). An interesting and charming phenomenon typical of the polydisperse granular materials and with no parallel in fluids is the segregation, the tendency of particles, with different physical properties, to separate from the mixture. Because of these differences, the homogeneity of the granular mixtures can be compromised by segregation during handling operations and particles motion results from the effects of mechanical actions such as tumbling or stirring, and external forces, primarily gravity (Hogg, 2009). Especially the free-flowing materials tend to segregate in a large scale due to the preferential movement of individual particles.

Segregation onset and its drawbacks are well known in the industrial practice since a long time; notwithstanding several studies, segregation remains an open issue. A qualitative understanding of the phenomenon exists from long time.

One of the oldest studies in the Literature considers free surface flow on inclined chutes. Brown (1939) reports the principles of segregation and suggests that the main mechanism of segregation is the inter-particle collisions, which cause deceleration of small particles and their concentration close to origin of flow, whereas larger particles concentrate at the end of the chute. Later, Williams (1963) suggests that inter-particle percolation is the main mechanism. Still studying free-surface flows, he observes small particles traveling through the voids on the surface, whereas large particles roll down the surface without any chance to percolate into the smaller voids. Savage and Lun (1988) also consider the inclined chute; they model the granular material as several moving layers under shear where segregation is caused by percolation through voids and by particle migration from one layer to another. Bridgwater (1994) shows that there are three fundamental mechanisms of segregation on free flowing granular materials, which are inter-particle percolation and particle migration, occurring in the bulk, and a free surface segregation. Tapping and vibrations are also studied. Barker and Mehta (1993) conclude that segregation is driven by convection and diffusion, while Knight *et al.* (1993), through uniaxial vibration experiments, suggest that the principal segregation mechanism is convection. Finally, different types of segregation mechanisms were identified (De Silva *et al.*, 2000), but there are mainly four important mechanisms that it is worth keeping in consideration: percolation, bulk convection, surface and interstitial fluid effect (Scott and Bridgwater, 1975). One of the most frequent and important cause of segregation is inter-particle percolation (Williams, 1963), that occurs when small particles fall down through the voids between large particles as result of a local shear in the presence of a gravitational field.

After this brief overview, it appears clear that segregation is a widespread phenomenon that involves different types of mechanisms and occurs in different types of devices. Furthermore, every device is dominated by its mechanism of segregation and the development of a flexible framework able to describe all the

mechanisms in different devices is an hard challenge. Recently, different efforts were done to deepen the compehension and the description of the segregation during the dense flow of a granular material, and in particular on shear induced percolation with a creation of a broad theorethical framework.

1.3.1 Theoretical approaches to segregation

Despite the physical evidences of the phenomenon, there exist few models that give a quantitative description of it. Cooke *et al.* (1978) were the first to develop a continuum model for the segregation based on competition between percolation and diffusion mechanism. The model is written in terms of concentration ω of a component i expressed as a fraction on the solid volume and the segregation flux is proportional to $\omega_i(1-\omega_i)^2$. Both the percolation and the diffusion act in the direction parallel to the gravity. Cooke *et al.* (1978) also identify the physical variables that contribute to segregation and use a shear apparatus to investigate the dependence of the percolation velocity on these variables.

Savage and Lun (1988) develop a model to describe the particle size segregation in inclined chute flows. For slow flow, they assume that the percolation is a combination of two mechanisms: ”kinetic sieving” and ”squeeze expulsion”. The former is a mechanism caused by gravity and dependent on voids between the particles that provides the drop of the finer material inside a ”sieve” formed by the bed of coarse particles; it is based on the statistical assumption that small particles have more probability to fall down into voids with respect to the bigger one when they are sheared down a slope. The second mechanism is introduced to satisfy overall mass conservation. This model is used to predict the concentration profile of a bidispersed mixture flowing down an inclined plane, assuming that the velocity profile is linear.

Using a phenomenological approach, Dolgunin and Ukolov (1995) propose a model for size and density segregation for rapid flow that depends on particle

concentration and granular temperature. Their segregation flux, proportional to ω(1-ω), is based on the consideration that it must switch off when the large or small particles are in a pure phase. This model is very similar to that formulated by Cooke *et al.* (1978), but it also contains the particle transport by bulk velocity convection.

Recently, other theoretical models to predict the size segregation in dense flow have been proposed (Gray *et al.*, 2015; Thornton *et al.*, 2012; Fan *et al.*, 2014). These models, developed for a binary mixture, are based on a transport equation for the volume concentration of the species that incorporates a term of advection due to mean flow, a diffusion and a percolation term. The model of Thornton *et al.* (2012) contains two dimensionless parameters, which in general depend on both the flow and particle properties. The model of Fan *et al.* (2014) is applied to a bounded heap flow and it has not adjustable fitting parameters. In fact, the model contains two dimensionless parameters that are functions of physical control parameters and kinematic parameters that were measured from DEM simulations. Also Gray and Ancey (2011) develop a model similar to these, where the segregation flux is proportional to ω(1- ω). Hajra *et al.* (2012) arrive at similar relation, starting from the consideration that the velocity of segregation for fine particles is proportional to the diameter of fines d_f and the average diameter of the mixture $\langle d \rangle : v_S \propto (d_f - \langle d \rangle)$. Expanding the previous right term, they obtain that the velocity of segregation is proportional to the size ratio and to the concentration of fine and coarse particle. This type of relation guarantees for ω=0 or (1-ω)=0 that the velocity of segregation tends to zero and increases when ω approaches to zero. Khola and Wassgren (2016) simulate a simple shear flow of bi-dispersed granular materials via DEM simulation to study the segregation varying the shear rate, the concentration of fines particle and the size ratio. Some correlations for the velocity of percolation and for the coefficient of diffusion are found. These relations are valid for low shear rate, in the quasi-static regime.

The models previously described can be qualitatively or, in some case, quantitatively predictive in highlighting the critical points in a process in term of segregation, but they do not give practical instruments to minimize the problem.
McCarthy (2009) pointed out the recent studies developed to minimize the segregation. Hersey (1975) was the first to say that the cohesive forces between particles could affect the segregation. In cohesive materials, individual particles have less freedom to move and relocate and most of the mechanisms of segregation valid for the free-flowing material are not relevant (Nienow *et al.*, 1997). He elaborated the concept of "ordered mixing", different from "random mixing". The first one occurs also when the grains have different size or weight, and it is provoked by strong particle interactions between fine and coarse particles.

Nomenclature

Symbol	Units	Description
ω	-	volume fraction

From the next Chapter, with the same symbol it will be considered the mass fraction because we will consider the density as a constant.

Chapter 2

Rheological and segregation continuum models

2.1 Introduction

In this Chapter the continuum models used to describe the flow and the segregation of granular materials are presented. The behavior of free flowing segregating mixtures was simulated with a Finite Element Method (FEM) using an existing hydrodynamic model for powder rheology (Artoni *et al.*, 2009), that solves mass, momentum and energy fluctuation balance equations and uses specific constitutive relations to account for fluctuations in the velocity field, through the 'granular temperature' concept. This model was previously successfully used to simulate the granular flow of mono-dispersed mixtures in full industrial scale reactors and silos (Artoni *et al.*, 2011; Volpato *et al.*, 2014). The continuum model for granular flow was combined with a transport equation to describe transient phenomena of the granular flow, for instance the discharge of silos. The simulation of granular flow allowing for a free, moving surface was achieved by an Eulerian, continuum modeling of the two-phase flow (Olsson and Kreiss, 2005). The domain included two regions, accounting for the air and the solids, the latter treated with the model previously mentioned. Segregation was modeled with a mass transport equation applied to a bi-dispersed mixture of particles of different sizes that included the effects of two different mechanisms: advection due to flow

and segregation due to percolation. The percolation was modeled starting from Literature relation (Hajra *et al.*, 2012), modified according reasoned arguments.

2.2 Rheological model

The granular flow was modeled with the continuum approach already described by Artoni *et al.* (2009), Artoni *et al.* (2011), and Volpato *et al.* (2014) for silos discharge. The model includes mass, linear momentum and translational kinetic energy balance equations, under some simplifying assumption:

- the effect of the interstitial fluid is neglected;
- the pseudo-fluid representing the granular material is incompressible;
- the stress tensor defined as $\boldsymbol{T} = pI + \boldsymbol{\Pi}$ results splitted into its spherical and deviatoric part and it is considered symmetric.

With these assumptions the conservation equations reduce to:

$$\nabla \cdot \boldsymbol{u} = 0 \tag{2.1}$$

$$\rho \frac{\partial \boldsymbol{u}}{\partial t} + \rho \boldsymbol{u} \cdot \nabla \boldsymbol{u} = -\nabla p - \nabla \cdot \boldsymbol{\Pi} + \rho \boldsymbol{g} \tag{2.2}$$

$$\frac{3}{2}\rho \frac{\partial \theta}{\partial t} + \frac{3}{2}\rho \boldsymbol{u} \cdot \nabla \theta = -\boldsymbol{\Pi} : \boldsymbol{\nabla u} - \boldsymbol{\nabla} \cdot \mathbf{q^T} - z^T \tag{2.3}$$

where ρ is the bulk density, $\boldsymbol{u}$ is the velocity field, pI is the isotropic part of the stress tensor, $\boldsymbol{\Pi}$ the deviatoric stress tensor defined as $\boldsymbol{\Pi} = \eta(\nabla \boldsymbol{u} + \nabla \boldsymbol{u}^T)$ where η is the viscosity, $\boldsymbol{g}$ is the gravity vector, θ the granular temperature, $\mathbf{q^T}$ and z^T the diffusive flux and the dissipation rate of fluctuating energy, respectively. The system is closed with *ad-hoc* constitutive equations that describe the behavior of a granular material. The fluctuating energy flux is formulated as a function of the

gradient of granular temperature:

$$\mathbf{q}^{\mathbf{T}} = -k' \nabla \theta \tag{2.4}$$

where k', assumed constant, is the coefficient of diffusion of fluctuating energy. It scales with the bulk density ρ and the particle size d_p. The energy dissipation rate was defined as:

$$z^T = \mu p |\dot{\gamma}| \tag{2.5}$$

where μ represents the effective friction coefficient and is taken equal to the tangent of internal friction angle of the material; $|\dot{\gamma}|$ is the shear rate, a measure of the spatial velocity gradients. The effective viscosity has been formulated to depend on granular temperature in the form of a phenomenological relationship between bulk fluidity and local particle mobility analogous to that of glassy systems (Doolittle, 1951):

$$\eta = \eta_0 \rho_g d_g^2 exp\left(\frac{\theta^*}{\theta}\right) \tag{2.6}$$

where η_0 represents an analogous of the pre-exponential factor in the Eyring's equation for simple liquids and θ^* is a granular temperature scale.

2.2.1 Wall-boundary conditions

The Navier slip condition was used to describe the velocity at the wall. This approach related the tangential velocity u_t at the wall to its gradient in the normal direction through a constant parameter, λ, called "slip length" (Artoni *et al.*, 2009):

$$u_t = \lambda \left| \frac{\partial u_t}{\partial n} \right| \tag{2.7}$$

The condition above allowed for a certain amount of slip at the walls.

2.3 Numerical description of the free surface flow

The simulation of bi-dispersed granular flows, allowing for a free, moving surface was achieved by an Eulerian, continuum approach to the two phase flow. Accordingly, the static computation domain included two regions, accounting for the air and the solids, the latter treated as a pseudo-fluid with *ad-hoc* rheology reported in 2.2. The extension and movement of the two regions were tracked by means of their interface. The local pressure, p, and velocity field, $\boldsymbol{u}$, were determined by the conservation equations reported in Eqs. 2.1, 2.2, 2.3. The local density, ρ, and viscosity, η, were very different in the air and solids domains. The values used in the unique momentum balance were determined as:

$$\rho = \rho_a + (\rho_g - \rho_a)\varphi_p \tag{2.8}$$

$$\eta = \eta_a + (\eta_g - \eta_a)\varphi_p \tag{2.9}$$

where the volumetric fraction of solids, φ_p, was used and the subscripts a and g indicate respectively the air and the granular material. It determined the extent of the solid domain, treated as a non-porous pseudo-fluid. For numerical stability φ_p was treated as a continuous variable which changed from 0 (air) to 1 (solid) in a very limited layer of finite thickness at the interface between the two phases. It was determined by the convective equation for a passive scalar:

$$\frac{\partial \varphi_p}{\partial t} + \mathbf{u} \cdot \nabla \varphi_p = 0 \tag{2.10}$$

This approach to two phase flow is referred to as Level Set method (Olsson and Kreiss, 2005). It allows tracking the interface motion. Its implementation may require the addition of a small, artificial diffusion flux, to cope with the sharp discontinuity at the interface, Γ. The densities of air and of granular material,

as well as the viscosity of air, were assumed constant. The local viscosity of the granular pseudo-fluid was the key to determine its movement. It was defined through a sub-model, detailed in 2.2. Shortly, the local viscosity was determined using the equation 2.6.

2.4 Segregation model

The modeling of segregation required specifying the local fraction of different species. Focusing on bi-dispersed mixtures of solids, where the size was the only feature that differentiated the species, the local mass fraction of species i in the mixture, ω_i, was given by:

$$\frac{\partial \omega_i}{\partial t} + \boldsymbol{u} \cdot \nabla \omega_i = \left(\nabla \cdot \boldsymbol{J}_{s,i}\right)_y \tag{2.11}$$

that assumed a convective-segregating transport mechanism, where the segregating flux, $\boldsymbol{J}_s$, described the separation of fines from coarse material. The segregating flux can be described starting from different segregation mechanisms. Here, we considered that the percolation was the main mechanism that affects the segregation (Williams, 1963). The segregation flux acted in the direction of gravity (Christakis *et al.*, 2002; Christakis *et al.*, 2006), assumed to be y. We then neglected the segregation flux in x direction. The model was an original combination of Literature models (Fan *et al.*, 2014; Hajra *et al.*, 2012). The particle diameter ratio, used by Hajra *et al.* (2012), and the shear rate used by Fan *et al.* (2014) were considered as the two most important factors in the percolation mechanism. The segregation velocity of fine particles was assumed as:

$$v_{sf} = -K d_c (1 - \omega_f) \left(\frac{d_f}{d_c} - 1\right) |\dot{\gamma}| \tag{2.12}$$

where $|\dot{\gamma}|$ was the magnitude of the shear rate, d_f and d_c the small and the large particle diameter, respectively. K was a model parameter discussed later. Hajra

et al. (2012) develop their model assuming that the segregation velocity is proportional to the difference between the diameter of small (the segregating particle) and the average diameter:

$$v_s = -K(d_f - \langle d \rangle) \tag{2.13}$$

The average diameter $\langle d \rangle$ is the mass averaged particle size defined as:

$$\langle d \rangle = \omega_f d_f + \omega_c d_c \tag{2.14}$$

Expanding $\langle d \rangle$, the term contained in 2.12 is obtained. Hajra *et al.* (2012) state that the segregation velocity of each specie is proportional to the concentration of the other specie as previously found also by (Savage and Lun, 1988). This dependence is in agreement with the physical evidence that percolation of a fine particle increases when larger amount of coarse particles surround it because larger inter-particle void are available. Fan *et al.* (2014) introduce in the segregation velocity, the dependence on the shear rate, since percolation occurs when the material is dilated due to flow. With the increasing of the shear rate, larger inter-particle voids are created and fine particles can percolate more easily. The present percolation model was obtained through the product of the two independent sources of segregation proposed by Fan *et al.* (2014) and Hajra *et al.* (2012) respectively. It has to be considered just as a first attempt to tackle a complex phenomenon using an hydrodynamic continuum rheology in a two phase unsteady system (solid and air) where the solid phase is a binary mixture of particles (coarse and fine). Further refinements may indeed include inertial effects occurring in the free surface flows and segregation flux in the x direction. The segregation flux was obtained as the product between the segregation velocity and the mass fraction of small particles, as:

$$J_{s.f} = -K d_c \omega_f (1 - \omega_f) \left(\frac{d_f}{d_c} - 1 \right) |\dot{\gamma}| \tag{2.15}$$

$$J_{s,c} = -J_{s,f} \tag{2.16}$$

According to Eq. 2.15, percolation does not occur in the absence of bulk deformation, differently from the model of Christakis *et al.* (2002). The solution of Eq. 2.11 may require some artificial diffusion for convergence, particularly when sharp composition differences arise locally. It has no physical meaning, nor quantitative relevance; and it is a purely numerical artefact. The Eq. 2.11 coupled with the Eqs. of rheological model, 2.1, 2.2, 2.3, 2.10 has the general structure of nD, advection and diffusion conservation equations.

Nomenclature

Symbol	Units	Description
d	m	particle diameter
$\mathbf{g}$	m/s^2	gravity acceleration vector
$\mathbf{J}_s$	m/s	vector of segregation flux
K	-	segregation parameter
p	Pa	pressure
$\mathbf{q}^T$	Pa m/s	diffusive energy flux
t	s	time
$\mathbf{u}$	m/s	velocity vector
v_s	m/s	segregation velocity (y-component)
z^T	Pa/s	dissipation rate of mechanical energy
$\lvert\dot{\gamma}\rvert$	1/s	magnitude of shear rate
η	Pa s	viscosity
η_0	1/s	parameter in the viscosity coefficient
θ	m^2/s^2	granular temperature
θ^*	m^2/s^2	granular temperature scale
$\mathbf{\Pi}$	Pa	deviatoric stress tensor
ρ	kg/m^3	density
ϕ_p	-	volume fraction
ω	-	mass fraction

Sub- and superscripts

f	fine

c	coarse

Chapter 3

Simulation of free surface granular flows in tumblers

3.1 Introduction

Segregation is strictly connected with the flow of the granular material and they influence each others (Hsiau and Hunt, 1996). The first step of this thesis was to use the hydrodynamic model, coupled with the transport equation that tracks the evolution of the air-granular material interface, to describe the flow inside devices of industrial interest, such as tumblers. They are commonly used to process particulate materials in mixing, reaction, calcination, granulation and drying operations, to make few examples. When used for mixing purposes, they often work batch-wise as in the pharmaceutical industry. In the rotating drum, which represents probably the simplest type of tumbler, several flow regimes have been identified by Mellmann (2001) and Henein and Brimacombe (1983). The flow of the particulate material in the transverse plane can be classified into three basic forms: slipping, tumbling (or cascading) and cataracting motion. Froude number, Fr, filling degree and wall friction coefficient are used to discriminate between them. Here only the tumbling motion is studied, since it is the only one able to provide good mixing, by shearing the material. For a complete description of all the motion types the reader can refer to Mellmann (2001). In the tumbling motion, it is possible to classify three different regimes: slumping, rolling and cascading.

When the rotational speeds are low (Fr<10^{-3}), slumping of the bulk occurs. The solid bed is continuously elevated, and the flow is characterized by a series of subsequent distinct avalanches occurring at the surface. As the rotational speed increases (10^{-4}<Fr<10^{-2}) the discrete sequence of avalanches evolves into a continuous motion of the free surface and a transition to the rolling regime arises. The rolling regime is usually considered in industry the most desirable condition to promote good mixing of the particles, due to the formation of a steady superficial layer of sheared material (Henein and Brimacombe, 1983; Ingram *et al.*, 2005). In this regime two zones can be recognized: an active layer formed by particles on the free surface moving downwards and a passive layer, located below the active layer, where the particles are transported upwards as a rigid body, by the rotation of the mixer wall (Mellmann, 2001; Boateng, 1998). The bed surface becomes nearly flat with a characteristic slope, called dynamic angle of repose, which depends on material properties (resulting from internal friction and cohesion) and rotational speed. Further increasing the rotational speed (Fr>10^{-2}), the bed surface evolves in a characteristic S-shaped profile and the tumbling regime sets in. Since the granular material is intensely sheared in the surface layer, the surface dynamics is responsible for the mixing or for the segregation of the material. When the particulate material has a broad particle size distribution or differences in density between the particles, segregation can occur (Mellmann, 2001; Santomaso *et al.*, 2006). Brown (1939) gives the fundamental concepts about segregation and points out that it is mainly a surface phenomenon. More recent experimental and numerical works have shown that the segregation in a rotating drum can be related to the shape and slope of the free surface (Santomaso *et al.*, 2013; Zik *et al.*, 1994) and that the bulk motion plays no role in the generation of segregation (Boateng and Barr, 1997). Being able to correctly describe the free surface flow in a granular bed is therefore required not only to describe the mixing dynamics but also to tackle more complex phenomena such as segregation. The work reported in this Chapter used the rheological model (Artoni *et al.*, 2009)

reported in 2.2, based on hydrodynamic analogies between fluid and granular flows to simulate the behavior of the free surface dynamics in different types of batch mixers. We focused on the rolling regime. The model was first validated comparing the numerical simulation with the experimental velocity profile obtained by Ding *et al.* (2001) in a drum mixer. Also the active layer thickness as a function of angular velocity was compared with the available Literature correlations (MiDi, 2004; Orpe and Khakhar, 2001). The model was then used to compare the behavior of two traditional tumbler geometries (drum and symmetric double cone) and a modified geometry (asymmetric double cone) rotating at the same angular velocity. The simulated surface flow pattern, active layer area and granular temperature were used to infer information on the mixing efficiency of the three geometries.

3.1.1 The active layer

Several experiments for characterizing the surface flow in the rolling regime can be found in the Literature. Boateng and Barr (1997) use optical probes to obtain particle velocities, granular temperature and solid concentration for different materials in 3D cylinders finding that the velocity profiles in the active layer vary in a parabolic way while in the passive layer the profiles are linear. Tomographic techniques, based on magnetic resonance imaging (Nakagawa *et al.*, 1993) and on positron emission particle tracking (PEPT) (Ding *et al.*, 2001), allow to investigate the velocity field and the depth of active layer finding a nearly linear velocity profile in the flowing layer. Jain *et al.* (2002) measure the velocity profiles using the particle tracking velocimetry (PTV) by observing the material through transparent side walls in a quasi-2D drum. The same technique is used by Chou and Lee (2009) in 2D and 3D configurations. Other approaches measure peripheral particles velocity from images of the transverse plane using a high-speed video camera. In order to follow particle trajectories, time exposed photographs are

taken at sufficiently low shutter speeds (Felix *et al.*, 2007; Santos *et al.*, 2013; Orpe and Khakhar, 2001). The particles at the lower point of the base of the flowing zone appears to be at rest, defining a static point in the laboratory frame reference. The distance measured between each static points and the free surface, perpendicular to the free surface, is considered as the depth h of the active layer (Felix *et al.*, 2007). It represents the interface between the active and the passive zone and can be considered as a yield line (Boateng and Barr, 1996). The depth h has been correlated to experimental variables such as the Fr number or the angular velocity (Jain *et al.*, 2002; Felix *et al.*, 2007; Orpe and Khakhar, 2001). Different scaling laws are also proposed in the Literature. MiDi (2004), using the data from Literature (Felix *et al.*, 2007; Orpe and Khakhar, 2001; Rajchenbach, 2000; Bonamy *et al.*, 2002), find that for half-filled drums in an appropriate range of velocity it is possible to obtain a steady flowing layer with a depth proportional to a dimensionless flow rate Q':

$$\frac{h}{d_p} \propto \sqrt{Q'} \tag{3.1}$$

where dp is the particle diameter and Q' is equal to:

$$Q' = \frac{Q_0}{d_p\sqrt{g d_p}} \tag{3.2}$$

with Q_0 the flow rate defined as:

$$Q_0 = \frac{\omega\left(R^2 - h^2\right)}{2} \tag{3.3}$$

R is the drum radius and ω the rotational speed. If the term h^2 is small compared with R_2 , the Eq. 3.3 can be simplified as:

$$Q_0 = \frac{\omega R^2}{2} = \frac{\omega D^2}{8} \tag{3.4}$$

where D is the mixer diameter. The general scaling reported in 3.1 is valid for surface flows in a drums for different materials and different drum sizes, D/d_p, ranging from 40 to 2500. Hence, MiDi (2004) observes a power law trend, $h \propto Q'$ with a constant exponent n=0.5. This exponent is based on the assumption of constant shear rate along the bed depth. Pignatel *et al.* (2012), however, find out that the power law exponent is not constant but dependent on the range of Q'. In particular, they observed that h/d_p increases with ω as a power law with the exponent n ranging between 0.07 and 0.33, so $n < 0.5$. Felix *et al.* (2007) instead propose the following power law:

$$h \propto \omega^n \tag{3.5}$$

where n is a function of D/d_p and ranges from 0.17 to 0.68, including 0.5. Furthermore Chou *et al.* (2011) generalize the GDR Midi (MiDi, 2004) equation by introducing in the Eq. 3.4 drum filling degree f (typically $f < 0.5$) which is dependent on the filling segmental angle α (see Figure 3.1):

$$Q_0 = \frac{\omega D^2}{8}\left(1 - \frac{sin\alpha}{\alpha}\right) \tag{3.6}$$

In conclusion once the geometrical parameters and the filling of the drum are fixed, the thickness of the flowing layer can be generalized as:

$$h = kd_p(Q')^n \tag{3.7}$$

where k is a constant of proportionality and n is an exponent that can be constant and equal to 0.5 according to MiDi (2004)or variable according to Pignatel *et al.* (2012) or Felix *et al.* (2007). The proportionality is valid under a no-slip condition between the granular material and the drum wall (Chou and Lee, 2009). Chou *et al.* (2011) indeed show that the relative thickness of the flowing layer is reduced for the slipping case, so that k and n are expected to be different in case of partial

TABLE 3.1: Parameters of rheological model.

Parameter	Values	Units
μ	0.5	-
θ^*	12	m^2/s^2
η_0	4	$1/s$
k'	4	$1/s$
λ/d_p	4	$1/s$

slip between the material and the wall.

3.2 Simulation set-up

The continuous flow of the granular material inside the rotating tumblers was modeled through 2D finite element simulations using the commercial CFD software Comsol Multiphysics 4.4, with suitable adaptation to account for the rheological and surface flow models (see Sections 2.2, 2.3). The model parameters used are reported in Table 3.1. Three different geometries were simulated: drum (Figure 3.1), symmetric double cone (SDC) tumbler and asymmetric double cone (ADC) tumbler (Figure 3.2). In order to simplify the un-steady simulations and to avoid the use of moving meshes to follow the rotation of the mixers, the equation of motion and the Level Set equation were solved in a fixed coordinate system (x,y) and the rotation of the mixers was simulated by rotating the gravity vector g according to:

$$g_x = |\mathbf{g}|\, sin(\omega t) \tag{3.8}$$

$$g_y = |\mathbf{g}|\, cos(\omega t) \tag{3.9}$$

where ω is the angular velocity. For the visualization of the results, the velocity maps were rotated so that the gravity vector always appeared vertical, downwards oriented. The mesh was built with triangular elements in the domain and quadrilaterals elements on the boundary. Each simulation was carried out for 60

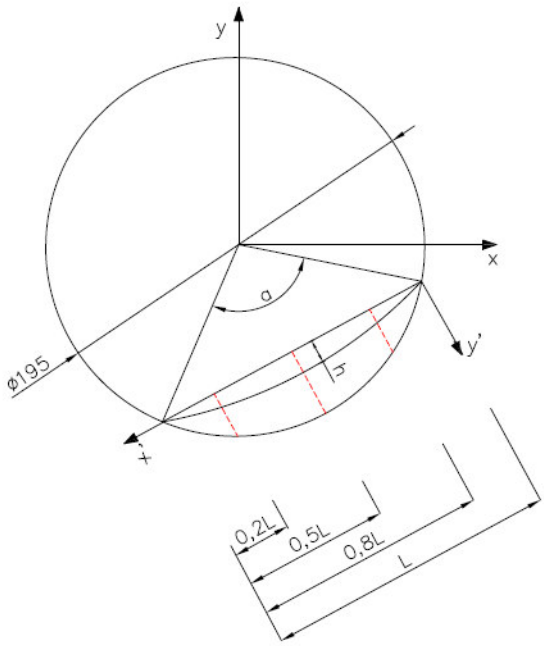

FIGURE 3.1: Geometry of the simulated rotating drum. Measures are in mm.

s with a time step of 0.001 s. The simulations were performed at different filling levels and, at the starting condition, the upper part of the cylinder, above the interface, was filled with air and the lower one with granular material. The wall boundary conditions explained in the subsection 2.2.1 was used for the granular material. Boundary conditions at the walls for the phase variable φ_p and for the translational kinetic energy were no flux and insulation respectively. We validated the model on a drum using the geometry and the operating conditions reported in (Ding *et al.*, 2001). A drum with diameter 400 mm, filling level 10% in volume and angular velocity 0.17 rad/s was therefore simulated. The granular material in the drum was constituted by glass beads 1.5 mm in size and 1600 kg/m^3 in bulk density. The material properties and operating conditions used in model validation are summarized in Table 3.2. The same parameters of Table 3.1 has been used, except for λ/d_p, which has been assumed 300 instead of 400. After validation, the simulations of this study were carried out in the three different geometries reported in 3.1 and 3.2, varying the angular velocities and

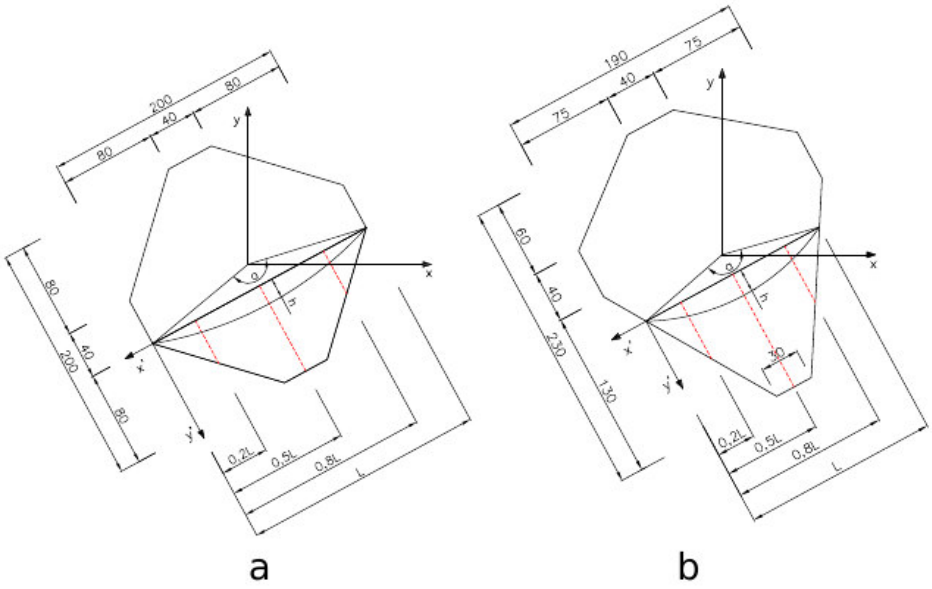

FIGURE 3.2: Geometry of the simulated tumblers: symmetric double cone (a) and asymmetric double cone (b). Measures are in mm.

TABLE 3.2: Materials properties and simulations conditions.

Property/condition	Validation	Simulations	Units
ρ	1600	1500	kg/m^3
d_p	1.5	0.9	mm
f	10	35	%
ω	0.17	0.3, 0.6, 0.9, 1.2	rad/s

the filling degree. Material properties and operating conditions used to perform these simulations are reported in Table 3.2. The different angular velocities selected correspond to Froude numbers between $9{\cdot}10^{-4}$ and $9{\cdot}10^{-2}$ consistent with a stable rolling regime (Mellmann, 2001).

3.3 Results and discussion

3.3.1 Model validation

The rheological model used in this work was previously validated for granular flows in silos and hoppers with and without internal inserts (Artoni *et al.*, 2009; Artoni *et al.*, 2011; Volpato *et al.*, 2014). Tumblers however differ from silos for the variable geometry, the larger impact of the surface flow and the more complex internal flow structure. To validate the model in tumbler geometries, we compared the simulations with experimental results on drum mixers by Ding *et al.* (2001). The coordinates for simulation (x,y) and post-processing (x',y') are shown in Figures 3.1 and 3.2. Ding and co-workers have measured the x'-velocity component, u'_x (x', y'), parallel to the surface against the bed depth in y'-direction at different x'-positions. They observe that the maximum value of $u_{x'}$ in the active region occurs at the bed surface in a position close to the mid-chord, $\mathrm{u}_{x'}$ (0.62L, y'). The velocity decreases with depth, inverting the direction at the local h and reaching a maximum negative velocity at the wall. The comparison between experimental values and our numerical $\mathrm{u}_{x'}$ (x', y') are reported in Figure 3.3. The nearly linear velocity profile in the active layer was captured in the simulation and the maximum velocity at the surface as well as the zero-velocity point at the transition between active and passive layer were well predicted. Also the decay of velocity in the passive layer was captured and the quality of fit was confirmed by R^2. Based on the simulations results an a posteriori verification of the model applicability was also performed. The inertial number, defined as:

$$I = \frac{|\dot{\gamma}|\, d_p}{\sqrt{p/\rho}} \tag{3.10}$$

quantifies the dynamics of a granular material (MiDi, 2004) and can be interpreted as the ratio of two characteristic timescales at particle level: a kinematic timescale (the characteristic time of deformation) and a mechanical timescale (the

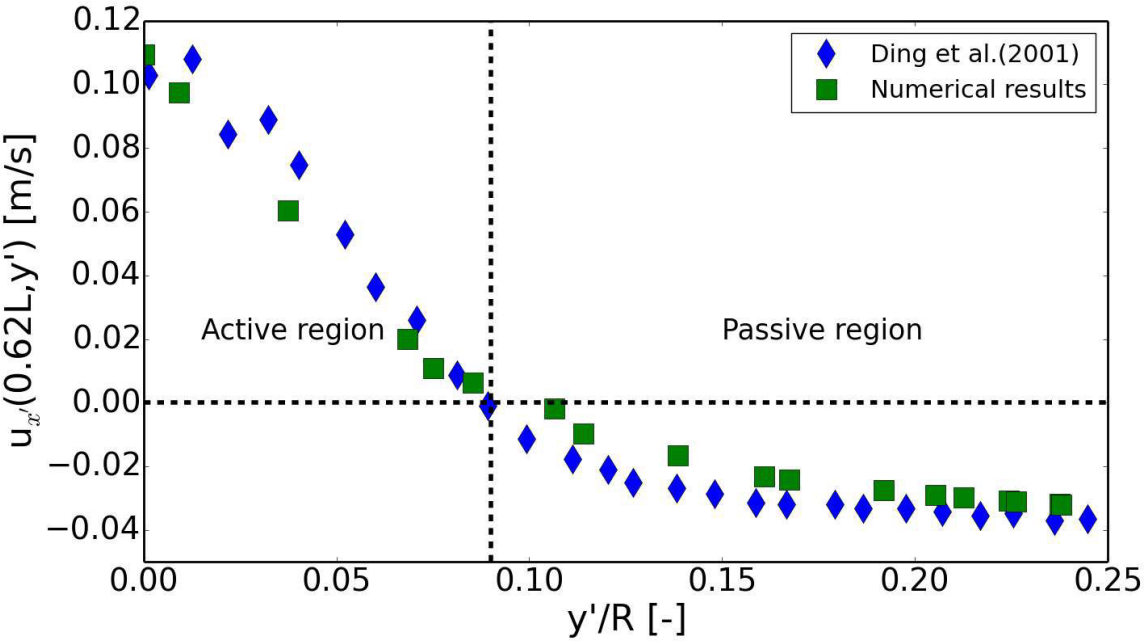

FIGURE 3.3: Comparison between experiments and simulation: x'-velocity component vs. the dimensionless bed depth.

confinement timescale). It can discriminate between three different regimes of motion: I<10^{-3} quasi static flow; 10^{-3}<I<10^{-1} dense flow and I>10^{-1} collisional flow (Da Cruz *et al.*, 2005). The rheological model used in this work was developed for the dense regime (Artoni *et al.*, 2009) so it was important to verify if the flow condition in the surface active layer were within the application range of the model. The average inertial number for Ding's experimental results was verified to be in the range of 0.026-0.036, therefore well within the dense flow regime described by the model.

3.3.2 Velocity maps in the tumblers

The main features of the granular bed behavior in rolling regime were qualitatively described in the Introduction. Summarizing, we therefore expected the simulations to be able to predict:

- the existence of two regions: active and passive region divided by a zero velocity line, at a depth h;

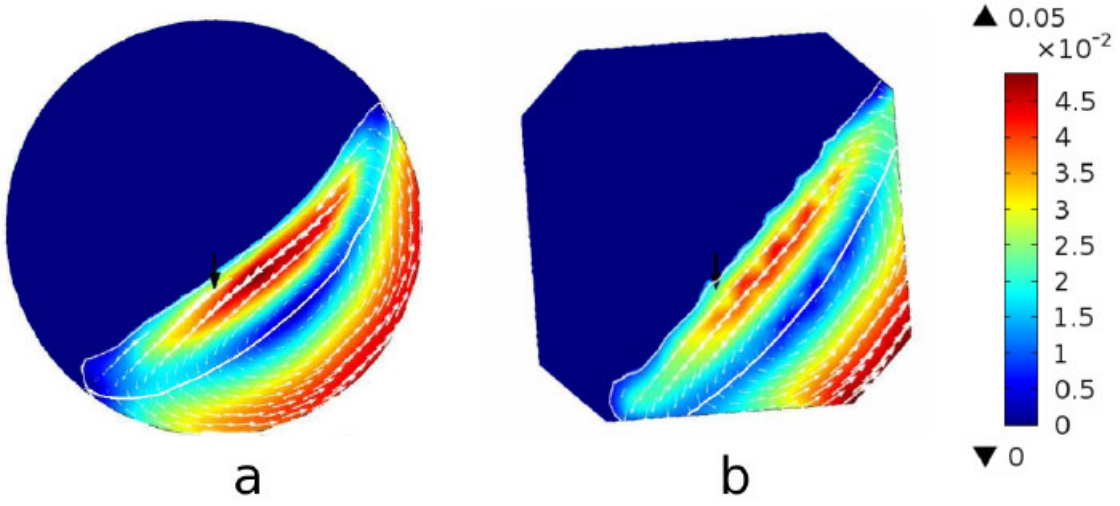

FIGURE 3.4: Velocities (m/s) of the granular solid phase for the drum (a) and for the SDC mixer (b). Filling level =35% and ω=0.3 rad/s in both mixers. The black arrow indicates the gravity vector, which rotated during the simulations. The white arrows represent the velocities vector. The continuous white line delimits the active area.

- a steady flow in the active region;
- the stabilization of a nearly flat bed surface with a characteristic slope.

This rich phenomenology was effectively simulated and observed to hold for the drum and the SDC tumbler, as shown in Figure 3.4. We observed the formation of the active surface in the form of a sheared layer that remained steady during several tumblers rotations. The bed surface was nearly flat, excepted close to the drum wall, with a constant slope. The active area was delimited at the top by the free surface and at the bottom by the zero velocity line which corresponded to the flow reversal (Ding *et al.*, 2001). It is know from dedicated experiments (Scanferla, 2015) that an ADC mixer, which is not a standard industrial geometry, can improve the homogeneity of the mixture at the discharge point if compared to the SDC tumbler and the rotating drum. Since simulation is a powerful tool to explore the internal flow structure, dedicated simulations were carried out in the alternative geometry (represented in Figure 3.2 (b)) in order to better understand

the superior mixing performance of the ADC mixer. Figure 3.5 reports four different flow configurations typical of the ADC tumbler. The steady state flow, typical of drum and SDC mixer, was replaced by a complex periodic flow. The velocity map changed continuously, depending on the position of the material inside the tumbler. In some flow configurations it was even difficult to identify the zero velocity line inside the granular bed since a large portion of the material slipped at the wall. In these cases the line separating the active and the passive regions disappeared at the intersection with the wall (this was particularly evident in configurations b and d), implying that the material did not yield internally but at the wall. This typically occurred when the material was moving predominantly parallel to the longest axis of the tumbler (Figures 3.5 (b) and 3.5 (d)). Instead when the material was moving along the shortest tumbler axis, (Figures 3.5 (a) and 3.5 (c)), the flow configurations were very similar to the SDC geometry, with a clear distinction between active and passive regions everywhere. These evidences coming from the simulations, were also observed by visual inspection in some experiments carried out in a 1:1 scale, transparent wall, ADC tumbler. The mixer was filled with a granulated free flowing powder (35% by volume) and operated in the rolling regime. An evident slip of the material at the wall was observed approximately in the same tumbler position predicted by the simulations.

3.3.3 Velocity profiles

The results presented so far are mainly qualitative. To develop quantitative considerations and comparisons, the velocity profiles along the bed depth at different surface positions will be studied in the following. Results for the drum and the SDC mixer after a rotation of 400 degrees (t=23 s), at a constant rotational velocity (0.3 rad/s) are presented first. In Figure 3.6 the velocity in the x' direction (i.e.

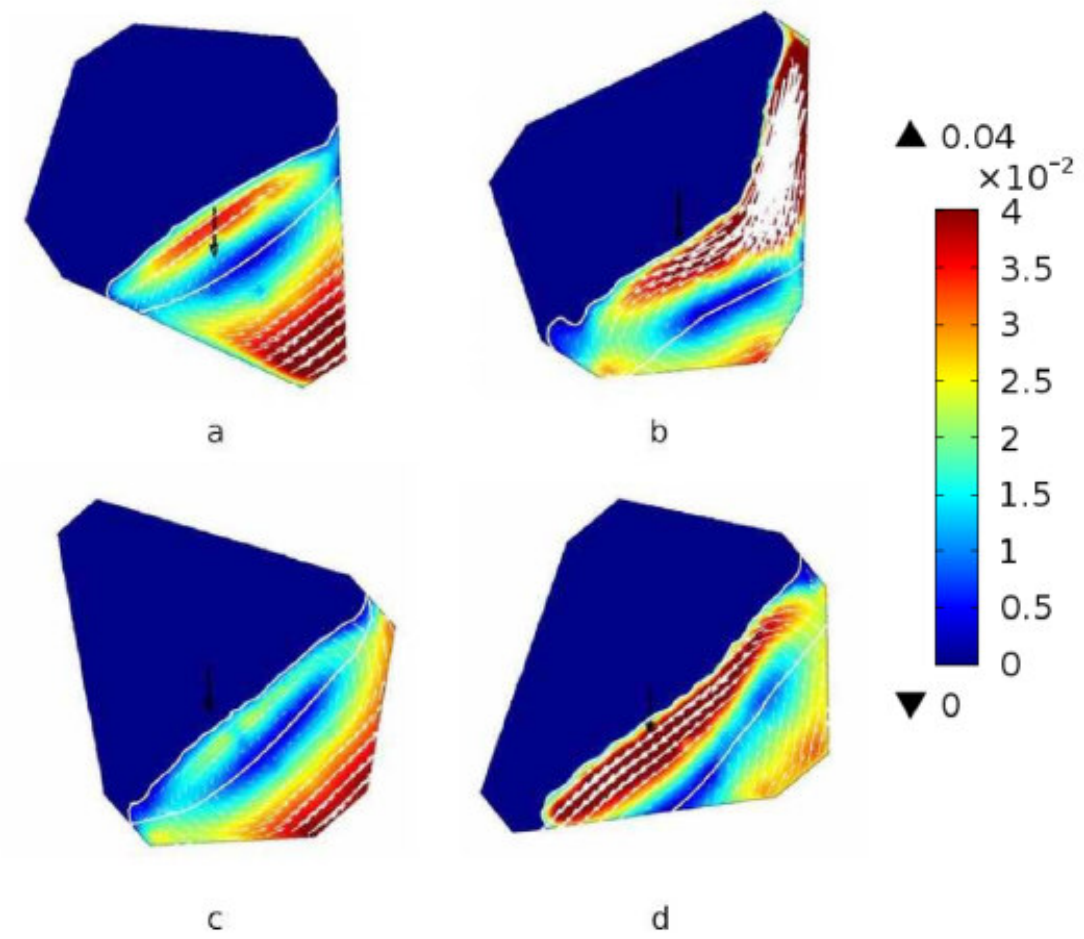

FIGURE 3.5: Velocity (m/s) maps for different configurations of flow in the ADC tumbler. a) rotation of 400° (t=23 s); b) rotation of 501° (t=29.2 s); c) rotation of 587° (t=34.2 s); d) rotation of 673° (t=39.2 s). Filling level=35% and ω=0.3 rad/s. The black arrow indicates the direction of gravity, which was rotated during simulation. The white arrows represent the velocity vector. The continuous white line delimits the active area.

parallel to the free surface) is plotted against the bed depth, y', at a given x' coordinate (in our case 20, 50, 80% of the free surface length L). The maximum positive value of u_x' occurs on the bed surface at the mid-chord position (0.5L,0), for both the drum and the SDC mixer. The velocity always decreases with depth (y' direction), reaching zero at the interface between the active and passive region. Here the velocity changes direction and increases in modulus simply because of the effect of the tumbler rotational velocity, reaching the maximum negative value at the wall. The velocity profiles of the solid phase in the drum qualitatively agreed with the experimental results of Boateng (1998) and Santos *et al.* (2013). The two symmetric chords, at 20% and 80% of L, show slightly lower surface velocity. Velocity along L was therefore slightly asymmetrical with respect to the mid-chord position in agreement with Literature data (Ding *et al.*, 2001). Also in the SDC mixer the surface velocity is larger at the mid-point. The velocity along the two symmetric chords (at 0.2 and 0.8L) is clearly different compared to the mid-chord; the wall velocity was different at different wall positions reaching the maximum value (in modulus) at the largest distance from the rotation center (mid-chord). The two symmetric positions correctly show similar, lower wall velocity since at these positions the wall was closer to the rotation center. As expected, after and exponential decreasing, u_x' converges at the same values that is equal to that measured at 0.5L. For the SDC mixer the profiles show therefore a different distribution of the velocity, breaking the symmetry observed in the rotating drum mixer. The loss of symmetry was even more evident in the ADC mixer, as expected. In Figure 3.7 the velocity profiles along 0.2L, 0.5L and 0.8L chords, in the configurations c and d of the ADC mixer, are shown. Configuration c was selected because it should be comparable to the SDC configuration of Figure 3.4b . Again, at the surface, u_x (0.5L,0) was larger than the velocities u_x (0.2L,0) and u_x (0.8L,0) in both configurations, but the absolute velocity magnitude in the two configurations is very different. Higher levels of shear (reflecting the slope of the velocity profile) are therefore experienced in configuration d at mid-chord, while

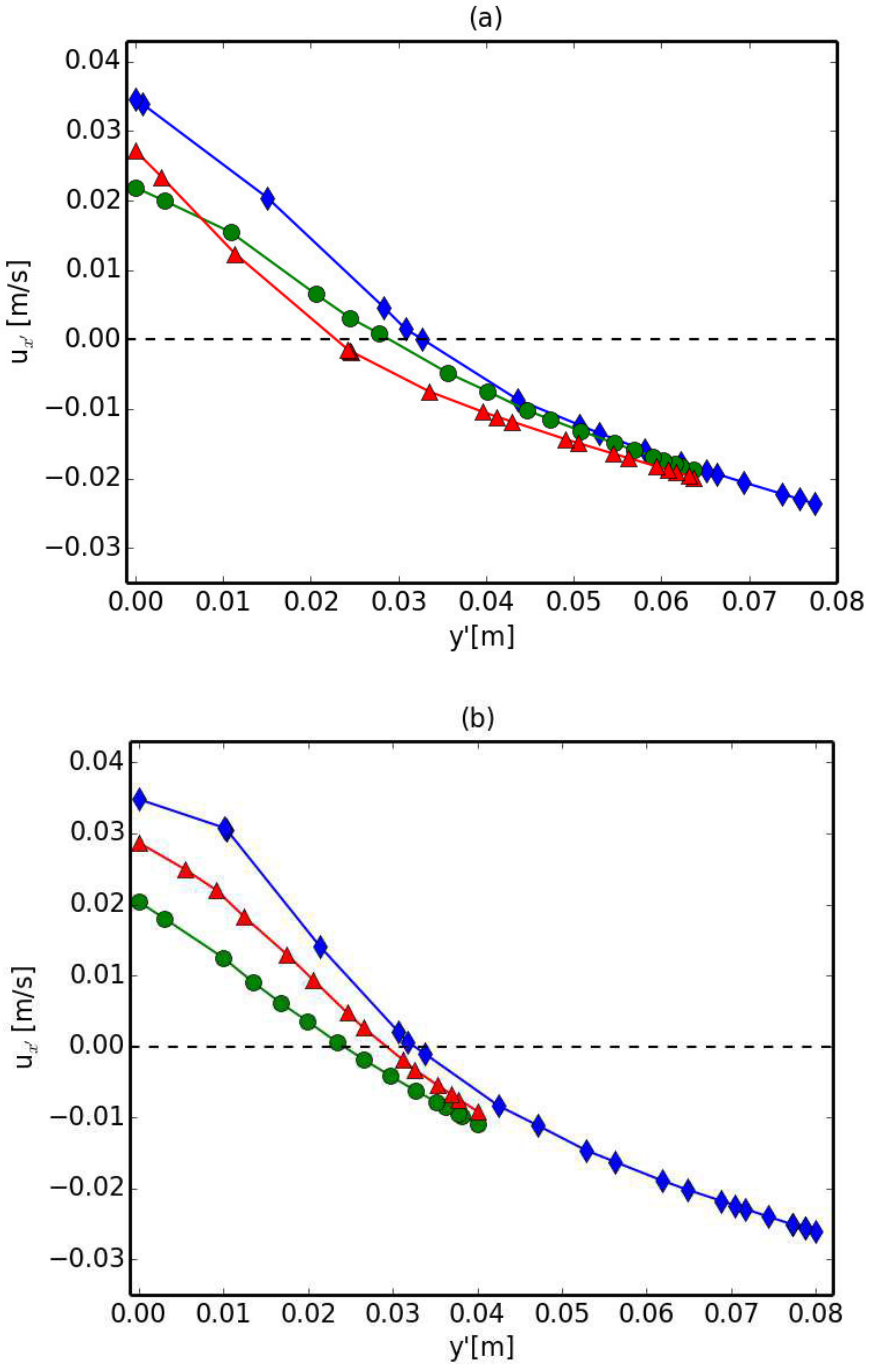

FIGURE 3.6: $u_x{}'$ along the depth for the rotating drum (a) and for the SDC mixer (b) after a rotation of 400° (t=23 s). •= $u_x{}'$ (0.8L, y'), ♦= $u_x{}'$ (0.5L, y'), and ▲=$u_x{}'$ (0.2L, y'). ω=0.3 rad/s.

TABLE 3.3: Active region depth in terms of numbers of particle at ω=0.3 rad/s and t=23 s.

	Active region depth, h/d_p		
Tumbler type	20% L	50% L (mid-chord)	80% L
Drum	27	31	27
SDC	29	31	29
ADC (config. 1)	25	32	30

much lower shear developed along the chord at x'=0.2L. Moreover, it appears that the velocities are always positive along this chord (0.8L) indicating that the zero velocity line intersected the tumbler wall. In configuration d the passive region disappears and all the bed thickness was sheared at some x' position. The same applies to configuration b.

3.3.4 Depth of the active region

The analysis of the velocity reversal points (the zero velocity line) allowed to determine the active region depth, at different position below the free surface. Table 3.3 reports the dimensionless depths h/d_p of the active region evaluated at 20%, 50% (mid-chord) and 80% of L. In the drum, the active region was observed to be roughly symmetric about the mid-chord position with a reduction in thickness of 13% at the two extreme positions (0.2L, 0.8L). A similar symmetric condition was observed for the SDC mixer, with only a 6.5% reduction in thickness at the extremities. Hence, the active region in the SDC mixer showed a more constant thickness along L than in the rotating drum, as can also be observed from 3.4. After the same rotation time, the ADC mixer (configuration a), developed an asymmetric distribution of the active region, as reported in 3.3. The depth of the active-passive interface was indeed thicker at the bottom of the free surface (0.8L). To further validate the results of the simulations, the active region depth at the mid-chord position in the drum was systematically investigated, as a function of the angular velocity. Results are shown in Figure 5.8. We found that the active

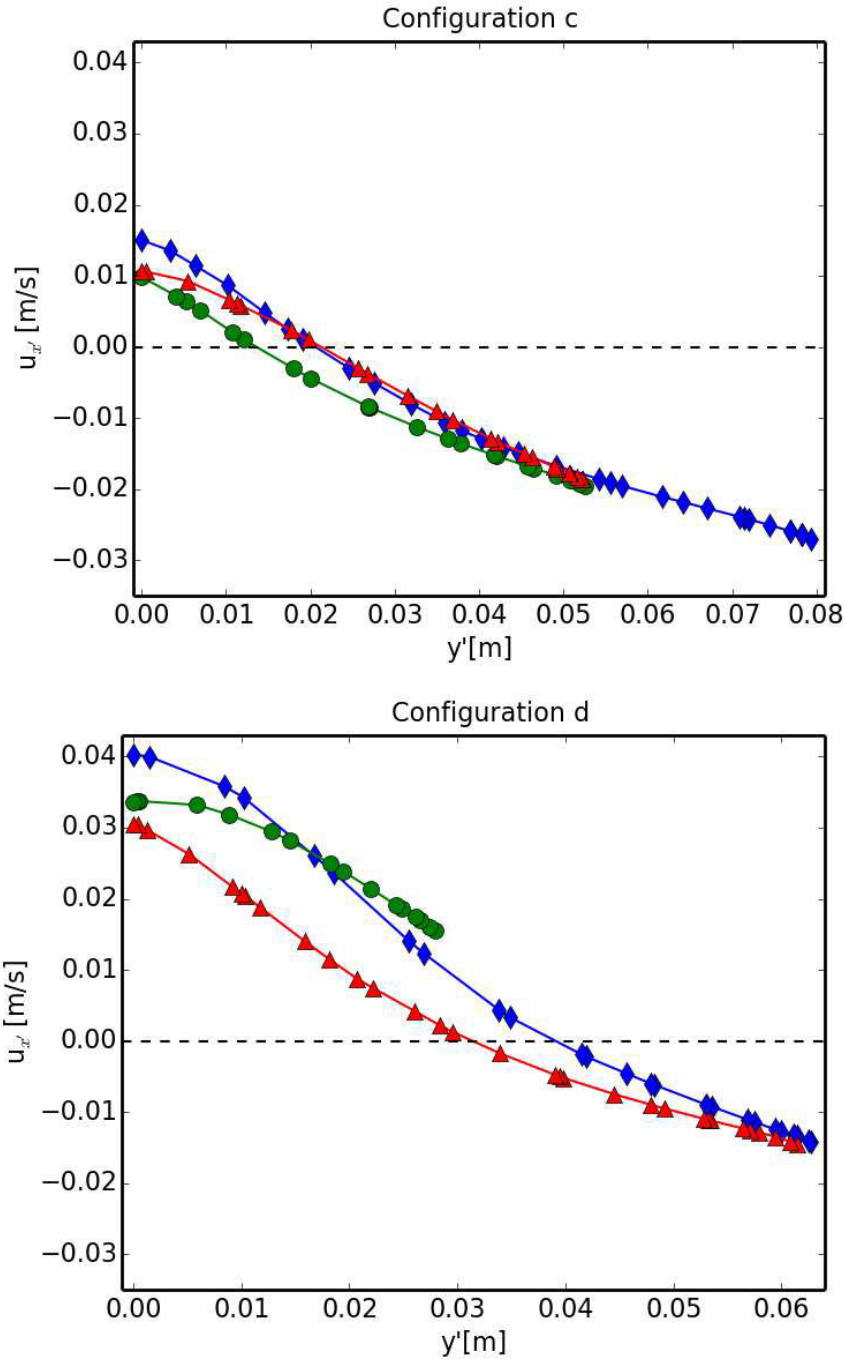

FIGURE 3.7: u_x'along the depth in the ADC tumbler, in the configuration c (above) and d (below) of Figure 5 3.5. •= u_x' (0.8L, y'), ♦= u_x' (0.5L, y'), and ▲=u_x' (0.2L, y'). ω=0.3 rad/s.

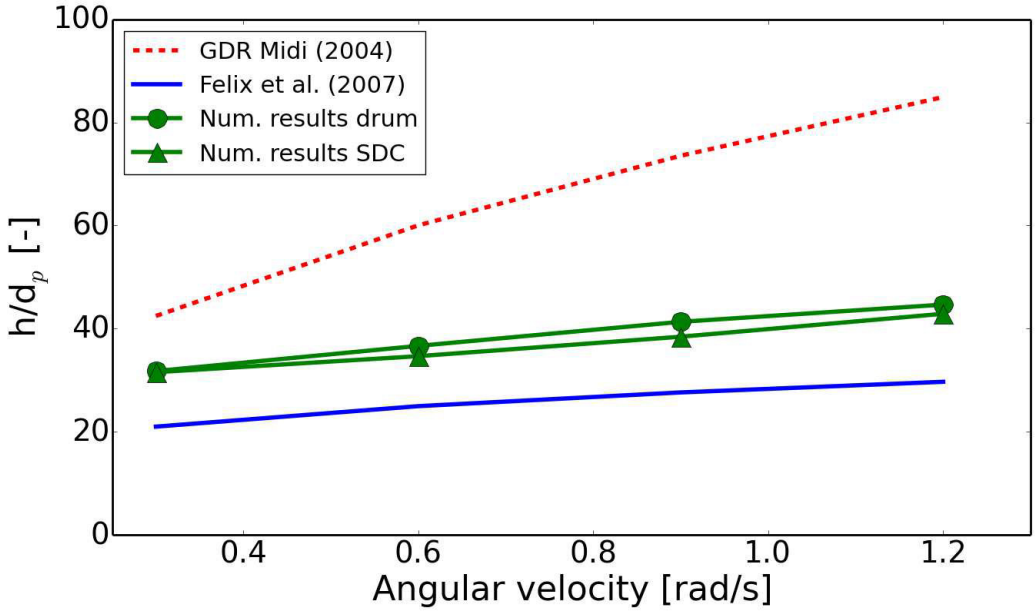

FIGURE 3.8: Active depth as a function of angular velocity.

depth increased with the rotational speed according to the following power law:

$$h = 0.038 d_p \omega^{0.5} \tag{3.11}$$

Also, the simulated values were between those predicted by the Literature correlations presented in 3.1.1, as clear from Figure 5.8. These are the correlations from MiDi (2004), with n constant equal to 0.5, and from and from (Felix *et al.*, 2007), with n being a function of the drum diameter and of the particle size and equal to 0.25 for our case. Note that MiDi (2004) and Felix *et al.* (2007) correlations were developed for half-filled drums while our study considered a 35% filling. The correction by (Chou and Lee, 2009) was then used to take into account the effect of filling degree. The segmental angle α in Eq.3.6 , calculated for 35% filling, was equal to 2.75 radians in our geometry. The good match with Literature correlations can be considered a further validation of the numerical results. For the SDC mixer the predicted active region depths at the mid chord were very similar to those obtained for the rotating drum shown in Figure 5.8, thus confirming the qualitative observations obtained from the maps in Figure 3.4. The

analysis of the active region depth for the ADC mixer was instead impossible. As previously reported, the unsteady motion of the material in the tumbler did not always allow to define a mid-chord position. To overcome this problem, instead of considering just the depth of the surface layer in one position (typically x'=0.5L), a further analysis was carried out, on the extension of the whole active region.

3.3.5 Analysis of the active region extension

The extension of the active area, A_a, differently from the depth at the mid-chord, took into account the variations of the whole flowing area and was therefore affected by any change in bed shape occurring during a tumbler revolution. In the rotating drum, because of the fully developed steady state, the expected nearly constant area was confirmed by results of Figure 3.9. Its extension was approximately 1/3 of the whole solids domain. For the SDC and ADC mixers instead periodic oscillation of the area occurred. In particular in the SDC tumbler we identified eight extreme values of area occurring with a constant frequency and amplitude at each rotation, reflecting four similar cycles per rotation (Figure 3.9). They corresponded to precise displacements of the granular material with respect to the tumbler position. A maximum was reached each time the bed surface was aligned to one diagonal of the tumbler; this corresponded to the maximum distance between surface and the walls, and also the maximum extension of the free surface. The minimum active area was reached with the material bed surface aligned to one of the walls of the tumbler, corresponding to the minimum length of the chord between two opposite walls, and also to the minimum extension of the free surface. Such observations and correspondences in Figure 3.11 are also highlighted by the insets indicating the tumbler positions. Also for the ADC mixer periodic peaks were evident, but with a different periodicity with respect to the SDC; the frequency appeared halved and intensity varied between

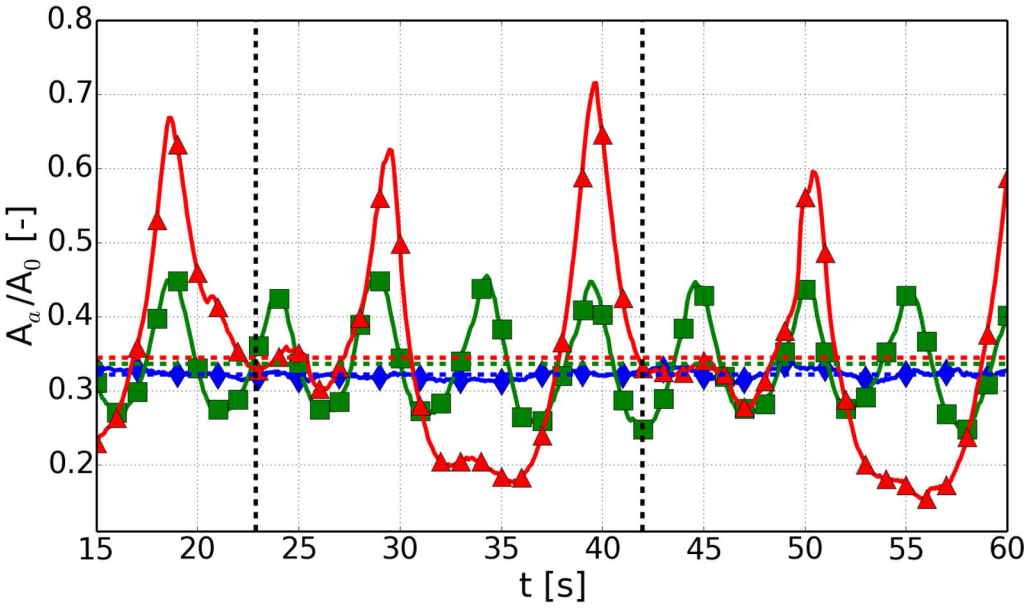

FIGURE 3.9: Extension of the active layer, A_a , scaled to the initial filling area A_0 as a function of time for a drum (⧫), SDC (■) and ADC (▲) tumbler. The vertical lines mark a whole rotation of the tumbler. The horizontal dashed lines reflect the time average extension for the 3 types of tumblers.

the two cycles. The maxima corresponded to the configurations where the material flowed aligned to the longest diagonal of the double cone (configurations b and d in Figure 3.5). In these cases however the flow was no longer a surface phenomenon, but it extended to most of the granular bed thickness. The material was mobilized not only internally but also at the walls. In these configurations the active region for the ADC mixer was clearly larger than in the other two tumblers. On the contrary when free surface was aligned to the shortest axis the active area dramatically dropped, reaching a minimum. This was clearly different from the SDC, which at the same position presented a maximum. The reason was that only in the ADC geometry the effect of the longest diagonal dominated, so that the other diagonal and chords did not correspond to maxima in the extension of the free surface. Clearly the flow pattern in the ADC was strongly influenced by the shape of the tumbler; mixer geometry induced an unsteady motion which, even if continuous at the surface, was discontinuous at the wall, bearing some

similarity with the slumping regime existing in drums rotating at lower rotational speed (Mellmann, 2001; Henein and Brimacombe, 1983). It is interesting to observe that the average values of active area, Figure 3.9, were quite similar for the three geometries, notwithstanding the large differences in the flow patterns. This suggests that the active area extension is not meaningful per se, but it is its variation that affects the efficiency of mixing.

3.3.6 The granular temperature and the mixing potential

To deepen our understanding of the granular bed dynamics and mixing potential of each tumbler, we analyzed the variations of the granular temperature, θ. The mobility of the particles in the tumblers, taken into account by θ, can be associated to the two main mixing mechanism, i.e. shear in the bulk and particle collisions at the surface (Boateng, 1998). According to the analysis carried out in 3.1.1 it was verified that the material moved in a dense flow regime. The dominant granular activation mechanism in the active region could be therefore associated to the shear rather than to the collisions between individual particles. θ was therefore supposed to be generated in the bulk and proportional to the local velocity gradient. Based on the active area results, we expected that also the granular temperature, averaged inside the active region, θ, could vary with some time periodicity in the SDC and ADC mixers. Numerical results indeed confirmed that in such geometries, θ did not remain constant during one rotation, differently from the drum (Figure 3.10). The periodic variations of θ were compared to those of the active area extension for the SDC and the ADC mixer in Figures 3.11 and 3.12 respectively. Profiles appeared to be similar, but θ the position of the peaks was delayed, almost in phase opposition with respect to that of active area. In particular in the ADC mixer we observed two peaks of θ, with different intensity and in phase opposition (configurations a and c of Figure 3.5) with respect to the active area (configurations b and d of Figure 3.5). The lag observed between θ and

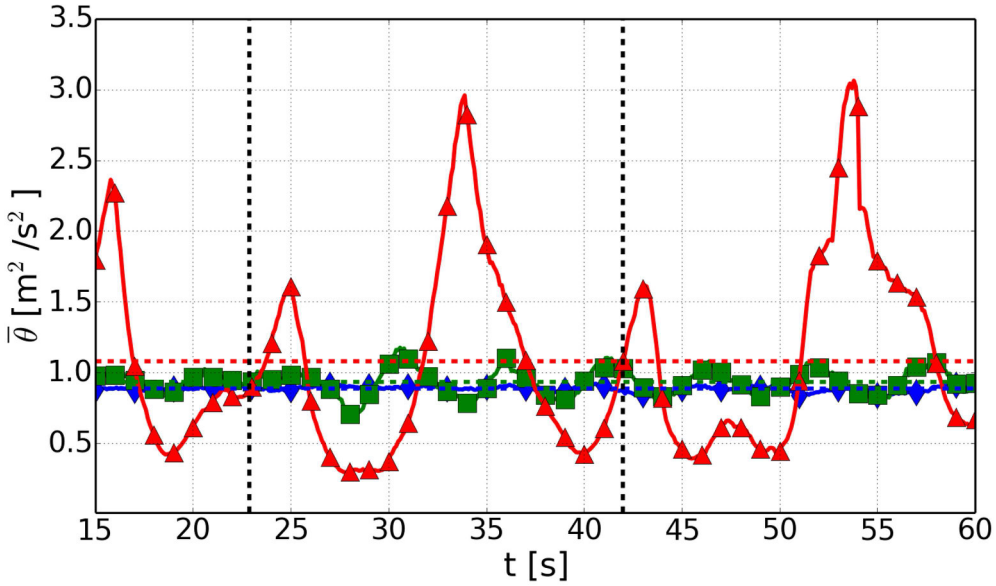

FIGURE 3.10: Average granular temperature in the active area θ as a function of time of rotation for a drum (♦), SDC (■) and ADC (▲) tumbler. The vertical lines mark a whole rotation of the tumbler. The horizontal dashed lines reflect the time average for the 3 types of tumblers.

A_a depended on the level of shear existing in the bulk in the different tumbler positions. In particular the largest value of θ corresponded to a bed configuration where the material was poorly sheared, since in some portion it yielded almost rigidly at the bottom wall (configurations b and d). These portions of bed dramatically contributed to reduce the average θ of the active layer. On the contrary when the active area was minimum the bed yielded only internally, increasing the level of shear (and therefore of θ) in the active layer. These observations suggested the possibility that the ADC tumbler could not provide good mixing performances. It is however intuitive that two elements of the granular dynamics in a tumbler can concur to improve the mixing performance: the extension of the active area and the average level of shear within it. Large active area associated to large shear rate levels (i.e. high θ) are expected to give the most efficient mixing, however a large active area with moderate shear levels inside, as in the ADC mixer, could result in poor mixing performance or longer mixing time. To

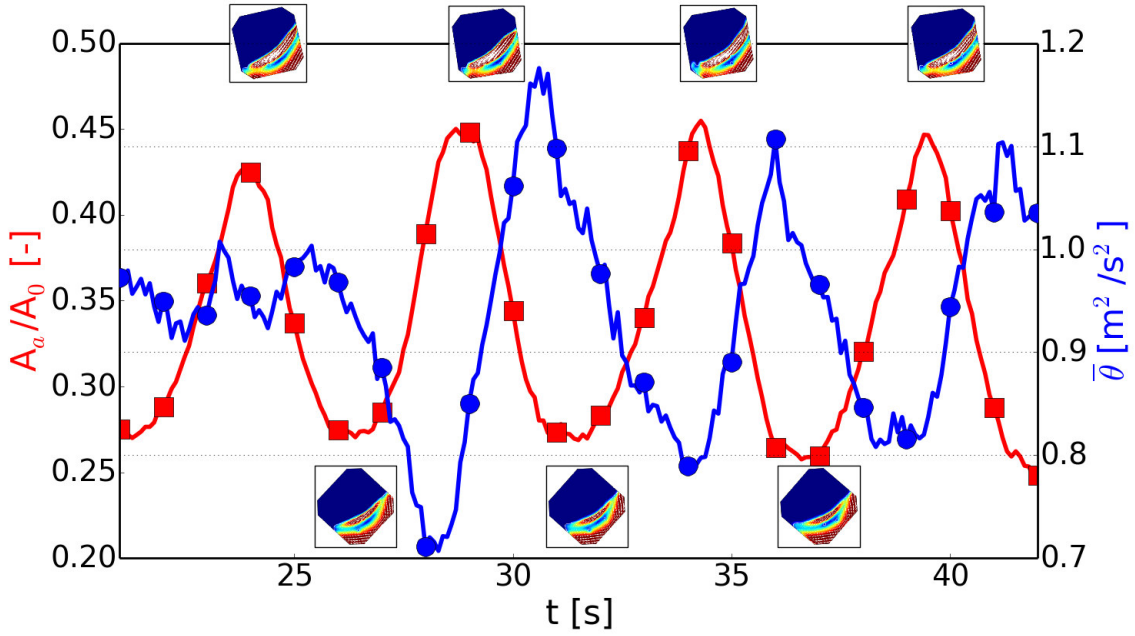

FIGURE 3.11: Variations in the active layer extension, A_a (■), and granular temperature, θ (•) in a SDC mixer.

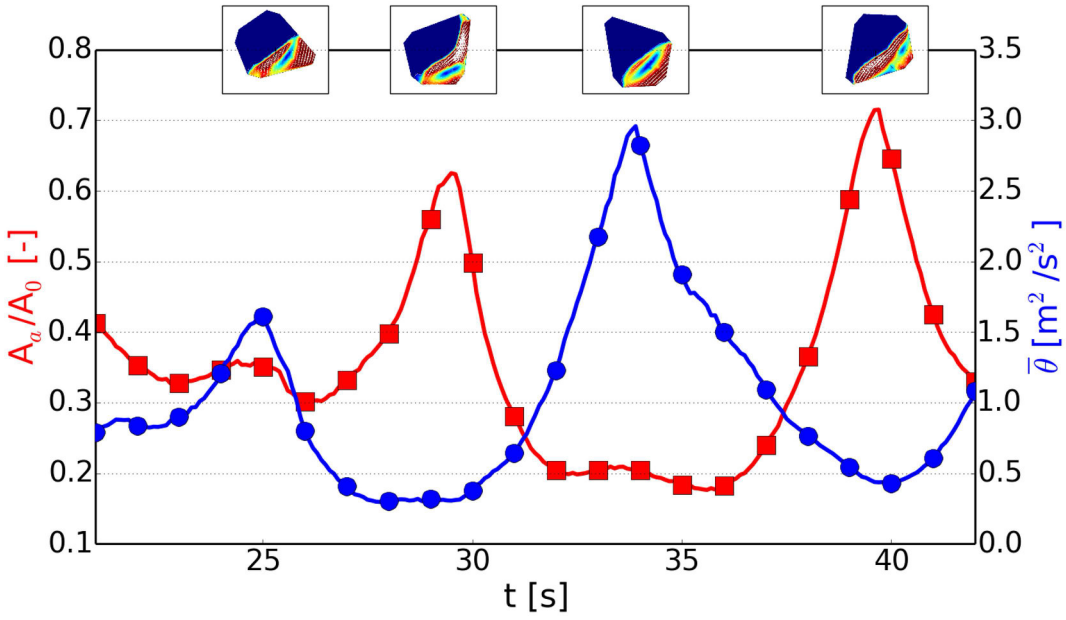

FIGURE 3.12: Variations in the active layer extension, A_a (■), and granular temperature, θ (•) in a ADC mixer.

formulate a quantitative comparison of the mixing potential of each geometry, we defined a dimensionless index accounting for the two mechanisms described above:

$$M_p = \frac{A_a}{A_0}\frac{\theta^{0.5}}{\bar{u}} \tag{3.12}$$

where A_0 is the initial filling area and u is the average velocity in the active layer. The ratio A_a / A_0 takes into account the possibility of comparing tumblers with different amount of material. The ratio $\theta^{0.5}/\bar{u}$ contains the contrasting effect of shear (represented by θ) and convection (represented by $\bar{u}$). A fast bulk motion not necessarily gives a good mixing if low particle activation is provided to the mass (as in configuration b of Figure 3.5) and vice-versa. The average value of mixing potential M_p (average over two complete mixer revolutions) for the drum, the SDC and the ADC were calculated to be 16, 19, and 24 respectively. Notwithstanding the unsteady flow conditions in the ADC which alternated high shear to low shear levels, this tumbler showed the highest mixing potential (26 and 50% higher than the SDC and the drum respectively). In addition considering that segregation is enhanced by steady state conditions typical of the drums, while irregular breakage of the flow symmetry disturbs segregation and enhance mixing (Santomaso *et al.*, 2013), the ADC could be even more favorable to mixing. It is clear that an analysis based on the study of flow patterns can not predict the final level of homogeneity of a mixture; moreover the effects of transverse flow (parallel to the rotational axis) are missing in this study. However the above observations, suggesting some potential benefits of using non traditional mixer geometries, justify additional efforts for future experimental or numerical studies able to provide more quantitative correlations between flow patterns (in time and space) and mixing potential. Finally, to evaluate the overall mixer performance also the flow patterns during the discharge of the material from the vessel needs to be considered. Flow during mixer discharge is certainly different in the three

geometries considered in this study and the effects of such difference still need to be addressed in a similar way it has been done for silos (Bertuola *et al.*, 2016) for example and reported in the Chapter 5.

3.3.7 Conclusions and perspectives

In this chapter the kinematics of granular material in rotating tumblers with different geometries was analyzed. A continuum hydrodynamic rheological model was used to simulate the behavior of the particulate material. The model was first validated with Literature experimental data for drums mixer in terms of velocity profiles at the mid-chord and active-layer thickness. The analysis was then extended to three different geometries: drum mixer, symmetric and asymmetric 2D double cone mixer. Simulations allowed to study the flow patterns, the active layer extension and the level of granular activation (through the granular temperature). The flow patterns in the symmetric double cone mixer were found to be similar to that in the simple drum with the formation of steady surface layer, with a flat air-solid interface at a constant slope. The extension of the surface area varied periodically in the symmetric double cone, following the changes in free surface length imposed by the tumbler geometry during rotation. In the asymmetric double cone tumbler instead the granular flow was more complex and periodicity more irregular, reflecting the asymmetric geometry. The analysis of the average granular temperature and of the convective velocity in the active layer suggested the enhanced mixing potential of the asymmetric geometry. This work, limited to a kinematic analysis of the granular flow, suggested the opportunity of extending the study to multicomponent mixture in order to correlate the granular flow fields to the final level of mixture homogeneity. The coupling between flow fields and composition maps will be helpful to create a unique predictive tool for mixer performances also at industrial level. In the next Chapter, in fact, the study of the effect of composition of the mixing was investigated.

Nomenclature

Symbol	Units	Description
A_a	m^2	active area
A_0	m^2	initial filling area
d_p	m	particle diameter
ω	rad/s	angular velocity
D	m	drum diameter
f	-	filling degree of mixers
g	m/s^2	gravity acceleration vector
H	m	bed depth
h	m	depthof the flowing layer
I	-	inertial number
L	m	lenght of the free surface
Q′	-	dimensionless flow rate
Q_0	m^2/s	flow rate
z^T	Pa/s	dissipation rate of mechanical energy
R	m	drum radius
ū	m/s	average velocity in the active layer
M_p	-	mixing potential

Chapter 4

Effect of PSD on mixture quality in double cone mixers

4.1 Introduction

In this Chapter, the effect of mixture composition on the mixing was investigated. In the Chapter 3, we studied the kinematics of flow in different granular flow and how it affect the mixing potential, but we did not have information on how the flow affected the homogeneity of the mixture. In dry granular materials composed of heterogeneous particles, the individual species often segregate under mechanical agitation. This is particularly problematic when occurring in industrial devices designed to increase the level of homogeneity such as the mixers. During the mixing operations, particles with different physical properties (size, shape, density) may not uniformly distribute in the mixer selectively accumulating in different parts of the bulk. The interplay of mixing and segregation is critical to the analysis and design of industrial mixing operations. The difference in size is the strongest driving force of segregation. There is a category of mixer particularly plagued by segregation: the tumblers. When binary mixture of particles differing only in sizes is tumbled in a rotating drum, high concentrations of the finer particles are collected around the center of the bed after few revolutions and form a segregated core in the radial direction (Boateng and Barr, 1996). In the

pharmaceutical industry, even if the tendency is to move, under a PAT perspective, to continuous processes, batch operations and mixing in particular are still the rule. Among the mixers used in the pharmaceutical industry, the tumblers are the most common. This type of mixer provides low shear stress conditions on the materials so that they can not be used with cohesive powders. For cohesive powders, higher levels of shear are required to break down the small aggregates originated by electrostatic and Van Der Waals forces. For that reason tumblers are often used to blend free-flowing powders. Unfortunately the flow patterns originated by the tumbler rotation are favorable to segregation mechanisms. This is particularly evident for horizontal drums where spectacular radial and axial segregation patterns develop after few mixer rotation (Cantelaube and Bideau, 1995; Hill *et al.*, 1997). In this mixer low axial mixing is given because of the geometry. Some study to increase the axial mixing in drums has been carried out by Wightman *et al.* (1998) by introducing a rocking motion to the mixer. For this reason other tumblers, able to provide higher level of axial mixing, are used in the pharmaceutical industry: V-blenders, double cone mixers, cubic mixers. Among these mixers, double cone mixers are commonly used in industrial application. Even if a certain axial mixing is provided by the geometry, the existence of a surface active layer where the powder is free to flow can promote axial segregation while percolation can give radial or core segregation. Radial segregation, not induced by percolation, but by ineffective flow patterns, can also develop when the filling level of the mixer exceeds the 60%. As a general conclusion all the tumblers suffer some drawbacks related to the fact that powders are free to flow in an uncontrolled manner, which limits their performances and reduces mixing efficiency. Breaking the symmetry of the flow patterns can be a way to reduce the segregation as we saw in Chapter 3; however other strategies are possible to improve the level of homogeneity of the final product. From a practical and industrial point of view the important thing is not the level of homogeneity in the mixer after mixing, but the degree of mixture homogeneity withdrawn from

FIGURE 4.1: White and blue TAED

the mixer. Powder needs to be discharged and this implies the formation of new flow patterns completely different from those used to previously mix. This can be an exceptionally good occasion to segregate. In this chapter, we investigate the mixing mechanisms typical of double-cone mixers, focusing the analysis of the composition of the mixture after the discharge. The double cone mixer was filled with a poly-dispersed mixture and the effect of the initial mixture on the discharge was investigated. Furthermore some considerations are done about other two types of tumblers: asymmetric double cone and conical tumblers.

4.2 Experiments and method

4.2.1 Mixing and sampling procedure

The material used in mixing experiments was tetraacetyldiamine (TAED) powder; it is typically used in detergent industry as bleaching activator and it is commercially available in different colors. Here, white and blue powders were used, but also red and green powders exist. In Figure 4.1 the white and blue TAED particles are shown. The TAED powder has a bulk density of 900 kg/m^3 and is available with a broad particle size distribution (PSD) in the range between 400 and 1000 μm. This allowed to sieve the material in several size ranges and to recombine them with the appropriate amount in order to obtain a controlled PSD. In a first set of experiments the overall PSDs were kept constant, as well as the amount of blue TAED particles that represented the 10% of the mixture by

weight, but the 'position' of the blue fraction was changed according to Figure 4.2. In a second set of experiments, a simpler binary bidispersed mixtures were considered as shown in Table 4.1 .

TABLE 4.1: Granulometric distributions used in the second set of experiments.

Experiments	Types of TAED	Diameters
1A	blue	200-300
	white	400-500
2A	blue	200-300
	white	500-600
3A	blue	200-300
	white	700-800
1B	blue	200-300
	white	400-500
2B	blue	400-500
	white	500-600
3B	blue	500-600
	white	700-800

Powder flowability was assessed by shear cell measurements (Brookfield PFT). The flow functions of the mixtures, i.e. the representation of the unconfined yield stress vs. the major principal stress, are reported in Figure4.3. Powders were free flowing, the internal friction angle and the wall friction angle are reported in Table 4.2.

TABLE 4.2: Internal and wall friction angle of TAED

Internal friction angle	Wall friction angle
35°	22°

A double cone mixer, scaled-down from a real industrial mixer, was used to perform the experiments. The volume of mixer was 1.855 cm^3. It consisted of two identical cones, joined by a cylinder 160 mm in diameter. The loading/discharging opening was 25 mm wide. The mixer, realized in trasparent PVC, is sketched in

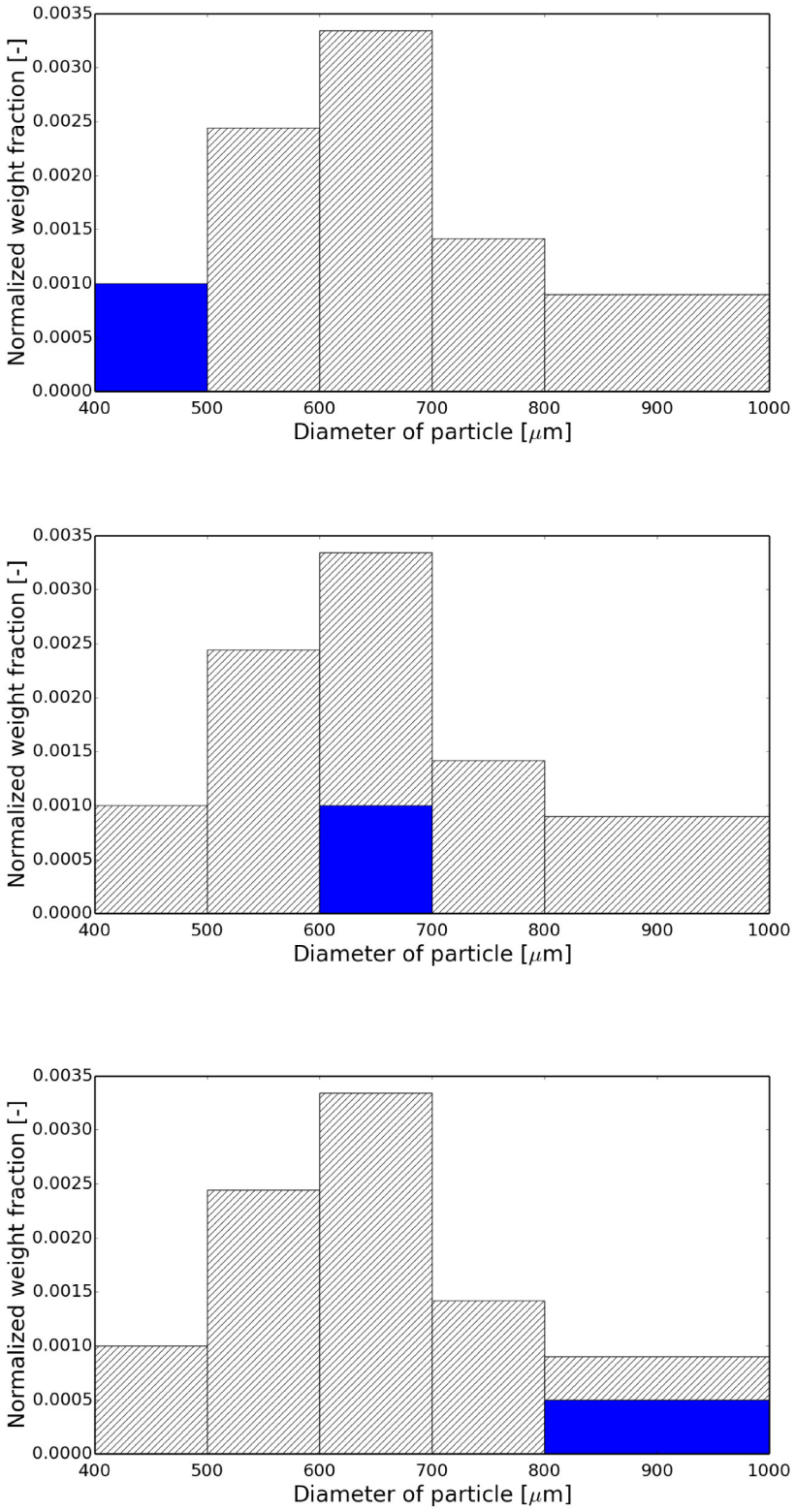

FIGURE 4.2: Different PSDs used in the experiments.

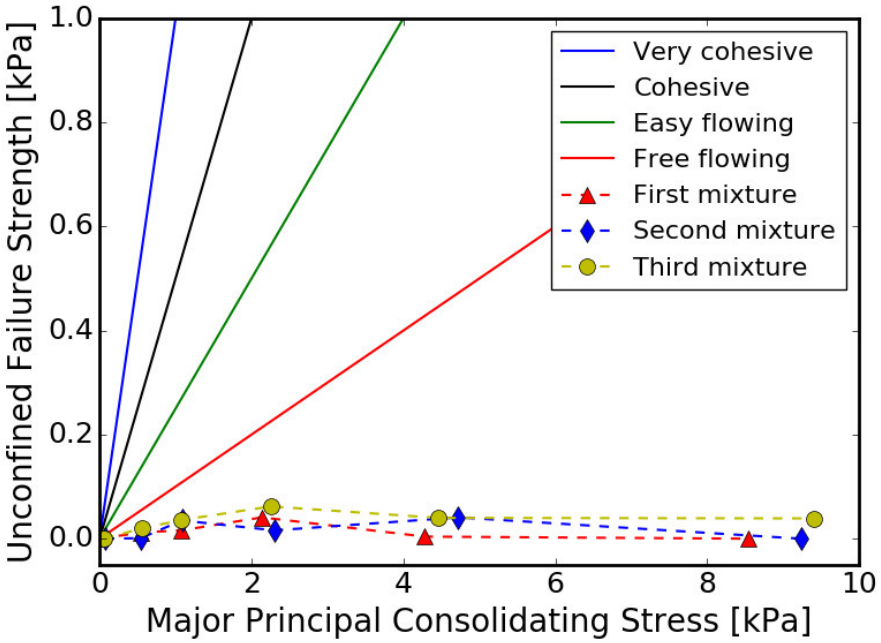

FIGURE 4.3: Flow functions for the three different mixtures reported in Figure4.2.

Figure4.4. The double cone mixer was filled with the powder necessary for the test, the mixture amount was kept fixed, closed with a magnetic cap placed inside a cylinder of Plexiglass used as support during rotation. The cylinder containing the double cone was then placed on two rollers driven by an electronic control motor for the necessary number of revolutions, at constant speed of 30 rpm (see Figure4.5).

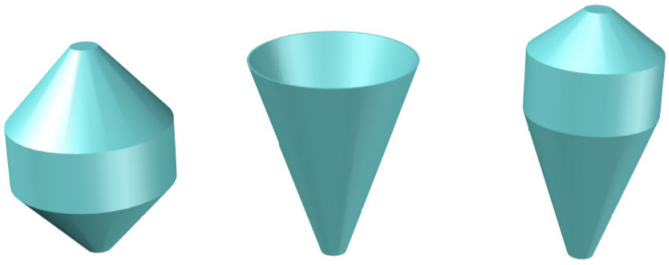

FIGURE 4.4: Mixers used in the experiments; from left to right:symmetric double cone mixers, conical mixer and asymmetric double cone mixer.

FIGURE 4.5: A picture of the cylinder containing the double cone placed on two rollers.

After mixing, particular care was dedicated to the unloading procedure of the material from the tumbler. A graduate paper strip 10 m long was placed on the floor. After the mixing step the double cone was placed on a mobile carriage at one end of the paper strip. A second magnet on the floor allowed the automatic opening of the discharge acting on the magnetic cap. The trolley was then moved at constant speed along the graduated paper strip letting progressively discharge the double cone mixer.

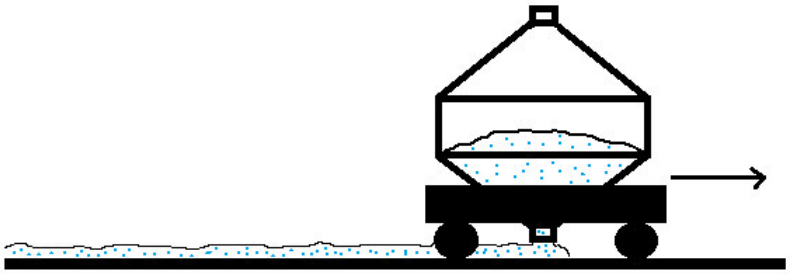

FIGURE 4.6: A picture of the double cone during the discharge.

After the complete discharge of the material, the strip of powder was divided to collect fifteen samples at equal distance of sampling, making sure to collect the same amount of material in order to standardize the sampling. Although this method may seem somewhat unusual, it respects the "golden rules" of sampling described by Allen (2013): " sample from a flow of powder in motion, by the whole discharge section and on the entire volume of the mixture".

4.2.2 Mixture analyses

Image analyses was used to evaluate the quantity of blue and white TAED; the intensity of blue pigment was measured and correlated to the quantity of blue TAED inside the mixture. To calibrate this measurement system, seven different reference samples with known composition of blue TAED were used. The total amount TAED for each sample was kept constant and equal to 30 g. Every sample was blended with 24 g of water and the paste obtained from the blending was put in a plate of transparent polystyrene (25 x 15.5 cm) provided with 15 cells. Every cell measured 2.5 x 2.5 x 0.3 cm. After drying the paste, images of the plate were acquired using a digital camera (DBK-61BUC02 CMOS9 with resolution 2048x1536 (RGB). The Lab color space method was used to evaluate the color of the sample. The Lab color space is a space with dimension L for lightness and a and b for the color-opponent dimensions, based on non-linearly compressed coordinates. The lightness, L, represents the darkest black at L = 0, and the brightest white at L = 100. The color channels, a and b, represent true neutral gray values at a= 0 and b= 0. The red/green opponent colors are represented along the a axis, with green at negative a values and red at positive a values. The yellow/blue opponent colors are represented along the b axis, with blue at negative b values and yellow at positive b values. For every sample it was possible to identify a value for the color channel b. In Figure4.7, the calibration curve is reported.

The color method was also compared with an alernative method based on sieve analysis. Three different mixture samples with different concentration of blue TAED were taken as reference: 5%, 10 % and 15 %. Every sample was composed by white TAED with a range size equal to 400-500 μm and blue TAED in a range size equal to 200-300 μm. This choice of particles ensured the complete separation of the differently colored particles by the sieving. For every composition, the sifting was on five samples. In Figure 4.8 we reported the parity plot with the measured % of blue TAED with sieving and with the color analyses method. It

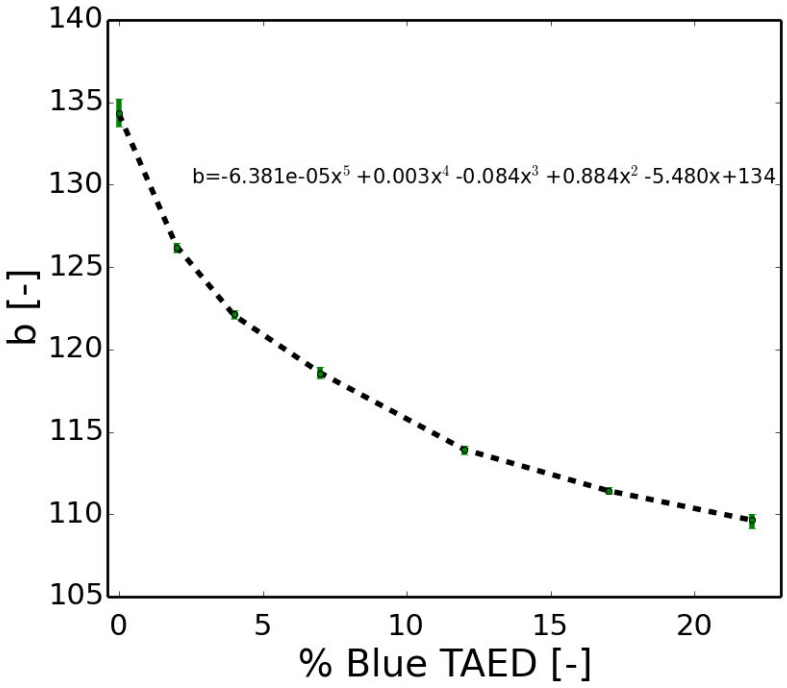

FIGURE 4.7: Calibration curve.

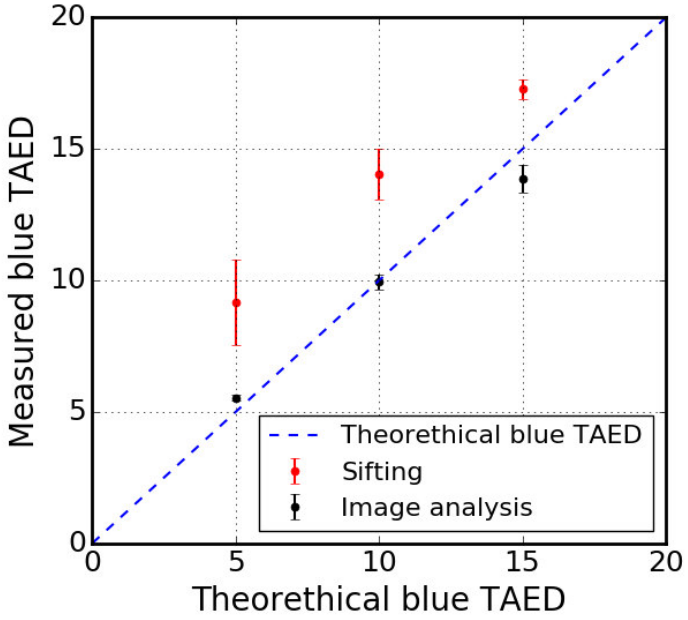

FIGURE 4.8: Parity plot

can be observed that the method based on image analyses was more reliable than that based on sieving because of the higher linearity of the error bars.

4.3 Results and discussion

4.3.1 Effect of the PSD

As reported above, a first set of experiments was conducted using the three mixtures shown in Figure 4.2. Every mixture, loaded in the double cone mixer, was discharged after mixing and the average variance of the discharge material, σ^2, was considered. Fifteen different samples of material were collected, blended with the water and then put in the each cell. Three different images for every cell were taken. Through the calibration curve, the b value, derived from the analyses of the images, gave a measure of the fraction of blue TAED present in the sample.

The mixture quality was evaluated through statistical method using the definition of variance σ^2:

$$\sigma^2 = \frac{\sum_{i=1}^{n}(y_i - \mu)^2}{N} \tag{4.1}$$

where y_i is the fraction of TAED blue measured in every samples, μ is the known fraction of TAED blue (0.1) and N is the number of the considered samples (N=15). The measured variance of a system was influenced not only by the mixing itself but also by other factors, for example the variance caused by the analytical method. For this reason, in order to consider only the variance due to mixing, it was necessary to subtract the variance due to the analytical method of analyses:

$$\sigma^2_{mixing} = \sigma^2 - \sigma^2_{analyses} \tag{4.2}$$

Figure 4.9 shows the evolution of the variance of mixture composition performed at 30 rpm and 40 % fill level. In each Figure, it is also reported the logarithmic value of the variance in the case of perfect mixing, σ^2_R, and in the case of complete

segregation, σ_0^2. The first and the third mixtures, showed a minimum variance after 45 revolutions; for this value the best degree of mixing was obtained, also if it resulted quite far from the perfect mixing meaning that a some degree of segregation remained in the mixture. Increasing the number of revolutions, the degree of mixing worsened in the first mixing and remains approximatively the same in the third mixture. The second mixture did not show optimal mixing at 45 revolutions, but increasing the number of revolutions, the quality of the mixing increased progressively. To better quantify the mixing performance, a mixing index was used. Several mixing indexes are reported in Literature and in this work, we used the Poole *et al.* (1964) defined as the ratio of the standard deviation of a completely random mixture, σ_R, and the experimental value, s:

$$MI = \frac{\sigma_R}{s} \tag{4.3}$$

This index tend to increase when the mixture approaches to the random mixing state. The mixing performance must be related with the three different PSDs used in the experiments (see Figure 4.2) and another index, representative of the three different PSDs of the mixture, was defined:

$$I = \frac{\left|\bar{d}_{blue} - \bar{d}_{mix}\right|}{\bar{d}_{mix}} \tag{4.4}$$

The index I took in consideration the distance of the diameter of the blue fraction from the average value of the distribution. The term $\bar{d}_{blue}$ represented the average diameter in the range constituted only by blue diameter. Considering the PSD reported in Figure 4.2, the average diameters in the three cases are equal to 450, 650, 900 μm respectively. The average diameter of the mixture $\bar{d}_{mix}$ was calculated as:

$$d_{mix} = \sum_{i}^{n} f_i \cdot d_i \tag{4.5}$$

where i represents the $i-th$ granulometric range. The greater the distance of the

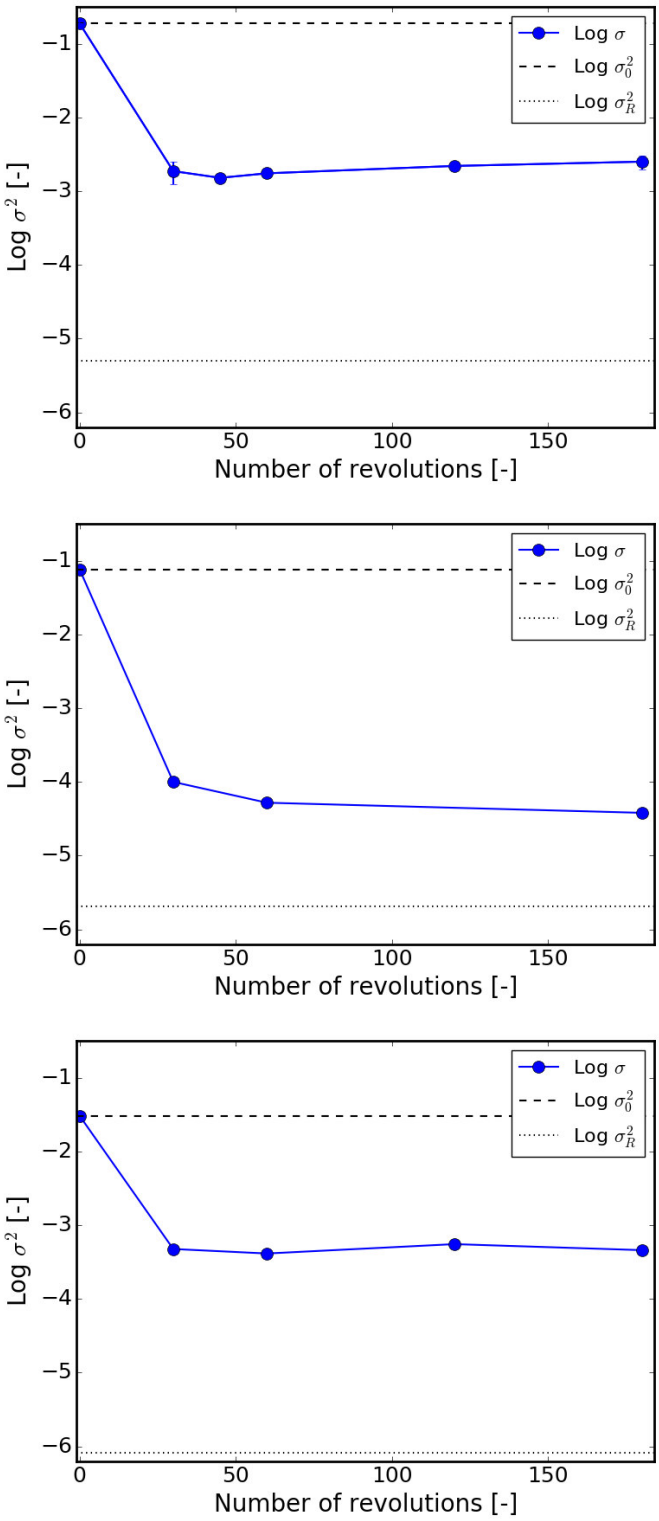

FIGURE 4.9: Logarithm of the variance plotted versus the number of rotation of the double cone mixer for mixture reported in figure 2a, 2b and 2c respectively.

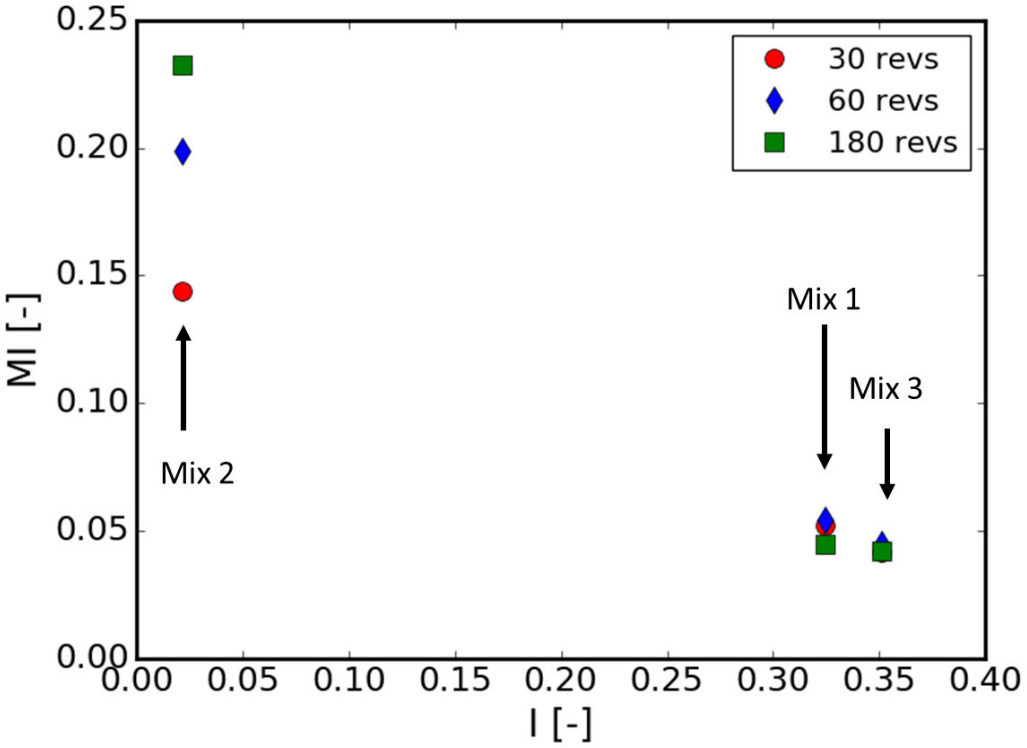

FIGURE 4.10: Mixing index versus I index.

blue diameter with respect the average diameter of the mixture, the greater the index I. As expected the index I was lower for the second PSD showed in Figure 4.2, and it was greater for the other two cases: in the first case the value of I is equal to 0.02, in the third case the value is equal to 0.35. In terms of I index, the worse mixture was the third that had a greater I index. In fact, as shown in Figure4.10, the mixing index MI got worse using the first and the last PSD. For these two cases, the number of revolutions did not seem to affect the degree of mixing. Blending a mixture with the second PSD reported in Figure 4.2 gave better results with respect the other PSDs. Furthermore, the mixing was more sensitive to the variation of the revolution numbers. The Figure4.10 clearly showed that the better number of revolution in this case was 180 revolutions. Increasing the revolutions of the double cone mixer it is possible to see an improvement of mixing only for the second mixture, instead for the first and the third mixtures, there are not a relevant variations of the variance increasing the revolutions. A simi-

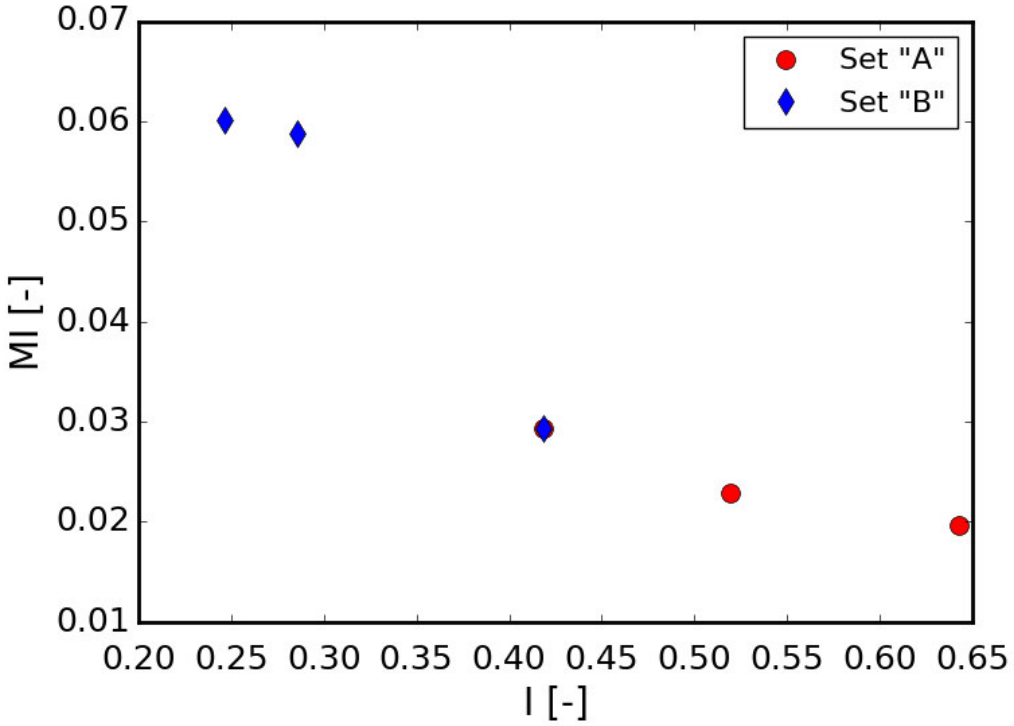

FIGURE 4.11: Mixing index versus I index for the simplified mixtures.

lar study was conducted using the simplified mixture reported in Table 4.1. The mixtures were blended as reported in previous section at an only number of revolutions equal to 240. In the first set of experiments (1A, 2A, 3A), the size range of TAED blue remained constant (200-300 μm) and the white TAED was inserted in the mixture with a diameter gradually increasing; in the second set of experiments (1B, 2B, 3B), instead, the same granulometric distance was maintained between TAED blue and white (200 microns). For the mixtures of the group "A" the I indexes were equal to 0.4, 0.5, 0.6 for the mixtures 1A, 2A, 3A respectively; the indexes I, instead, was equal to 0.4, 0.3, 0.1 for the mixtures 1B, 2B, 3B respectively. The mixture 1A presented the same PSD of the mixture 1B. The mixing index plotted against the I index for the simplified mixtures was reported in Figure4.11 showing that the mixing index decreased, increasing the I index for both the cases "A" and "B". The Figure confirmed that the distance between the average diameters of blue with respect to the average size of the PSD seems to be the

most important factor that influenced the mixing/de-mixing behavior

4.3.2 Effect of mixers discharge

A further investigation was done in order to assess whether the construction of mixers of different geometry could positively influence the mixing of non-cohesive powder, in particular by reducing the effect of segregation during the discharge of the material. From visual checks of the discharge from the symmetric double cone mixer, it was observed that the material moved in funnel flow regime, exacerbating the degree of de-mixing of the material. Thus, we have identified two alternative geometries candidate to be used for this experiment: a conical mixer and an asymmetrical double-cone mixer with similar volume to standard one, 1615 and 1766 m^3 respectively. Their geometries and size are sketched in Figures 2b, c. For both geometries a hopper, which allowed the discharge of the material in a mass flow regime, was realized, to promote a different flow pattern of the mixture during the unloading stage of the mixers with respect to those of the symmetric double cone. In these two new types of mixers, the hopper angle necessary to ensure a mass flow regime of discharge was calculated. The flow depended on the internal friction angle ϕ_e, the wall friction angle ϕ_x and the hopper angle θ_c (Schulze, 2007). These values were determined by shear cell test. The results shown in the graph of the mass flow in Figure4.12, allowed calculating a value for the angle of the hopper, approximately of 20°. The test was performed by filling each mixers with the same amount of material used for the study of the symmetrical double-cone mixer (500 g), with the same particle size distribution (PSD) and the same percentage of blue TAED with respect to white TAED (10% wt.). Because of the different sizes of mixers, the percentages of filling were respectively 40% for the symmetrical double-cone mixer, 55% for the conical mixer and 50% for the asymmetrical double-cone mixer. In order to perform the comparison, it was decided to evaluate the degree of mixing in the

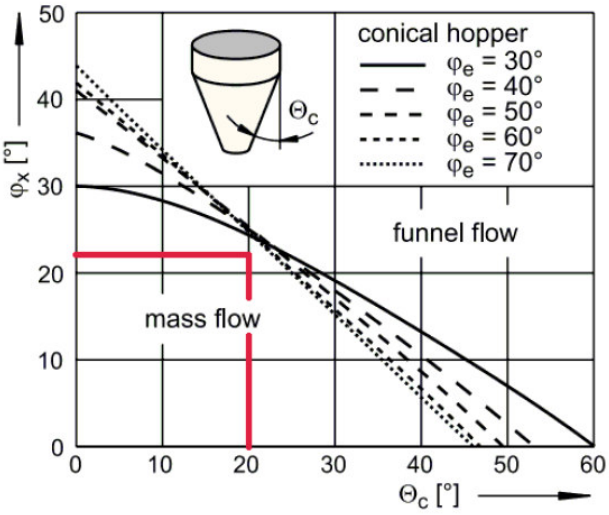

FIGURE 4.12: Internal friction angle against hopper angle

three mixers at a constant mixing time, equal to the optimal number of revolutions found with the symmetric mixer in the case of the mixture with the first PSD reported in Figure4.2 (45 revolutions).

In general, the double cone mixers ensured a better mixing degree. This result was explained considering two positive aspect of this mixer. The asymmetric geometry guaranteed an asymmetric flow pattern during the mixing able to promote the mixing, as seen the Chapter 3 and the mass flow discharge ensured a uniform discharge, with no formation of stagnant zone enriched of fine or coarse material. A further analyses will be carried out with FEM in Chapter 5.

4.3.3 Conclusions and perspectives

The flow of non-cohesive powder was investigated using an experimental approach. To perform these experiments, it was necessary to adopt some methods for the sampling and the analysis of samples of powder mixtures. The analysis of the composition was made by mixing these samples with an appropriate amount of water and analyzing the semi-solid paste through colorimetric analysis. The technique has allowed to relate the intensity of the blue pigment present in a

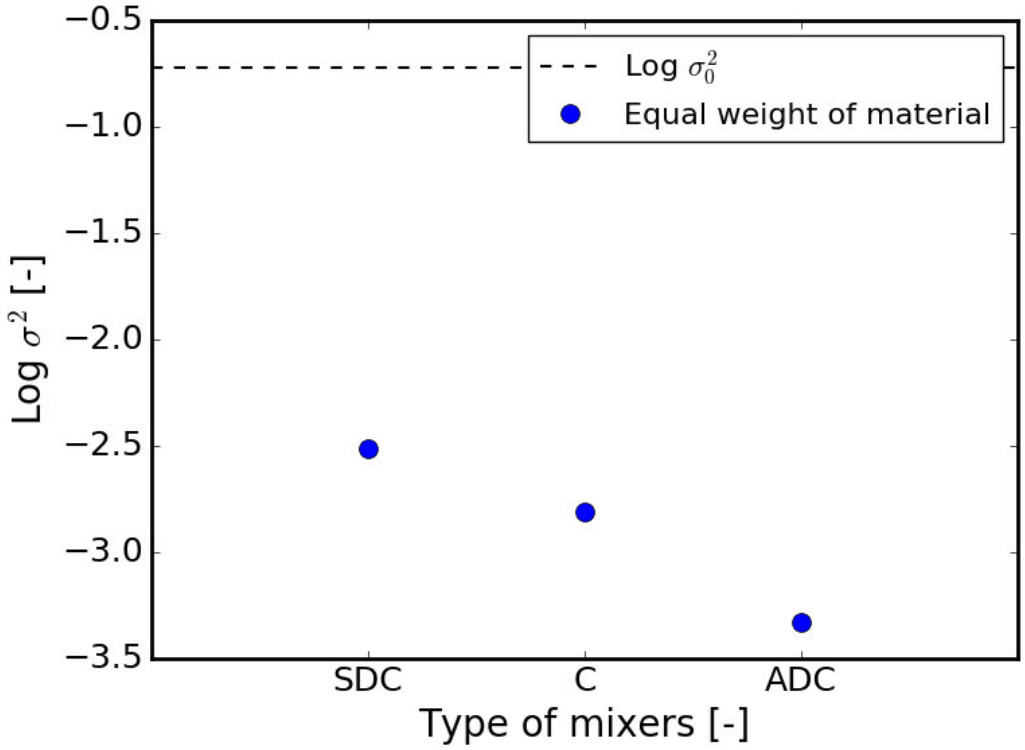

FIGURE 4.13: Logarithmic of the variance plotted for different type of mixers at the same number of revolutions.

mixture with the amount of the component of interest. After several attempts it was found a color space, the Lab, able to distinguish the intensity of the blue pigment. The technique was particularly effective since it avoided the introduction of probes for the analysis and followed to the so-called "golden rules" necessary for a good sampling. The quality of the analysis was also tested by comparison with a screening technique. The test showed that the development technique based on the image analysis may be much more precise and accurate than the screening. Once developed the system of investigation the mixing degree of an asymmetric double cone mixer was evaluated and we found that it was influenced by the difference between the diameters of the particles of interest and the average diameter of the mixture. A comparison between symmetrical biconical mixer, conical and asymmetrical biconical mixer was done. In particular the use of mixers designed to operate in mass flow regime allowed to considerably increase the degree of mixing achievable. The best results were obtained with the

asymmetric biconical mixer: the mixing index increased compared to the symmetric case.

Nomenclature

Symbol	Units	Description
σ^2	-	variance
N	-	number of samples
ϕ_e	-	internal friction angle
ϕ_x	-	wall friction angle
θ_c	-	hopper angle

Chapter 5

Prediction of segregation in funnel and mass flow discharge

5.1 Introduction

In this Chapter the application of the rheological model to the composition evolution of mixtures is fully addressed. The model used to describe the segregating velocity reported in Eq. 2.12 starts from the simple consideration that the percolation velocity is proportional to the difference between the diameter of the fine material and the average diameter of the mixture. This relation was also found with the experimental study conducted in Chapter 4.

Different geometries were studied in the Literature, focusing on model arrangements, such as rotating drums, chutes, vibrating vessels (Santomaso et al., 2004, 2006; Taberlet et al., 2006; Shi et al., 2007; May et al., 2010; Hajra et al., 2012; Fan et al., 2014). Still, the most common configuration, in the industrial processing of granular materials and powders, is the silo, with a converging hopper at discharge. To model the flow of granular materials, a discrete or a continuum approach can be chosen. In the first, known as DEM (Discrete Element Method), forces balance is applied at each particle (Cundall et al., 1979). DEM can provide detailed information about the micro-mechanics of granular material on a local scale. DEM remains limited in simulating full scale industrial equipments because of the computational costs. Alternatively, a continuum approach can be

used (Savage 1988), in which the granular material is considered like a pseudo-fluid with a peculiar rheology. Christakis et al. (2002, 2006) investigate silo segregation through continuum models. The model is applied to the discharge of a binary mixture (60% of fines and 40 % of coarse) from a mass flow silo and funnel flow silo and to the discharge of ternary mixture to a funnel flow silo. The velocity of segregation is considered as the sum of three contributes: velocity due to diffusion, velocity induced by shear and velocity by percolation. The percolation term depends on the particles diameter, on the available void in the control volume and on the gravity vector, allowing the material to move and percolate even when the material do not flow. Here, we extended a previously developed hydrodynamic model (Artoni et al. 2009), to predict segregation. The model was successfully used to simulate the granular flow of mono-dispersed mixtures in full industrial scale reactors and silos (Artoni et al., 2011; Volpato et al., 2014). The continuous model for granular flow is here combined with single species transport equations, to describe the changes in granular material composition due to segregation. Since segregation is strongly connected with the free surface displacement, a convective equation for air is included in the comprehensive model, to track the air/pseudo-continuous granular material interface. Two types of flow regimes in silos are studied: funnel and mass flow. These determine different segregation patterns and intensity, as demonstrated by Sleppy and Puri (1996) in their experiments on sugar mixtures. The experiments by Ketterhagen et al. (2007) and Arteaga and Tüzün (1990) nicely prove that the funnel flow regime promotes segregation, at the discharge point, whereas mass flow regime keeps segregation bounded. These experiments were used to critically evaluate our model predictions and to assess its reliability on different scales and geometries.

5.2 Initial and boundary conditions

The initial configuration assumed zero velocity everywhere, a specified partitioning of the domain between air and granular material (better specified in each example, see Figures 5.1 and 5.2) and a given distribution of fines consisting of a uniform initial concentration at a specified mass fraction. Boundary conditions for Eqs. 2.1 and 2.2 were the following: atmospheric pressure on the open top of the silo, slip at the walls where there was air and partial slip where the granular material was flowing. The partial slip condition at the wall set the ratio of the tangential velocity to its gradient in the normal direction, by means of a constant slip length (Artoni *et al.*, 2009). It allowed for a limited tangential velocity at the walls, as common in granular flow in contact to many comparatively smooth solid surfaces. At the silos discharge point, the flow rate was fixed, as common in industrial practice where rotary, screw or belt feeders withdraw material at a constant mass flow rate. This was simply expressed as a constant, plug flow velocity at the outlet. Among several options, depending on the extractor, in our computations we set the outlet velocity according to the Beverloo' s equation (Nedderman, 2005), valid for gravity discharge of granular materials through an orifice. Two different flow rates were imposed at the outlet: $2.2 \cdot 10^{-5}$ m^3/s for the funnel flow silo and $1.5 \cdot 10^{-4}$ m^3/s for the mass flow silo. Boundary conditions for the phase variable φ_p were no flux at the walls and φ_p=0 (for numerical reason the value is not equal to 0, but it is a very small number, i.e 10^{-29}) at the inlet boundary. For the translational kinetic energy, insulation was imposed at the walls whereas at the open top boundary a constant granular temperature was set, with a value equal to the average temperature of the cylindrical part. Mass fractions, ω_i were bounded by a condition of zero orthogonal flux across the walls and convective flux at the outlet.

5.3 Model parameters

Viscosity of the granular, pseudo-fluid is a function of the particle diameters. In our case the two species differed just by the size, so that an average particle diameter was used. The parameters in the rheological model were calibrated so that a unique set predicted both the mass and funnel flow, depending on geometry. We used η_0 equal to 0.2. The most relevant parameter was factor K in the segregation velocity, Eq. 2.12. As a first attempt, a constant value of K was assumed. It was however clear from comparison with experimental data that a K dependent on the composition could give better results. Hajra *et al.* (2012) indeed assume that the parameter K has both an intrinsic and a concentration-dependent component (K_T and K_S, respectively) that can be considered a complex functions of granular temperature, local void fraction, gravity, particle sizes, density, shape, roughness, coefficient of friction and coefficient of restitution. They suggest:

$$K = \frac{[K_T + (1 - \omega_F)K_S]}{d_c} \tag{5.1}$$

i.e. a linear dependence on the fine mass fraction. The parameters in Eq. 5.1 were tuned on the experimental data and the same values used for all the simulations done.

5.4 Reference experimental studies

The granular flow model accounting for segregation presented above was tuned and validated with experimental data from literature. Two sets were used, reflecting quite different silo geometry. Ketterhagen *et al.* (2007) report data in short silos, Artega and Tüzün (1990) carry out measurements in tall silos. They all use binary mixtures of the materials as reported in Table 5.1.

TABLE 5.1: Properties of materials used in the experiments from literature.

	Ketterhagen et al. (2007)			Arteaga and Tüzün (1990)	
Material	Glass beads			Acrylic granules	Radish seeds
Size (μm)	521	1160	2240	605	2410
Bulk density (kg/m3)	1450			600	

5.4.1 Experimental studies on short silos

Ketterhagen *et al.* (2007) perform their experiments in silos with dimensions dictated by ASTM D 6940-03 standard. The cylindrical part of their silos is very short so that they mainly evaluate the amount of segregation occurring in the hopper. This is consistent with the purpose of the standard, because segregation develops mostly in the hopper, where the shear rate is higher. A larger hopper also enhances the shear dependence of the segregation flux in Eq. 2.15, as in Hajra *et al.* (2012). Ketterhagen and co-worker (Ketterhagen *et al.*, 2007) use two transparent, acrylic silos, quite short, with very different hoppers to achieve distinct discharge regimes. They are reported in Figure 5.1, with the original dimensions. One operates in funnel flow (Figure 5.1 a) while mass flow regime prevails in the taller (Figure 5.1 b), with a longer, slender hopper. The silos are filled with binary mixtures of glass beads; the level of filling is determined to load the same amount of material in both silos. The experiments use different loading policies. In this work, however, only the experiments starting from a homogeneous filling are considered. The silos are discharged with a discontinuous start-stop method, following the ASTM Standard for evaluating the segregation propensity of the materials. 18 samples of 55 ml are withdrawn after each stop. The material collected in each sample is sieved to determine the mass fraction of each species. The experimental data from Ketterhagen *et al.* (2007), selected for model validation, include 2 types of regimes (mass and funnel flow), with mixtures of 2 different size ratios (1.9 and 4.3) and 3 different mass fractions (5, 20 and 50 %

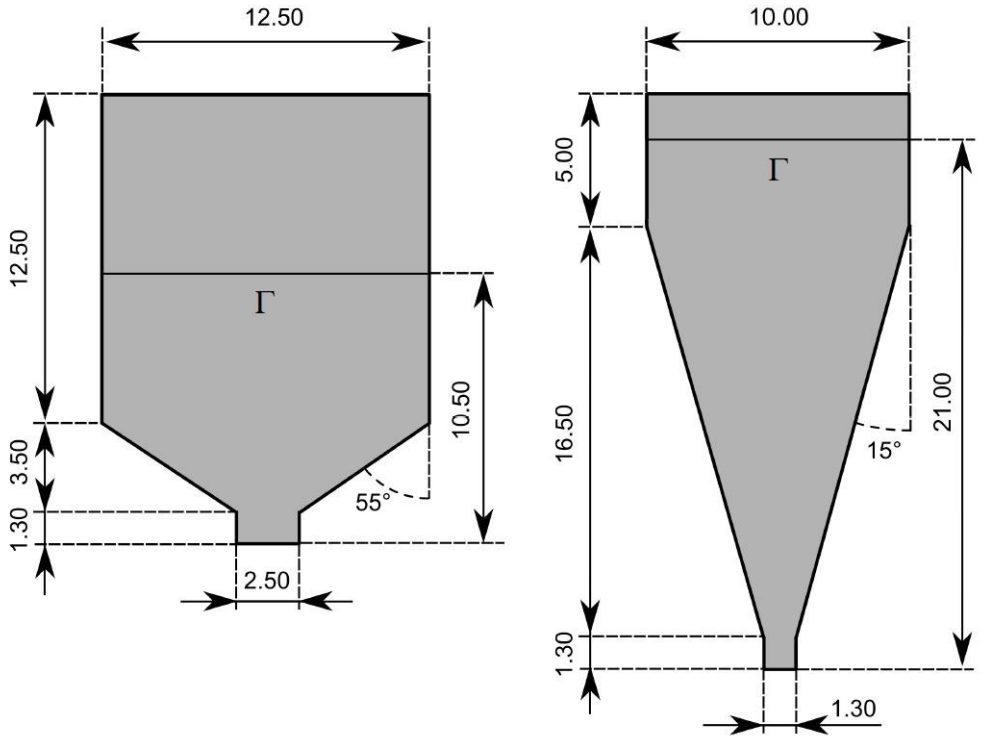

FIGURE 5.1: Silo geometries used in Ketterhagen et al. (Ketterhagen *et al.*, 2007) experiments, operating in (a) funnel flow regime and (b) mass flow regime. Γ indicates the initial interface between the two phases. The measures reported are in cm.

of fines). Hence, a total of 12 experiments are simulated. Simulations have been carried out in 2D.

5.4.2 Experimental studies on tall silos

In the industrial practice silos have a longer cylindrical section, compared to those used by Ketterhagen *et al.* (2007) which follow the ASTM standard to measure segregation. To consider a more realistic configuration and study the interactions between the upper cylindrical and the lower conical section during segregation, the experiments by Artega and Tüzün (1990) are considered. They use two silos as well, made of Perspex, shown in Figure 5.2 with dimensions. The first one operates in funnel-flow regime (Fig. 5.2 a) and the second one in mass-flow regime (Fig. 5.2 b). These silos are loaded with a mixture of nearly spherical granules, made of ABS or acrylic particles, turnip and radish seeds. The mixtures initially loaded in silos are homogeneously premixed. Here we considered the experiments with mixtures of radish seeds and acrylic particles (see Table 5.1). Specifically, a mixture having 20% of fines with a coarse/fine diameter ratio equal to 4 was simulated.

5.5 Results and discussion

5.5.1 Short silos

The evolution of uneven distribution of fines from initially uniform mixtures was simulated and shown in Figures 5.3 and 5.4, in case of funnel and mass flow, respectively. Conditions reflected the experiments of Ketterhagen *et al.* (2007). The time marks suggested that the segregation evolved quite rapidly. In funnel flow regime, Figure 5.3 , the small particles accumulated below the shearing regions, shown in Figure 5.5. Shear concentrated below the free surface, particularly approaching the outlet; the material was mainly stagnant in the other regions of the

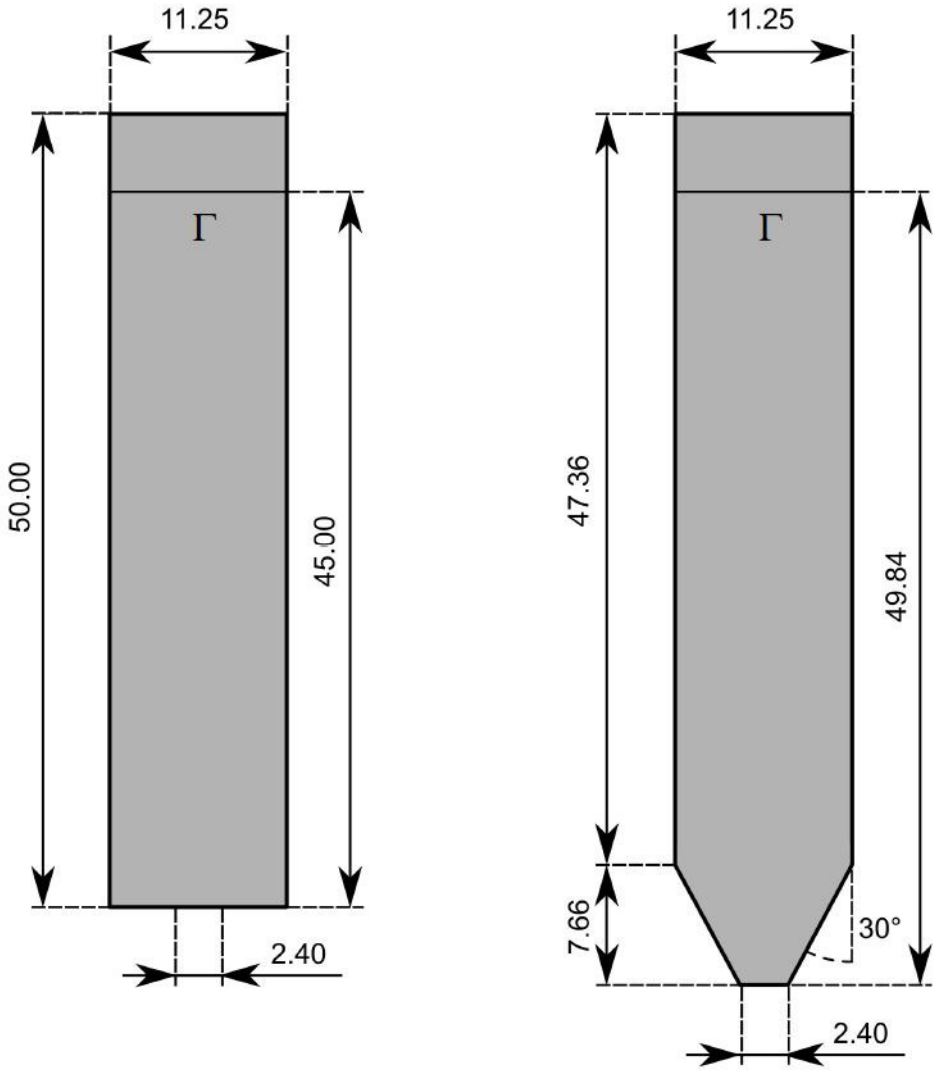

FIGURE 5.2: Silo geometries used in Arteaga and Tüzün (Artega and Tüzün, 1990) experiments, operating in (a) funnel flow regime and (b) mass flow regime. Γ indicates the initial interface between the two phases. The measures reported are in cm.

hopper, close to the walls and the corners. The finest material migrated downwards where the shear was higher, then it remained trapped near the hopper wall. Since the nature of the funnel flow discharge is first in-last out, small particles rapidly accumulated in the hopper and they remained there until the end of discharge. This created an inhomogeneous outlet flow composition during time, where the coarse particles preferentially exited first. On the contrary, mass flow, Figure 5.4, followed a first in-first out discharge pattern. The material was mainly sheared at the walls, as shown in Figure 5.6 , contrary to the funnel flow where shear developed within the bulk (Figure 5.5). Fines accumulation occurred along the whole length of the inclined walls, where the shear was larger. Segregation appeared to be less localized than in funnel flow regime, with a large core region that became almost devoid of fines. This was consistent with some shear to propagate throughout the whole hopper section (Figure 5.6), because of the converging flow, giving a chance for percolation of fines everywhere in the hopper. However, since all the material was flowing, including the most peripheral one, the average composition across the outlet section remained close to the initial value, even during the initial transient, when fines accumulated at the walls. The composition maps shown in Figures 5.3 and 5.4 are intuitive and useful to understand the nature of the discharge mechanism and qualitatively visualize the effect of flow field on segregation. However, a more quantitative comparison is needed. It is formulated in the next section. Mimicking the experimental procedure, we calculated the average composition in samples of fixed volume, collected at the outlet of the silo over discrete time intervals. Following the representation of the experimental results in the original literature, we reported the progress of discharge as normalized fines mass fraction (= fines mass fraction in each sample / initial fines mass fraction) vs. fractional mass discharged, up to a given time, for each experimental case analyzed

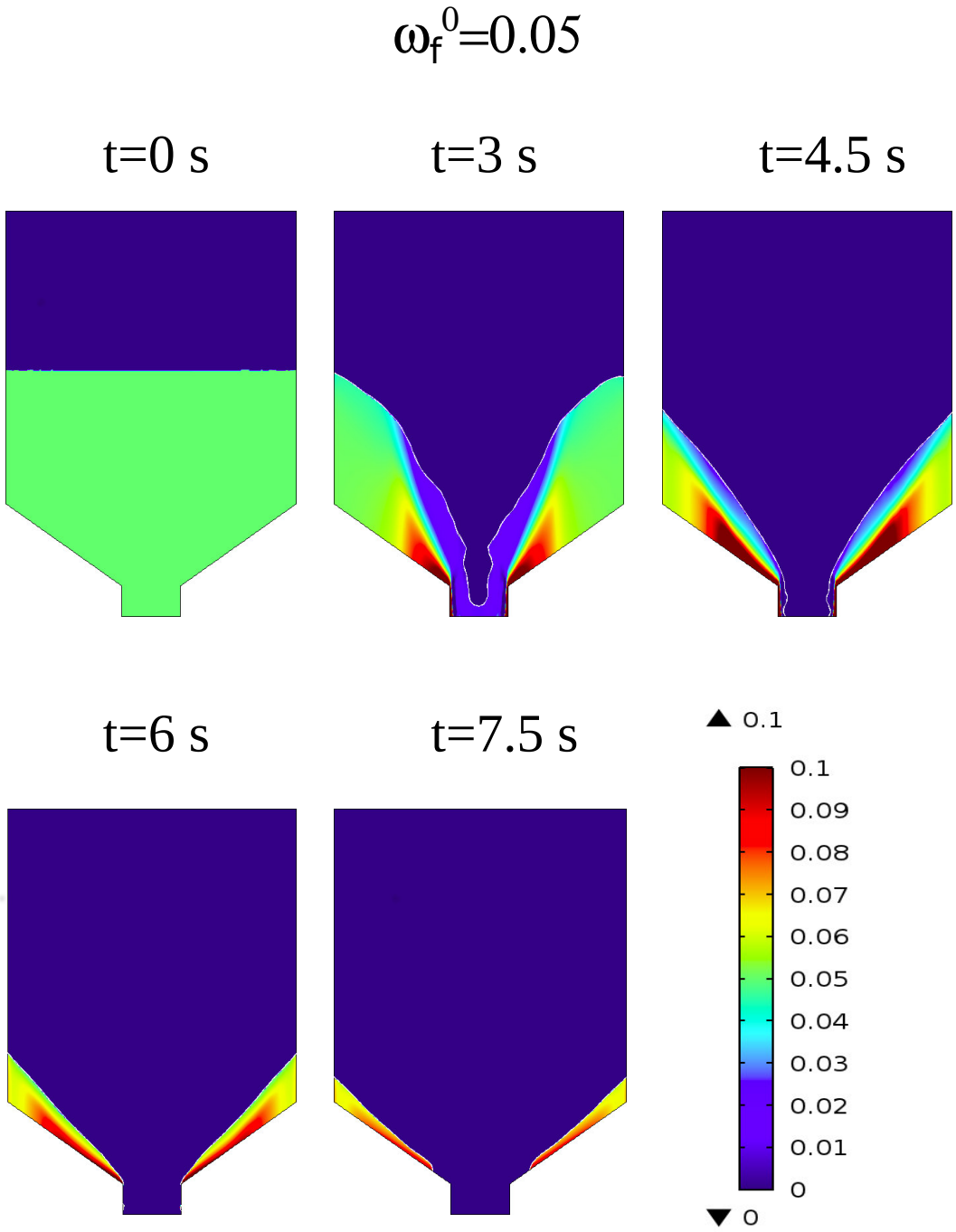

FIGURE 5.3: Evolution of segregation in funnel flow regime for ω_f^0= 0.05; d_c/d_f = 4.3. The color indicates the fines mass fraction.

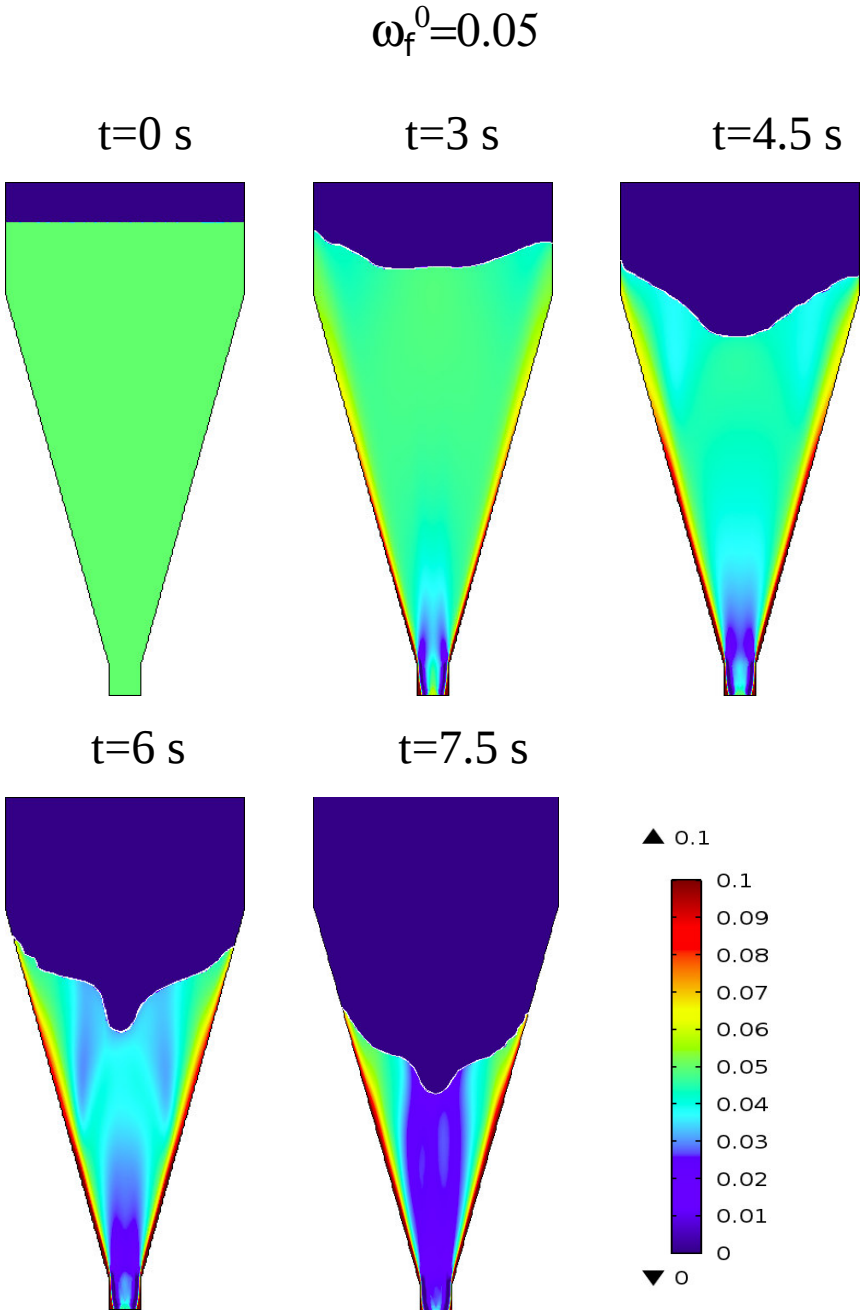

FIGURE 5.4: Evolution of segregation in mass flow regime for ω_f^0= 0.05; d_c/d_f = 4.3. The color indicates the fines mass fraction.

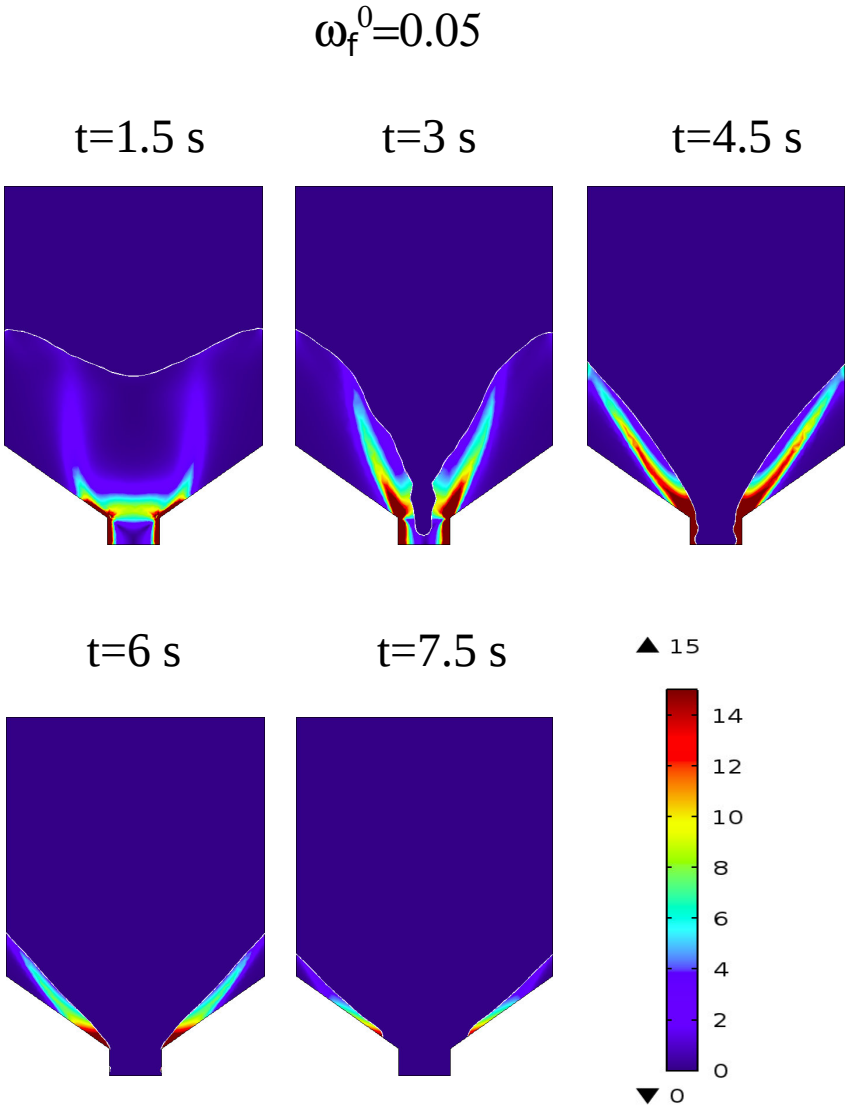

FIGURE 5.5: Evolution of shear rate [1/s] in funnel flow regime for for ω_f^0= 0.05; d_c/d_f = 4.3.

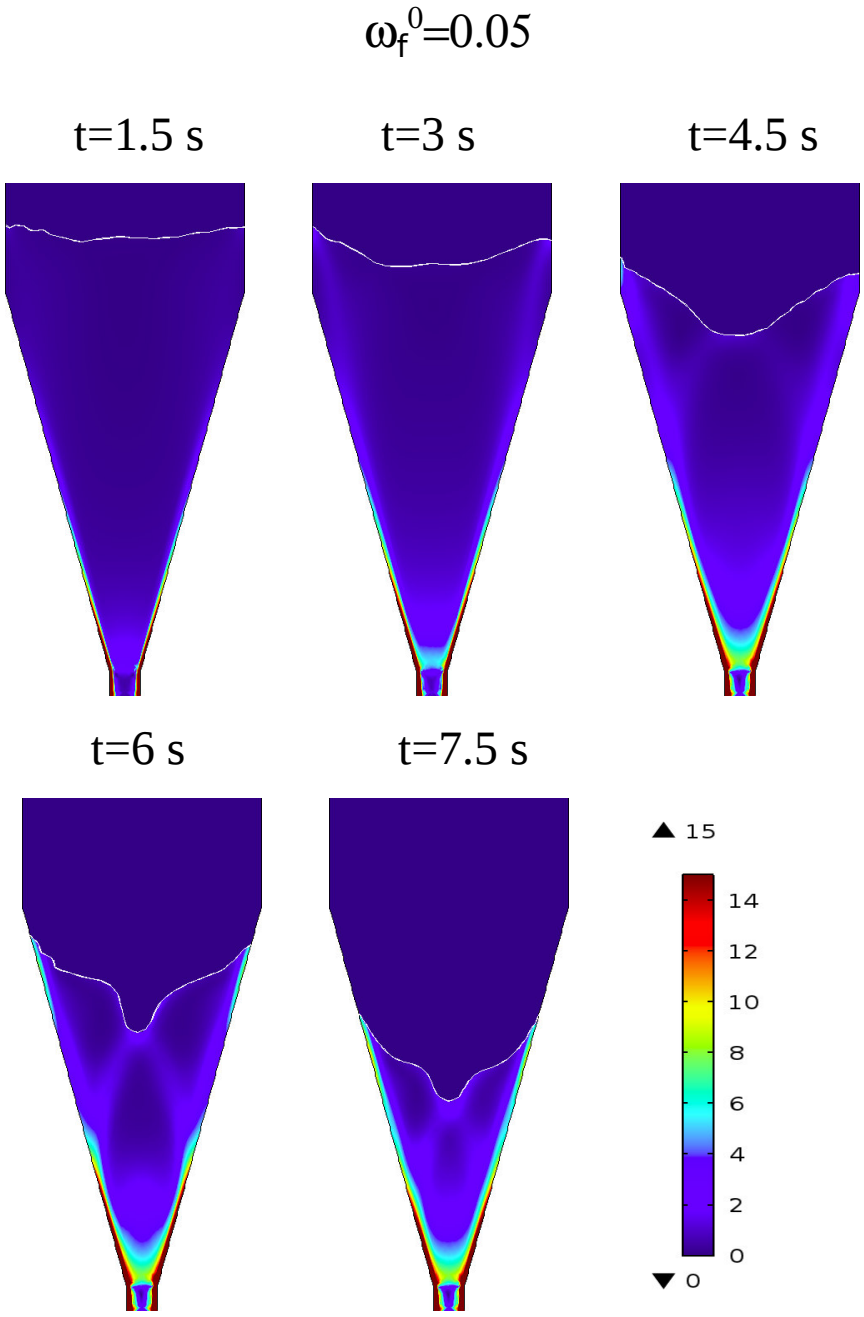

FIGURE 5.6: Evolution of shear rate [1/s] in mass flow regime for ω_f^0= 0.05; d_c/d_f = 4.3.

Tuning of the segregation flux

In this work the segregation process was modeled through the species material balance, where the transport mechanisms were convection and percolation. Convection was ruled by the granular flow model, already validated in our previous works. The precise rheology of the granular materials in the experiments considered, could not be validated because neither the velocity, nor the stress fields inside the silos or at the walls are reported in the referenced literature. Still, we could successfully reproduce the discharge regime experimentally observed, either funnel or mass flow, at changing hopper geometry. This was a solid confirmation of the capability of our continuous granular flow model. Finally, the discharge velocity was always imposed in the experiments, further reducing the importance of a precise definition of the rheological parameters, as far as the flow regime was captured. It should be underlined that a good prediction of the local granular flow determined the accuracy of the segregation model, which was affected by the local shear rate. It impacted on the segregation flux through Eq. 2.15, where the relative importance of was ruled by $|\dot{\gamma}|$. The segregation flux was proportional to the shear rate through a parameter K. However, a constant K led to predictions that were not sufficiently accurate, when compared to the experimental data, particularly in the funnel flow. It was observed that different values of K were required to fit the data satisfactorily when the initial amount of fines varied ω_f^0= 0.05, 0.2, 0.5).

Optimal, constant K linearly correlated with ω_f^0, as shown in Figure 5.7. The correlation recalls the findings of Hajra *et al.* (2012), that suggest a linear dependence of $K(\omega)$ with an intrinsic- and a concentration-dependent component, K_T and K_S, respectively, as in Eq. 5.1.

The linear correlation found could be recast as K=2.4–7.9 (1–ω_f^0), which was consistent with Eq. 5.1 when K_T/d_c=2.4 and $_S/\mathrm{d}_c$=7.9. Adopting these values of

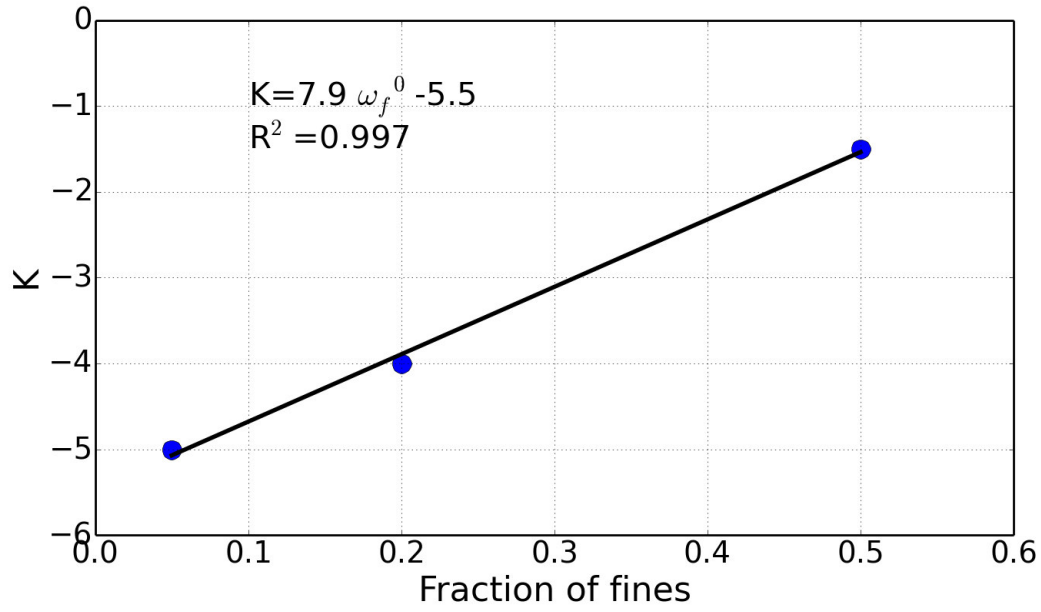

FIGURE 5.7: Optimal K values as a function of the initial fraction of fines.

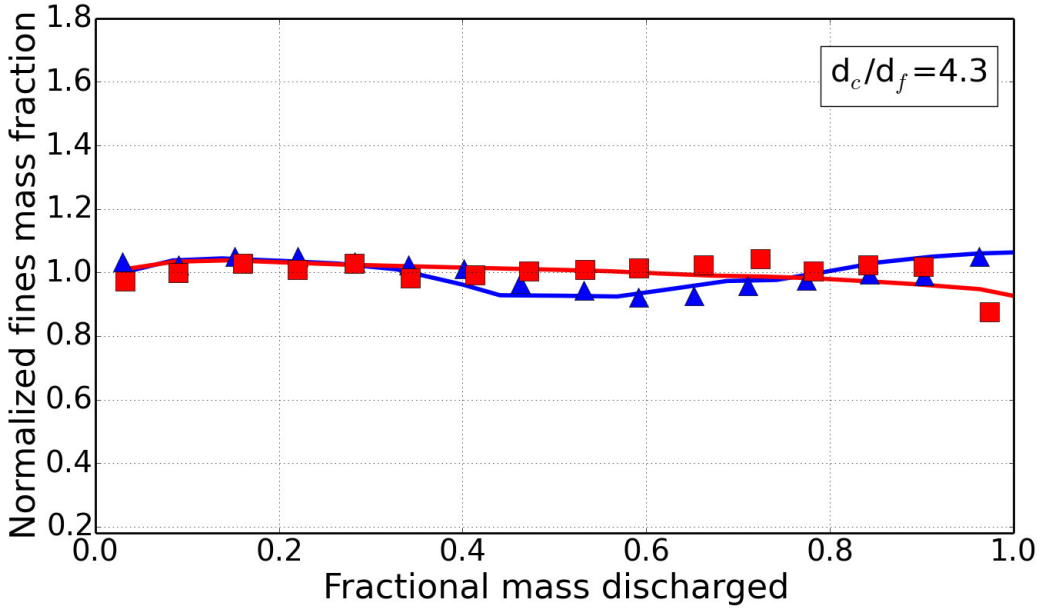

FIGURE 5.8: Comparison with experimental data of mass (■) and funnel flow (▲) regimes in short silos after $K(\omega_f)$ optimization with ω_f^0=0.5; solid lines are numerical predictions.

parameters K_T and K_S in Eq. 5.1 to determine K as a function of the local composition, even if estimated from the initial, average composition, led to a good agreement between the predictions and the experiments, during all the discharge, as shown in Figure 5.8 for a single case. Others will follow. The values of root mean square error, normalized with respect to the average value of the experimental fraction of fines (NRMSE), reported in Table 5.2, gave general information about the performance of the model. The implementation of the concentration-

TABLE 5.2: NRMSE for all tests in silos of Figure 5.1 for constant K and variable K

System	Fine mass fraction	NRMSE [%] for constant K	NRMSE [%] for variable K
Funnel-flow 1.9 diameter ratio	0.05	10.1	10.4
	0.20	9.2	7.6
	0.50	7.4	4.2
Mass-flow 1.9 diameter ratio	0.05	8.7	8
	0.20	7.6	6.8
	0.50	6.7	3.9
Funnel-flow 4.3 diameter ratio	0.05	18.3	18.2
	0.20	9.7	9.6
	0.50	10.1	2.9
Mass-flow 4.3 diameter ratio	0.05	33.2	39.4
	0.20	20	11.4
	0.50	6.1	2.9

dependent K in Eq.2.12 gave a general improvement of results in most of the cases examined enhancements were more significant with initial mixtures where fines were more abundant (ω_f^0=0.2 and 0.5). The NRMSE values, calculated considering concentration-dependent K, resulted less than 10%, except for some critical cases (d_c/d_f=4.3 and ω_f^0=0.05) that will be discussed later.

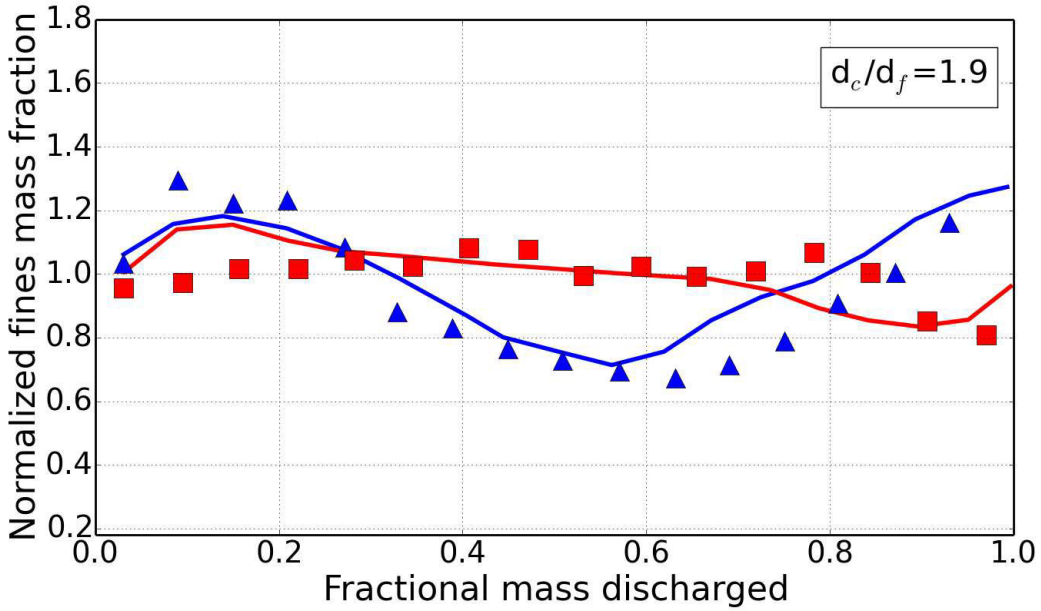

FIGURE 5.9: Comparison with experimental data of mass (■) and funnel flow (▲) in short silos ω_f^0=0.05.; solid lines are numerical predictions.

5.5.2 The effect of the particle size ratio and initial fines concentration

In the first mixture analysed, the fines mass fraction was 0.05. Figures 5.9 and 5.10 shows the comparison between experiments and simulations for two different particle size ratios, d_c/d_f=1.9 and 4.3. As a general comment we observe that the extent of composition inhomogeneity at the outlet increased with the difference in the two particle sizes. For the largest particle size ratio, large voids were expected between the particles so that fines could percolate more easily, giving a greater tendency for the mixture to size segregate. The variations were larger in funnel flow compared to mass flow. With the largest size ratio d_c/d_f=4.3, an excess of fines at the beginning of the discharge is reported in the literature experiments, both for mass and funnel flow (Figure. 5.10). It appears that even if the authors try to start the discharge with a homogeneous mixture, it is impossible in practice to obtain such initial condition. The size ratio is so large that the small

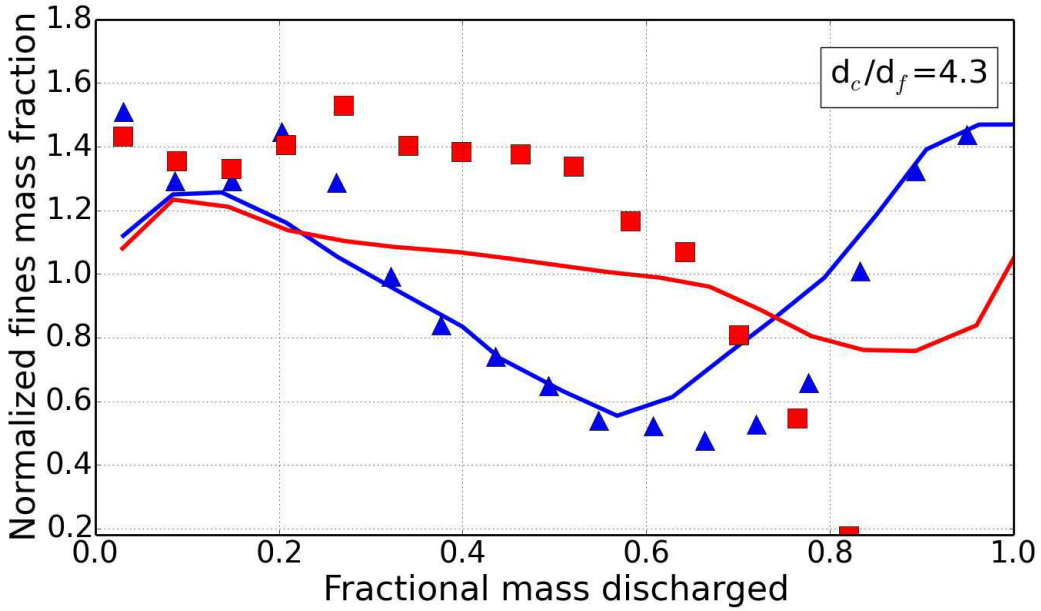

FIGURE 5.10: Comparison with experimental data of mass (■) and funnel flow (▲) in short silos ω_f^0=0.05.; solid lines are numerical predictions.

glass beads apparently percolate during silos loading, yielding an uneven initial mixture, before the material is set in motion. The difference in the initial composition between those assumed (i.e. implemented in the model) and those actually obtained experimentally weakened the validation, in the case of the largest size ratio. This was particularly evident for the mass flow regime. Clearly this represents a bias of the experimental data. After the initial phase, the qualitative trend was well reproduced by simulations and for the size ratio of 1.9 also a quantitative agreement with the experiments was obtained. With a larger initial amount of fines, ω_f^0=0.2, the intensity of segregation decreased, as apparent from Figures 5.11 and 5.12. The qualitative agreement between numerical results and experimental data remained quite good, including some fluctuations of composition during the discharge, particularly in the case of funnel flow. As expected, for the largest size ratio the difficulty to experimentally obtain an initially homogeneous composition is evident, jeopardizing the agreement with simulations for the mass

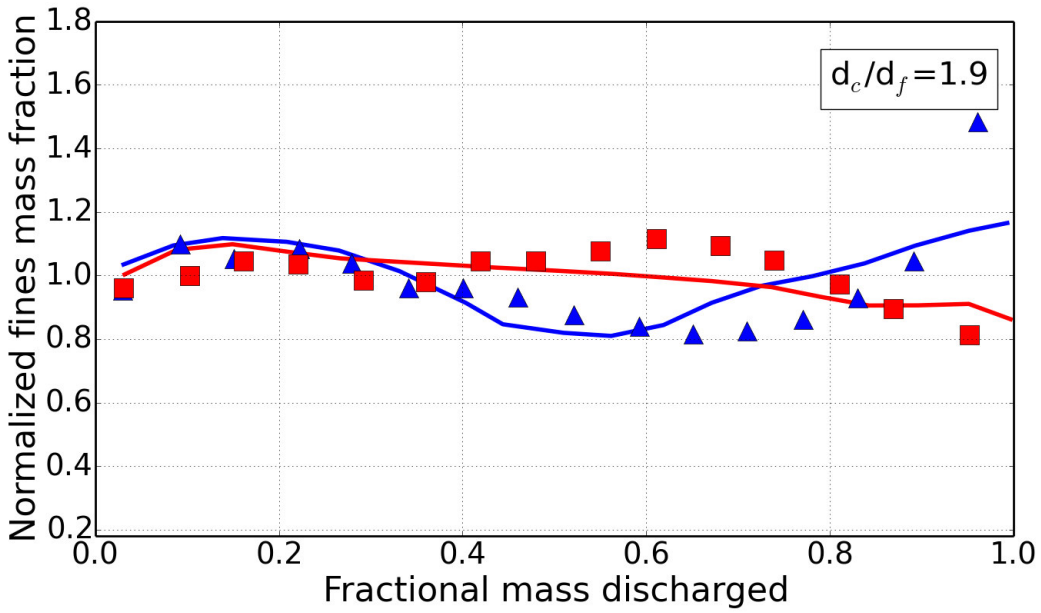

FIGURE 5.11: Comparison with experimental data of mass (■) and funnel flow (▲) in short silos ω_f^0=0.2.; solid lines are numerical predictions.

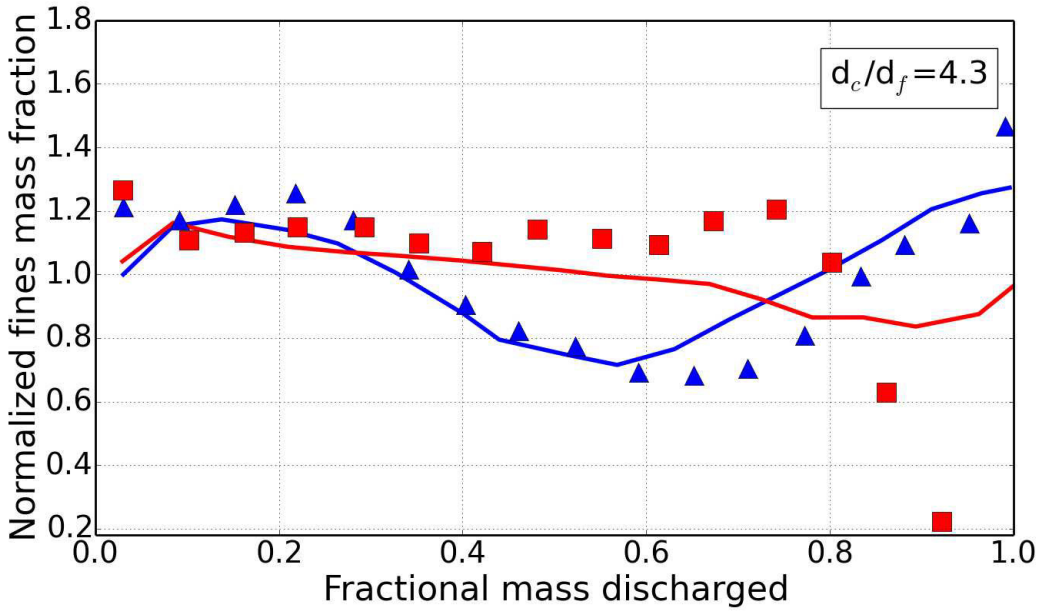

FIGURE 5.12: Comparison with experimental data of mass (■) and funnel flow (▲) in short silos ω_f^0=0.2.; solid lines are numerical predictions.

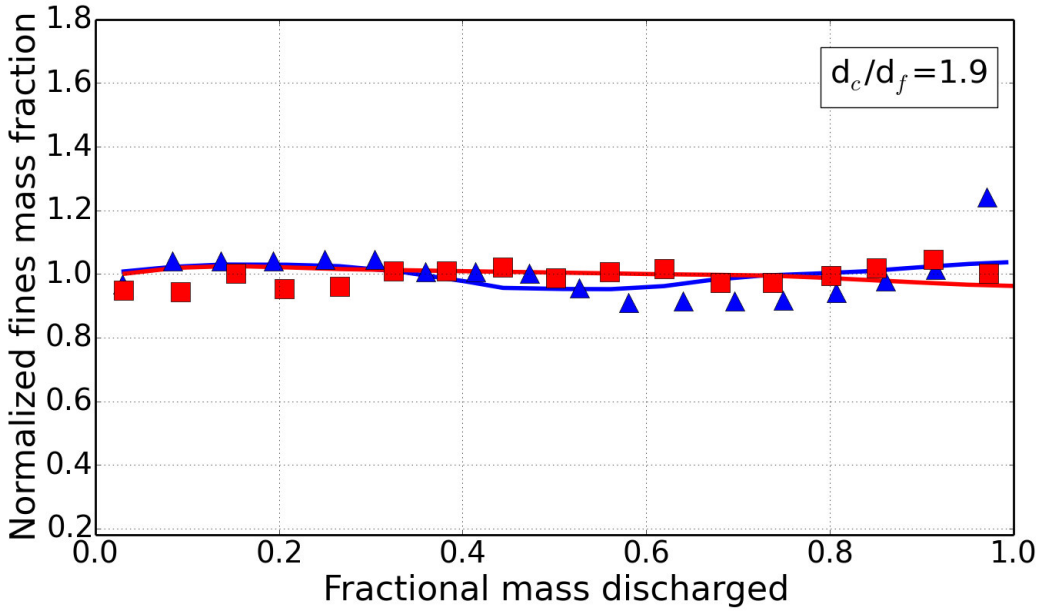

FIGURE 5.13: Comparison with experimental data of mass (■) and funnel flow (▲) in short silos ω_f^0=0.5.; solid lines are numerical predictions.

flow regime. However, for mass flow discharge and 4.3 diameter ratio the predictions were better than the more diluted case of ω_f^0=0.05. With a further increase of the initial amount of fines, ω_f^0=0.5, the segregation dropped dramatically, as evident from Figures 5.13 and 5.14, in both flow regimes. This was well captured by the simulations. Contrary to what occurred in the previous cases, also the mixture with the larger particle size ratio remained homogeneous during the filling stage, and the numerical results were consistent with the initial phase of the discharge. The results of Figures 5.9, 5.10, 5.11, 5.12, 5.13, 5.14 confirmed the qualitative observations suggested by the concentration maps, Figures 5.3 and 5.4. It could be observed that at the end of any funnel flow discharge, an increase of fines was observed at the outlet, more evident in the experimental data; this was not the case in the mass flow. It was an expected consequence of the first in-last out nature of funnel flow; the residual portion of fines accumulated at the wall left the hopper towards the end of the discharge.

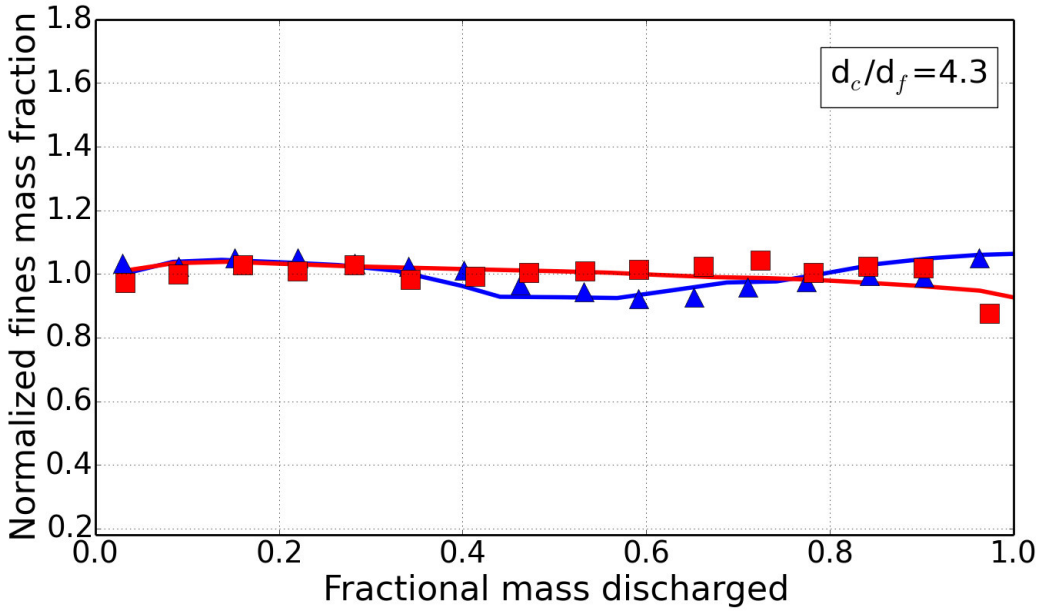

FIGURE 5.14: Comparison with experimental data of mass (■) and funnel flow (▲) in short silos ω_f^0=0.5.; solid lines are numerical predictions.

5.5.3 Tall silos

Tall silos experiments by Arteaga and Tüzün (1990) were used for comparison. We kept the same parameters (see Tab. 5.1) used for simulating the granular flow in short silo experiments, for consistency. Also the same $K(\omega_f)$ developed above for short silos was used for this configuration as well. We found that a constant linear dependence on $\dot{\gamma}$ was adequate for short silos, while a stronger dependence, $\dot{\gamma}^{3/2}$, was required in tall silos, where the flow patterns were quite different. Segregation was less intense than in short silos, as clear from Figures 5.15 and 5.16. However, there were quite significant deviations from the initial composition, particularly at the end of the discharge, that were well predicted by the model. Notwithstanding the crude choice of the parameters the agreement was good; the NRMSE values were always less than 10%, between 8.2% and 7%. The experimental data suggested that three different stages could be identified during the discharge: an initial transient, a pseudo-steady state and a final transient. According to Arteaga and Tüzün (1990) the initial transient, with

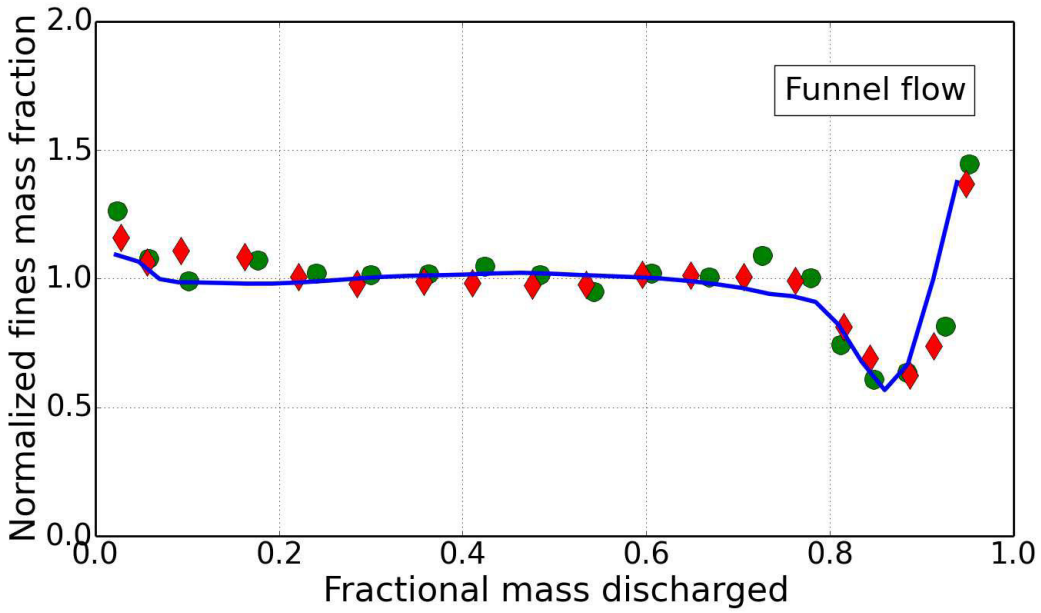

FIGURE 5.15: Comparison with experimental data of mass (■) and funnel flow (▲) in short silos ω_f^0=0.5.; solid lines are numerical predictions.

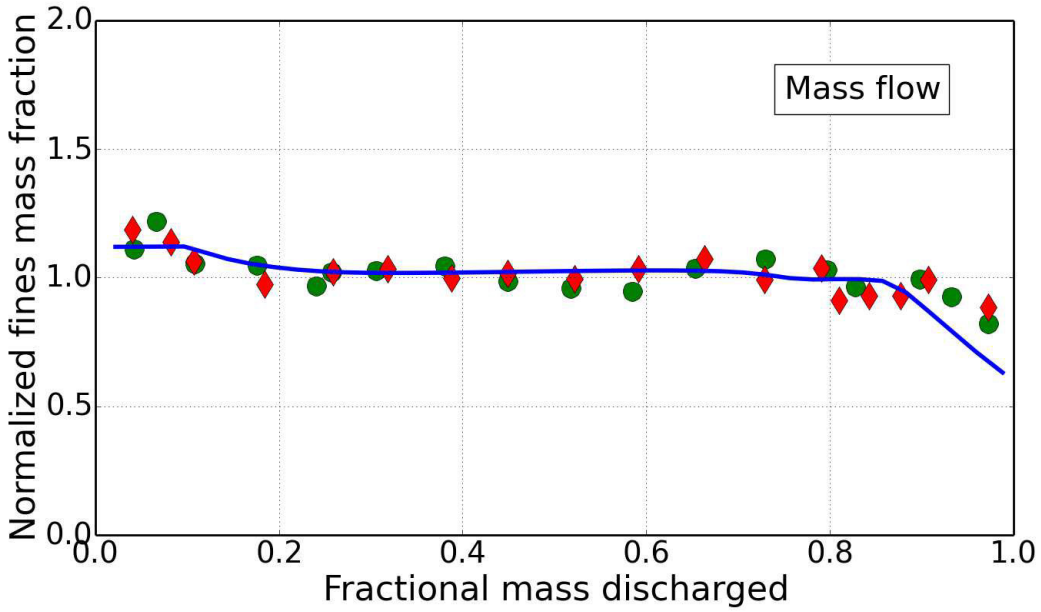

FIGURE 5.16: Comparison with experimental data of funnel and mass flow regimes in tall silos ω_f^0=0.2. d_c/d_f=4. Symbols (⧫,•) are two replicas of the same experiment. The solid line is the numerical simulation.

an enrichment of fines in the outlet flow is caused by the formation of a flame-shaped central core region, due to the granular bed dilation in the initial stages of the flow. In the dilated zone, percolation is favoured and accompanied by high value of shear rate in proximity of the outlet. The second stage, observed at 18% of the total discharge, is a pseudo-steady state in which no segregation is reported at the outlet. This is due to the absence of significant radial gradients of velocity in all the cylindrical section, except at the shear region adjacent to the walls. The third stage, finally, starts at approx. 78% of the discharge and is characterized by a larger segregation, greater in the funnel flow regime. Experiments and simulations showed that the segregation patterns on the short silos were similar to those observed in tall ones, in both discharge regimes, excepted for the absence of the pseudo-steady stage which was missing in short silos. All these stages were well captured by the simulations, thanks to a proper description of the segregation mechanism.

5.6 Conclusions and perspectives

In this work segregation in granular flow of bi-dispersed mixtures was simulated, using a continuum approach. Granular flow was described with a rheological model for free-flowing materials and adapted to multi-phase and multi-component conditions. The simulation of bi-dispersed granular flow, allowing for a free, moving surface was achieved by an Eulerian, continuum approach to the two phase flow. Segregation was modeled with a mass transport equation applied to a bi-dispersed mixture of particles of different sizes. The model included the effects of two different mechanisms: advection due to flow and segregation due to percolation. Two different types of flow regime occurring in silos were investigated: the funnel and the mass flow regimes. Simulations were compared with independent experimental data found in the literature, for short and tall silos. The simulations were carried out taking into account different size ratio (from

1.9 to 4.3) of the binary mixture and different initial fines concentration (from 5% to 50%). The segregation model, which primarily took into account the difference in size of the particles, was sensitive to the local mixture composition and the local shear rate, provided by the velocity field. The model was predictive for the spatial distribution of the mass fraction of the fines (or coarse) inside the silo at different stages of the discharge. Furthermore, it allowed to evaluate the fines weight fraction across the outlet with respect to the fractional mass discharged. The segregation model proposed was simple and its strength was the coupling with a rheological model able to predict the flow rate and a model able to follow the interface between air and bi- dispersed solid. Notwithstanding the simplicity of the proposed segregation model and the crude estimation of the parameters, the qualitative and quantitative agreement with experimental data was good. In tall silos the model correctly predicted the three different stages of discharge: initial transient, pseudo-steady state and final transient. Further work is however required to extend the model to more complex cases. These include additional percolation mechanisms originated by other physical properties such as differences in particle density and introducing inertial effects which typically occur at the free surface. Further refinements include considering polydisperse systems, where different size classes are present. So far, we implemented a one-way coupling between the granular flow and the segregation model, where the flow structure affected the segregation, but the local composition did not modify the rheology. Further development is therefore required on the two- way coupling, to also take into account the effect of local size difference on the flow patterns.

Nomenclature

Symbol	Units	Description
d	m	particle diameter
$\mathbf{g}$	m/s^2	gravity acceleration vector
K	-	segregation parameter
K_S	-	intrinsic segregation parameter
K_T	-	concentration-dependent segregation parameter
Π	Pa	deviatoric stress tensor
ρ	kg/m^3	density
ω	-	mass fraction

Chapter 6

Experimental study on shear induced percolation

6.1 Introduction

The relation for the percolation velocity used in Chapter 5 is based on the simple assumption that the velocity can be assumed proportional to the difference between the small and segregating particle diameter and the average diameter of the mixture (Hajra *et al.*, 2012) and on the shear rate (Fan *et al.*, 2014). The relation is very simple and it gave acceptable simulation results. However the functional dependence of the percolation velocity can be deepened, with dedicated experimental investigation. For this reason, it was chosen to explore the percolation in the simplest granular flow: the simple shear, that is a case of bulk deformation, in which only one component of the velocity vector has a non-zero value. This type of flow was achieved using a shear box, similar to that used by Bridgwater (1994) and Scott and Bridgwater (1975) which allowed for a quantitative and qualitative study of the percolation. The granular material inside the box was uniformly sheared and this permitted to easily determine the percolation velocity of small particles under chosen and controllable conditions. Normally, a small particle does not drop across the bed of coarse particles because it is supported by the underlying particles, but during the deformation of the bed a layer of material moves over another due to the imposed shear and between larger particles

some voids can be formed in which the smaller particles can drop. It may be that the void is large enough to let the small particle to drop in the bed, but it is even possible that the particle remains trapped between two layers of coarser material. Between these two layers a "failure zone" is formed (Bridgwater, 1994) and it is necessary that it persists long enough to let the percolation.

The experiments with the shear box allow to obtain a uniform shear rate inside the cell and it remains applied until the percolating particle crosses a bed of coarse particles with a known height. Bridgwater (1994) conducts his experiments only varying the size ratio, at given shear rate. He finds an exponential relation that linked the percolation velocity and the size ratio. He also gives a statistical mechanical interpretation to the percolation phenomenon by supposing that a large particles has a fluctuating amount of free space around it and that the percolation occurs when the length scale of this space exceeds a value sufficiently large for the small particle to pass (Cooke and Bridgewater, 1979). In this Chapter the experimental data obtained using a shear box were reported and discussed. The experiments allowed to obtain value of percolation speed at different size ratio and different shear rate for glass sphere and irregular particles. From experimental evidence, it was also possible to conjecture some percolation mechanisms that gave a theoretical relation for the percolation velocity. Finally, the experimental data and the theoretical relationship were compared, with a good agreement. This work was motivated by the possibility to find new relations accounting for the percolation velocity, better accounting for the physical phenomenon occuring in percolation.

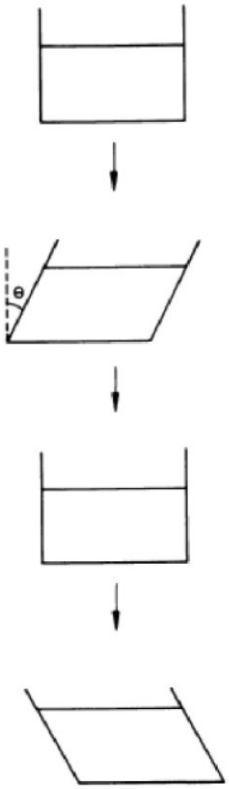

FIGURE 6.1: Principle of operation of the simple shear apparatus (Bridgwater, 1994)

6.2 Experimental method

6.2.1 The shear box

A simple shear box was used to measure the percolation velocity of a small particle tracer inside a bed composed of coarser material as a function of particle size ratio, shear rate and particles shape. In this type of device the bed of material was sheared in such a way that the cross section passed from a rectangle to a parallelogram as shown in Figure 6.1. Every points of the material inside the cell moved with the same shear rate and the percolation speed can be obtained measuring the time necessary to a tracer particle to cross the bed.

The experimental apparatus was composed of a box, 100 mm deep, 100 mm wide and 100 mm high. Two walls of the cell were fixed while the other two walls were hinged at a base and connected together; in this manner the mobile walls were

TABLE 6.1: Size of glass sphere used in the first set of experiments.

Fines diameter [cm]	Coarse diameter [cm]	Size ratio [cm]
0.1	0.5	0.2
0.15	0.5	0.3
0.2	0.5	0.4
0.25	0.5	0.5
0.3	0.5	0.6

TABLE 6.2: Size of glass sphere used in the second set of experiments.

Fines diameter [cm]	Coarse diameter [cm]	Size ratio [cm]
0.2	0.6	0.33
0.25	0.6	0.4
0.3	0.6	0.5

able to rotate up to 45 degrees remaining parallel to each other. A shear angle equal to 45 degrees allowed to obtain a deformation of the bed proportional to the diameter of one coarse particle d_c. The sidewalls of the cell was made of plexiglass that allowed to visualized the percolation of the tracer in the box. To avoid a regular-packing of the bulk material in the bottom layer of the cell that can disturb the passage of the tracer, the bottom of the cell was covered with a mixture of bi-dispersed particles with a smaller diameter of those that composed the bulk. It has been observed that during the experiments, an undesired recirculation phenomenon affects the upper part of the bed; to avoid this phenomenon, which could affect and un-validate the results, a cover has been built; it was made of plexiglass and had two vertical baffles which could penetrate into the particle bed limiting the re-circulation of the particles that compose the upper part of the bed.

The experiments were done using both glass spheres and granulated material. For the glass spheres, two sets of the experiments were done using different fine diameters and two different coarse diameters. The Table 6.1 reports the size of the particles used in the first set of experiments and the Table 6.2 shows the size in the second set of experiments. Using a bed of coarse sphere with 0.6 cm of diameter, the particles used for the bottom had a diameter of 0.5 cm, instead when

the size of coarse spheres was 0.5 cm of diameter, the bottom layer was a mixture of 0.3 cm sphere. Inside the bulk, the movement of the two mobile walls allowed a uniform shear rate; near the walls, the shear rate could deviate from the uniformity, but in the center of the cell it resulted uniform. For this reason the tracer was put in the central position of the cell.

A typical experiment started loading the cell with materials that composed the bed until an height equal to 4 cm. Four colored tracer particles were put at this height above the first layer of bulk. Then, other coarse particles were added at the bed until obtained a total height of the bulk equal to 7.4 cm. After the filling, the mobile walls of the cell were pushed to and fro by hand at a constant shear rate until the tracer particles arrived at the bottom of the cell. During the experiments the particles bed was dilated respect its initial state. The true density of the bulk material was calculated with liquid picnometric technique. From data of true density and bulk density, it was possible to obtain the porosity of the bed that for the spheres resulted equal to 0.4. To perform each experiments the frequency, f, with which the mobile walls were moved, was fixed. The shear rate was calculated through this relation:

$$\dot{\gamma} = \frac{2L \cdot f}{H} \tag{6.1}$$

where L is equal to 10 cm and represents the size of the cell and H is the total height of material. The experiments were carried out using four different frequency: 15, 30, 45, 60 bpm that corresponded to values of shear rate equal to: 0.66, 1.34, 2.02, 2.7 $1/s$. The percolation velocity was calculated with the following relation:

$$v_p = \frac{H}{t} \tag{6.2}$$

were t is the time that a tracer small particles spent to move from the initial position to the bottom.

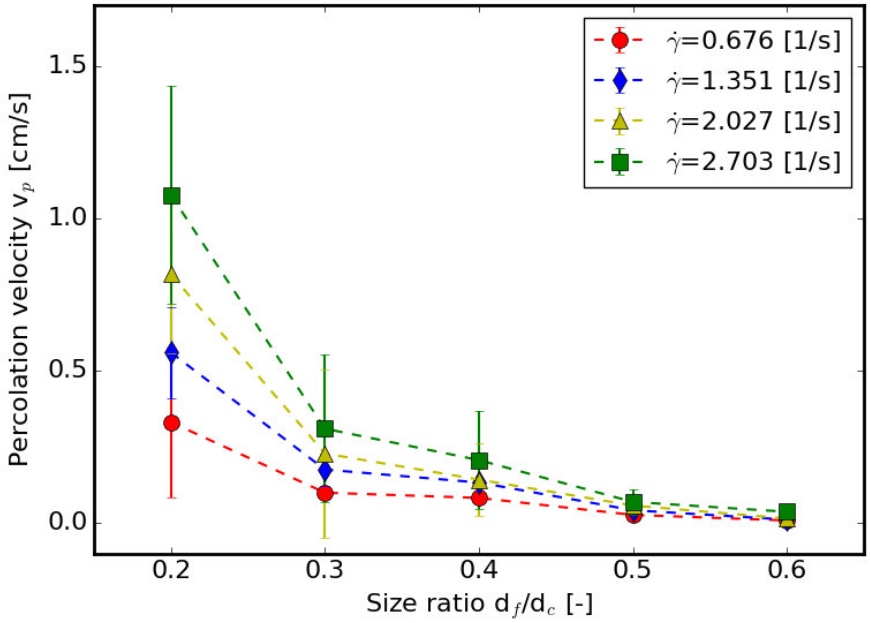

FIGURE 6.2: Percolation velocity against the size ratio varying the shear rate.

6.3 Results

Results from the experiments performed on the shear cell are reported in the following.

6.3.1 Percolating glass spheres

Velocity profiles of the glass spheres plotted against the size ratio are shown in Figure 6.2. This curve was obtained using a bed composed of 0.5 cm coarse particles. The profiles were obtained at different shear rate. As expected the percolation velocity increased increasing the shear rate and decreasing the size ratio. The percolation velocity was practically equal to zero at the larger size ratio examined (0.6), instead it resulted higher for smaller size ratio. This trend can be easily explained considering that when the difference of size between small and coarse material is high, the fine particles can drop in the bed freely undisturbed. This evidence will be better explained and discussed in the following Section. Figure 6.3 suggested that the percolation velocity varied linearly with the shear

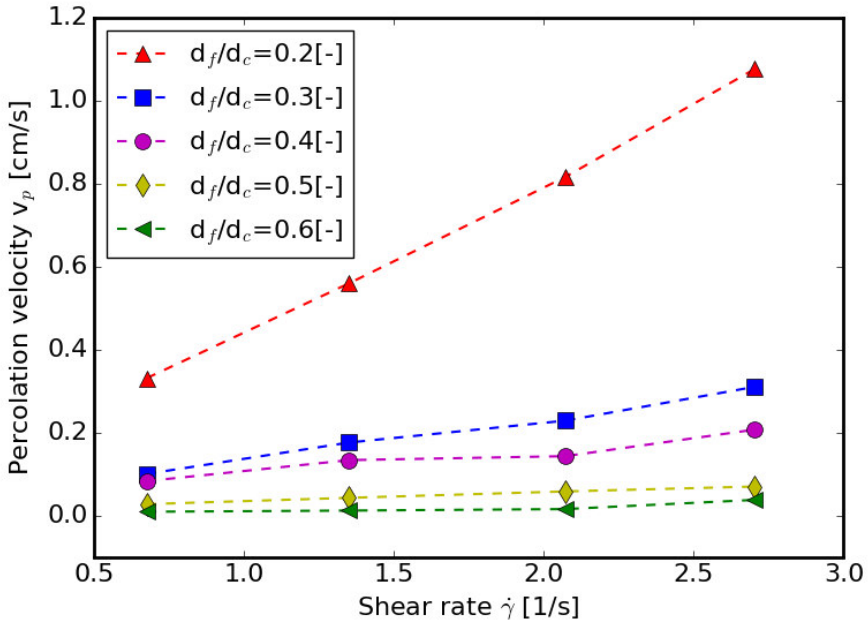

FIGURE 6.3: Percolation velocity against the shear rate varying the size ratio.

rate. This trend allowed to find four different interpolating lines with the intercept equal to zero. The slopes of each line were thus plotted as a function of the size ratio allowing to find a correlation between the percolation rate and the most important variables of the system, the shear rate and the size ratio:

$$v_p = f\left(\frac{d_f}{d_c}\right)\dot{\gamma} \tag{6.3}$$

Different interpolation curves were evaluated for $f\left(\frac{d_f}{d_c}\right)$. Bridgwater (1994) found a good fitting of his experimental data using an exponential law:

$$v_p = e^{A\frac{d_f}{dc}}\dot{\gamma} \tag{6.4}$$

with the parameter A in Eq. 6.4 equal to -8. The fitting done with expression 6.4 is reported in Figure 6.4. Remembering that in the segregation model used in the continuum simulations (see equation 2.12), different dependence between

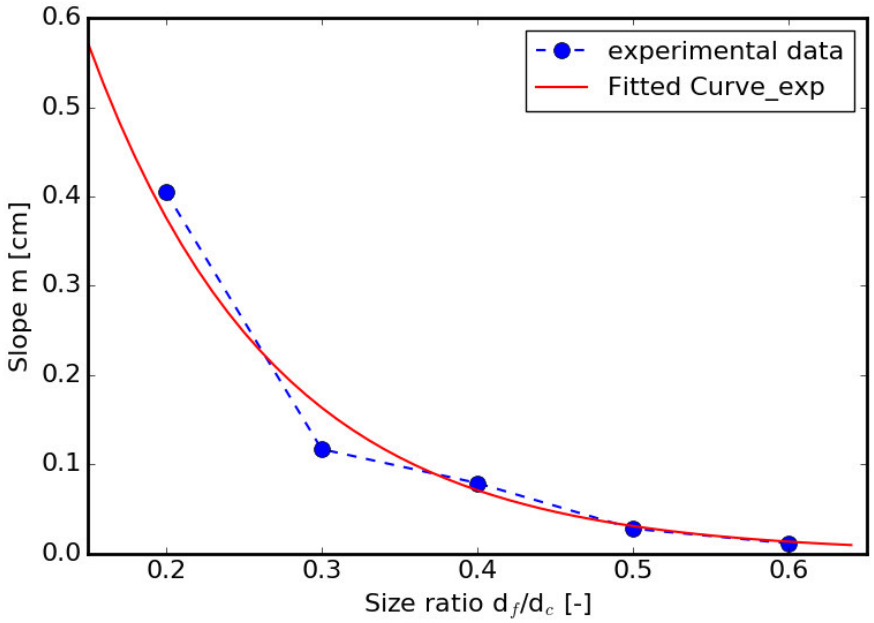

FIGURE 6.4: Exponential fitting of the experimental data.

the percolation velocity and the size ratio was considered as reported in the following:

$$v_p = k_1 \left(1 - \frac{d_f}{d_c}\right)^{k_2} \tag{6.5}$$

The new fitting reported in the Figure 6.5 resulted worse than the previous.This evidence was also confirmed by R^2 that resulted equal to 0.97 for the new fitting and equal to 0.99 for the previous one. The parameter values found were: k_1=2.2 and k_2=7.6.

So far, we considered that only the ratio between the diameter of fine and coarse particles played an important role in the percolation velocity without considering the effect of the absolute value of the coarse particles diameter. Thus, some experiments were devoted to understand if the magnitude of the particle bed diameter could play an active role in the percolation velocity. As it can be seen in the Figure 7.3 percolation velocity resulted larger increasing the diameter of the coarse particles, meaning that the diameter of the bed particles influenced the percolation. When the particles of the bed have a greater diameter is also greater the distance ("the jump") that a small particle have to perform before to meet the subsequent

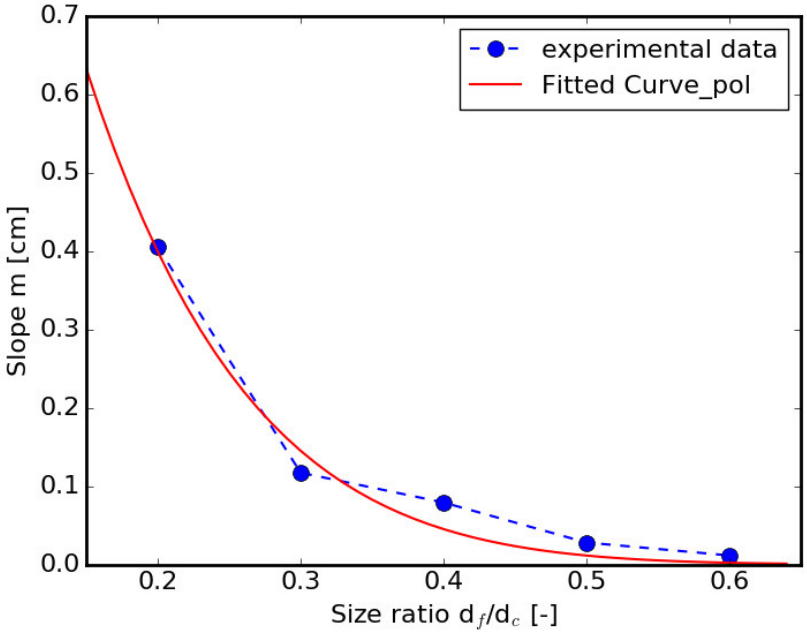

FIGURE 6.5: Polynomial fitting of the experimental data.

layer of coarse. As we explained better in the next section, this behavior resulted from the fact that in a bed composed of coarser particles, small particles present less occasion of remaining trapped between two layers of the bed, and thus they result faster during the percolation. In the Figure 7.3 only the comparison at the larger shear rate ($\dot{\gamma}$=2.701 s^{-1}) was reported, but the trend and the difference were similar also at at lower shear rate.

6.3.2 Dimensional analyses

A dimensional analysis of the system was performed to compare systems at different shear rate and coarse diameter with the experiments done. Such analysis allowed also to better understand which dimensionless parameter affected more the percolation. Three dimensionless numbers were identified to describe the system: the dimensionless percolation velocity, $v_p{}^*$, the size ratio, $d*$ and the dimensionless shear rate, $\dot{\gamma}*$:

$$v_p^* = \frac{v_p}{\dot{\gamma} d_c}; d^* = \frac{d_f}{d_c}; \dot{\gamma}^* = \dot{\gamma}\sqrt{\frac{d_c}{g}} \tag{6.6}$$

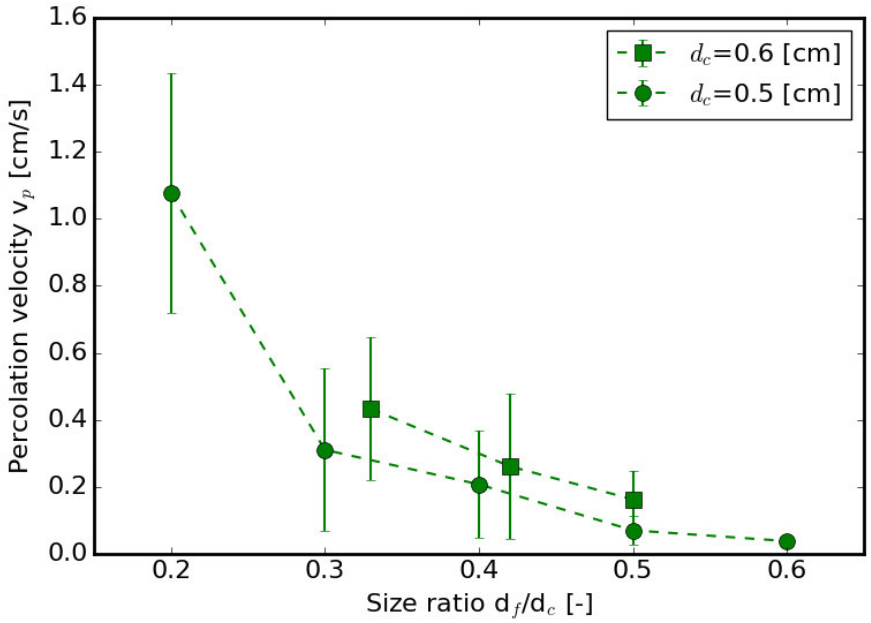

FIGURE 6.6: Percolation velocity against the size ratio using different size sphere bed at shear rate equal to 2.703 1/s.

TABLE 6.3: Size of granulated materials used experiments.

Fines diameter [cm]	Coarse diameter [cm]	Size ratio [cm]
0.07	0.45	0.12
0.126	0.45	0.28
0.18	0.45	0.4
0.23	0.45	0.51

From Figure 6.7 it can be appreciated that in dimensionless terms the data collapse in one curve and, thus, the identified dimensionless numbers well describe the percolating system.

6.3.3 Percolating granulated materials

We performed the same experiments described before using granulated microcellulose particles with irregular shape. The cellulose was granulated in such a way to obtain a wide size ranges and divided in small size ranges The diameter of the particles was calculated as the average of the maximum and minimum size in each size ranges. The size of the particles used in the experiments is reported in Table6.3. The figure 6.8 shows that at every shear rate the spheres percolate

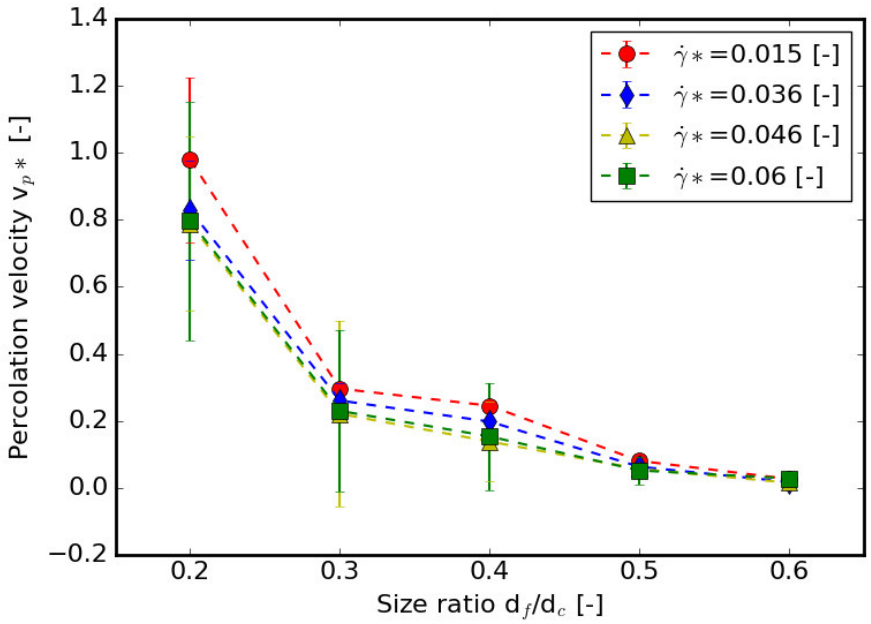

FIGURE 6.7: Dimensionless percolation velocity against the size ratio.

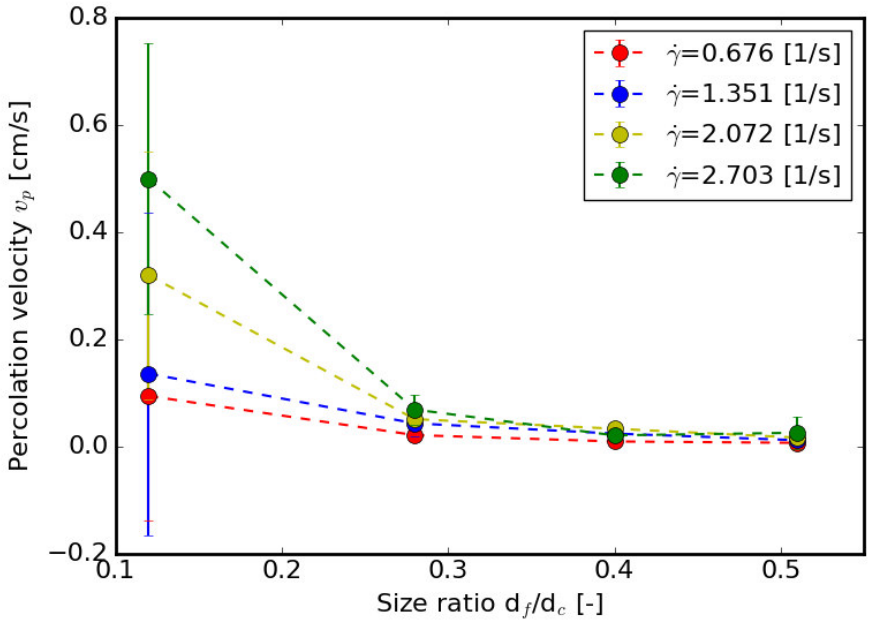

FIGURE 6.8: Percolation velocity of the granulated material against the size ratio at different shear rate.

faster than the granules as it can observed better in Figure6.9.

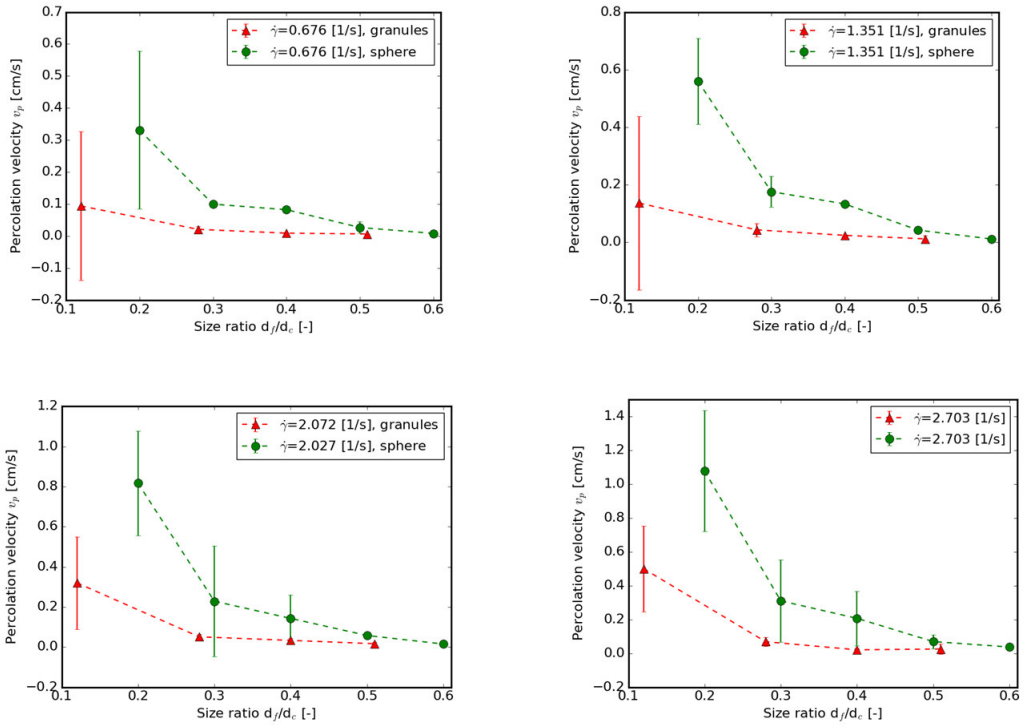

FIGURE 6.9: Comparison of the percolation velocity of two different materials:glass and granulated particles.

It can be observed that before the size ratio 0.3, the percolation speed decreases rapidly and becoming roughly constant for greater size ratios. The void between the coarse particles played an important role in the percolation. As general and simplified rule, we can say that greater is the void in the bed, greater is the probability for the fines to percolate. However despite the granulate bed presented a total higher bed porosity than the spheres bed, the granulated fine particles took more time to cross the bed. This behavior is probably due to the difference between the flowability of the two materials. A measure of flowability obtained with the angle of repose technique showed that the cellulose granules presented a repose angle of 46 degrees, while the angle of repose of the sphere was equal to 23 degrees. The irregular shape and the poor flowability of the granulated cellulose can compete to make difficult the percolation of fine materials.

6.4 Some theoretical considerations on percolation velocity

The percolating granular material sheared inside the cell can be in a state of movement or at rest. When a small particle falls inside the bed of coarser material, the fall is never continuous but it can be described as a results of a stop and go process. Every time the small particle find a void larger than its size it can fall for a distance which scales with the size of coarse particles, d_c minus the size of the fine one, d_f. The fall of the fine particle stops when it find an obstacle (typically a coarse particle) or the distance between the coarse particles is equal or smaller than d_f. The mechanical activation considered here will be the shear which occurs in bulk materials under strain deformation and is typically localized at the failure zones of the granular material. The voidage of the bulk material is an important variable which characterize the average distance between the coarse particles. Notwithstanding its important role Bridgwater (1994) did not considered bed porosity ε as an independent variable and not included it in his theory. We acknowledge that voidage is set by the stress conditions in the bulk material being at the critical state when sufficient strain is applied; however voidage strongly affects the average distance between coarse particles and i.e the possibility for fine to pass or not. This variable needs to be included as a fundamental ingredient of the theory.

6.4.1 Average distance between bulk particles

A further, practical reason, for including the bed porosity in the analysis is that the average distance between particles is difficult to be measured. Bed porosity instead is a much easier variable to be controlled and measured. In any case average particle distance and bed porosity are strongly related. For a bed of spherical

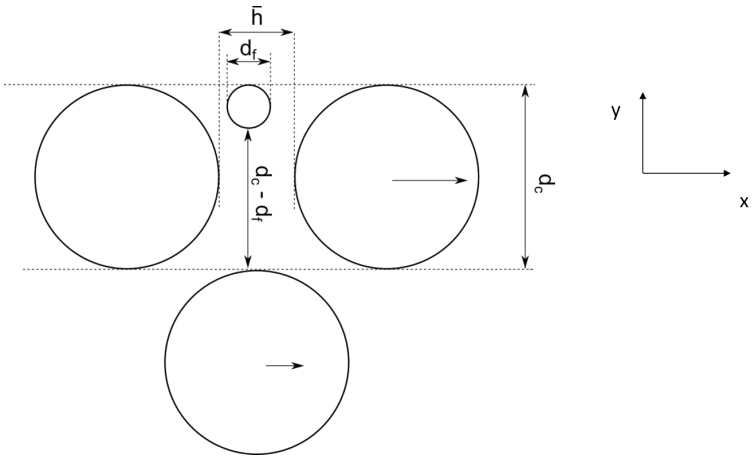

FIGURE 6.10: Percolation cage

particles in random packing it can be demonstrated that the average distance (intended as the average chord length between two surface points of two spheres) is:

$$\overline{h} = \frac{2}{3} d_c \frac{\varepsilon}{1-\varepsilon} \tag{6.7}$$

Experiments carried out in the shear box described in 6.2 have shown that for spheres the porosity of the bed during shear was $\varepsilon = 0.4$. This allow to find the average distance between particles to be:

$$\bar{h} = 0.44 d_c \tag{6.8}$$

6.4.2 Probability of passing for fine particles

Interparticle percolation is basically a random process. The percolation velocity strongly depends on the possibility, for a fine, to fall in a void of adequate size. Each coarse particle can be assumed to belong to a cage delimited by the other particles of the bulk. Because of the motion to which particles are subjected, the cage can be assumed anisotropic, and thus it can preferentially dilate in the direction of the motion (x-direction in Figure 6.10). The distance between the center of two adjacent particles in the direction of motion is therefore $d_c + \overline{h}$, while the

distance in direction normal to flow (y-direction) is assumed to be simply d_c. The probability for the fine particle to fall in direction normal to the direction of flow depends on the probability of finding a hole larger than d_f. As demonstrated by Cooke and Bridgewater (1979) on the basis of statistical mechanical arguments (but also from Pavlovitch *et al.* (1991)) the probability distribution of the distance between two particles is $P(h) = \frac{1}{\bar{h}} e^{-h/\bar{h}}$ where $\bar{h}$ was defined in eq. (6.7) .

The probability of finding an hole of aperture between h and $h + dh$ is:

$$P(h) = \frac{1}{\bar{h}} e^{-h/\bar{h}} dh \tag{6.9}$$

while the probability of finding an aperture h larger than d_f (which is the condition for a fine to pass) is therefore:

$$P(h \geq d_f) = \int_{dP}^{\infty} \frac{1}{\bar{h}} e^{-h/\bar{h}} dh = e^{-d_f/\bar{h}} \tag{6.10}$$

6.4.3 Falling conditions for fines

Two limiting cases can be thought:

- the free fall, occurring when $\bar{h} > d_f$, during all the time of flight so that the fine particle can move undisturbed in all the cage;
- the hindered fall when $\bar{h} = d_f$, which cover the case of multiple stops and go during the fall in each unit cage or shorter path.

Combining the condition $\bar{h} = d_f$ with eq. (6.8) gave the critical particle size ratio $d_f/d_c = 0.44$ discriminating between free fall and hindered fall.

Free fall time

The time of flight, t_f, in free fall conditions is proportional to the distance covered by the fine particle in the unit cage:

$$t_f \propto d_c - d_f \tag{6.11}$$

(and inversely proportional to the free fall velocity, v_f):

$$t_f \propto 1/v_f \tag{6.12}$$

As a first approximation lets imagine that the particle moves at uniform velocity equal to the final one (an average velocity can be also used as a further refinement of the theory). In free fall the sum of kinetic energy and potential energy can be assumed equal to 0, $\triangle E_k + \triangle E_p = 0$, therefore:

$$\frac{1}{2}\rho v_f^2 = \rho g(d_c - d_f) \tag{6.13}$$

and the free fall velocity results, hence, equal to:

$$v_f \propto \sqrt{g(d_c - d_f)} \tag{6.14}$$

The time of flight is thus:

$$t_f \propto \sqrt{\frac{d_c - d_f}{g}} \tag{6.15}$$

Stop time

After each jump the percolating fine particle find an obstruction (typically the coarse particle at the base of the cage) which, due the shear, is in relative motion with respect to the particles of the layer above (see Figure 6.10).

The stop time, t_s, is proportional to the size of the coarse particle plus the size of the fine (only when such distance has been covered by the obstructing coarse

particle, the fine can perform a new jump):

$$t_s \propto d_c + d_f \tag{6.16}$$

and inversely proportional the relative velocity between two layers of coarse particles, v_c:

$$t_s \propto 1/v_c \tag{6.17}$$

The relative velocity depends on the shear and is:

$$v_c = \dot{\gamma} d_c \tag{6.18}$$

The stop time results therefore proportional to:

$$t_s \propto \frac{d_c + d_f}{\dot{\gamma} d_c} \tag{6.19}$$

Total jump time

The total time spent by a fine particle in a cage is given by the sum between the falling time and the stop time. The time the particle spends in motion or in rest however depends on the probability of finding an aperture of adequate size or not. The total time can be considered therefore as an weighted average between the free fall time and the stop time weighted by the probability of finding holes of proper size (P) or an obstruction($1 - P$) respectively.

$$t_{tot} = P t_f + (1 - P) t_s \tag{6.20}$$

Percolation velocity

The percolation velocity can be computed as the ratio between the available space in the cage and the total time spent in the cage:

$$v_p \propto \frac{d_c - d_f}{t_{tot}} \tag{6.21}$$

After some manipulation we get:

$$v_p \propto \frac{d_c(1 - d_f/d_c)\dot{\gamma}}{(1 + d_f/d_c)(1 - P) + \dot{\gamma}\sqrt{\frac{d_c - d_f}{g}}\sqrt{1 - d_f/d_c}P} \tag{6.22}$$

that in dimensionless variables can be written as

$$v_p^* \propto \frac{(1 - d^*)}{(1 + d^*)(1 - P) + \dot{\gamma^*}(1 - d^*)^{0.5}P} \tag{6.23}$$

where:

$$v_p^* = \frac{v_p}{\dot{\gamma} d_c}; d^* = \frac{d_f}{d_c}; \dot{\gamma}^* = \dot{\gamma}\sqrt{\frac{d_c}{g}} \tag{6.24}$$

The comparison with the experimental data obtained with the shear cell is qualitatively good (see Figure 6.11); however it is clear that for higher size ratio the predicted percolation over predict the experimental one.

The hindered fall

The reason for that can be found in the fact that for large size ratios the percolation process do not evolve through free falls but hindered ones; $d^* = 0.44$ can be considered the limit above which the percolating particle trajectory is strongly affected by the coarse particles of the cage. Consider also that the vertical distance between two layers of coarse particle can be lower than d_c so that the free fall distance will be smaller than $d_c - d_f$. In theory it should be zero when $d_c = d_f$ i.e.

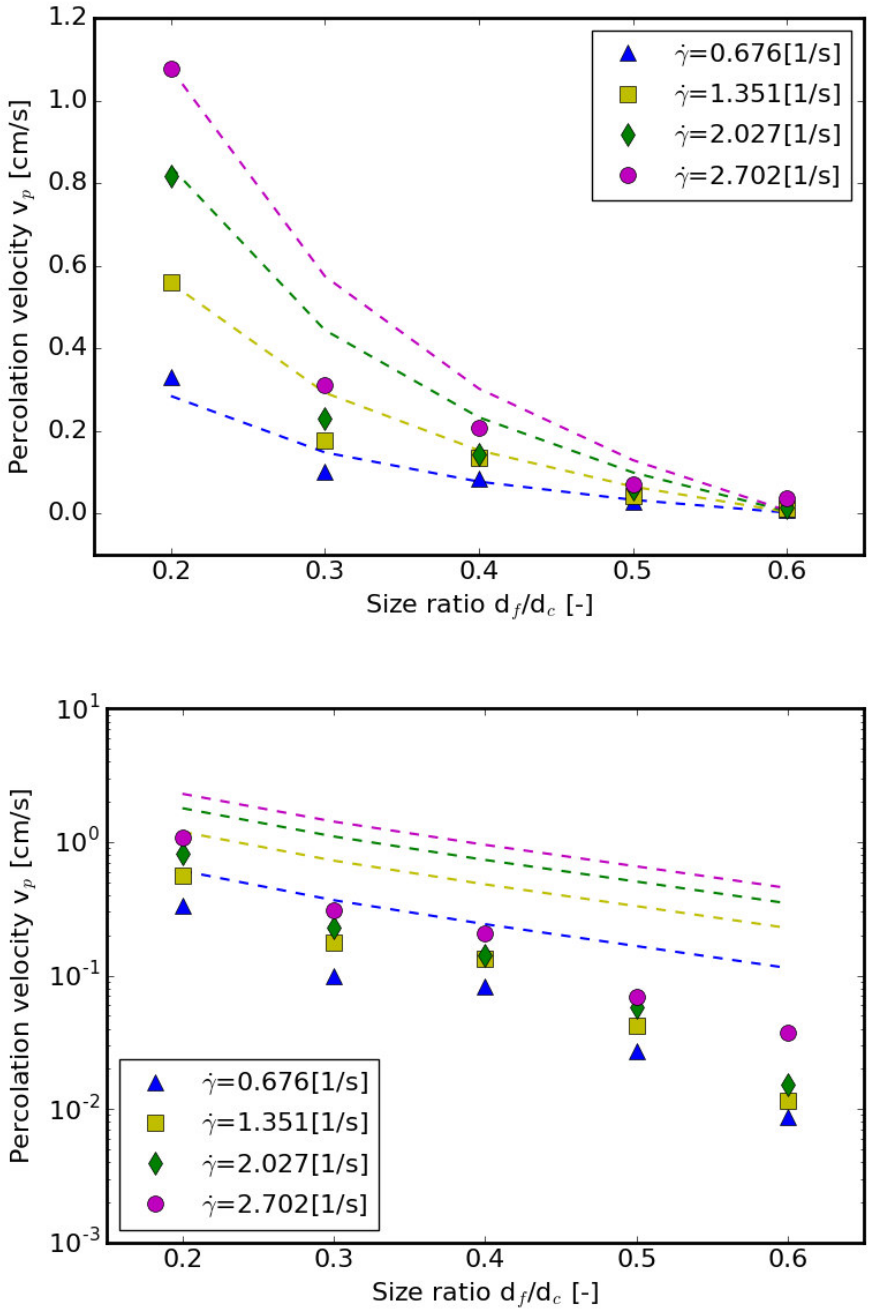

FIGURE 6.11: Percolation velocity as a function of d^* for a range of shear rates in linear (above) and semi-logarithmic scale (below).

when $d^* = 1$; however experiments show that for a size ratio $d^* = 0.6$ the percolation velocity is already very close to zero. A correction factor can be introduced to take into account the hindering effects of the cage of coarse particles on fines when $d^* > 0.44$. The free fall distance can be reduced by a factor k as $d_c - kd_f$ where $k \approx 1.2$. This correction bears some analogies with that used by Beverloo to predict the mass flow rate of free falling particles through an orifice. Notwithstanding the correction done, the theoretical formulation did not match very well the experimental data. According to the fitting found from them, we elevated the term $(1 - d*)$ to an exponent equal to 3. Finally, the relation found to describe the percolation velocity results equal to:

$$v_p^* = A\frac{(1 - kd^*)^n}{(1 + d^*)(1 - P) + \dot{\gamma}^*(1 - kd^*)^{0.5n}P} \tag{6.25}$$

with k=1.2, A=0.7 and n=3. Figure 6.12 shows the improvement in the prediction of the percolation velocity after introducing the corrections in the model.

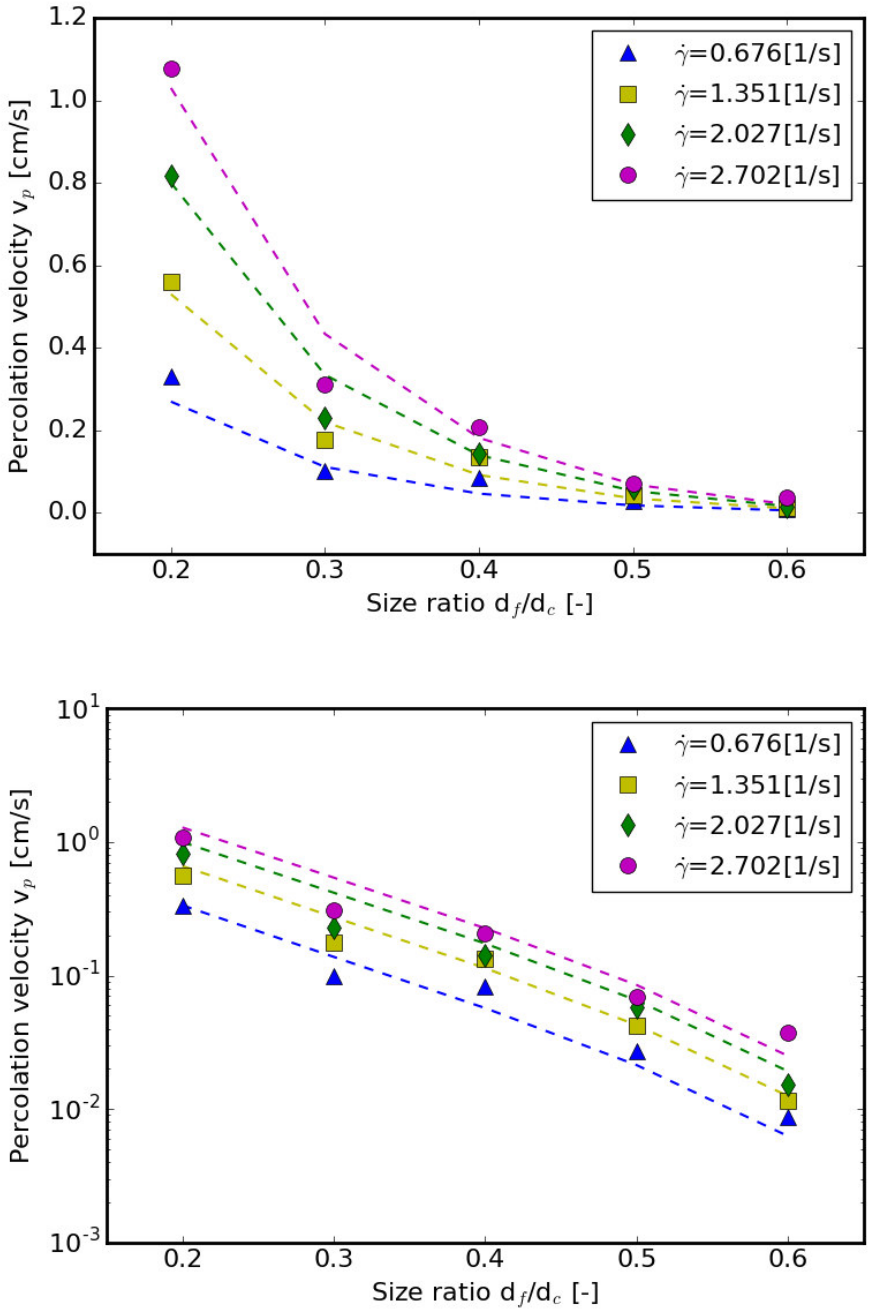

FIGURE 6.12: Percolation velocity corrected at high d^* for a range of shear rates rates in linear (above) and semi-logarithmic scale (below).

Also the trend of percolation velocity as a function of shear rate agree with the experimental data after introducing the correction for hindered fall (Figure 6.13).

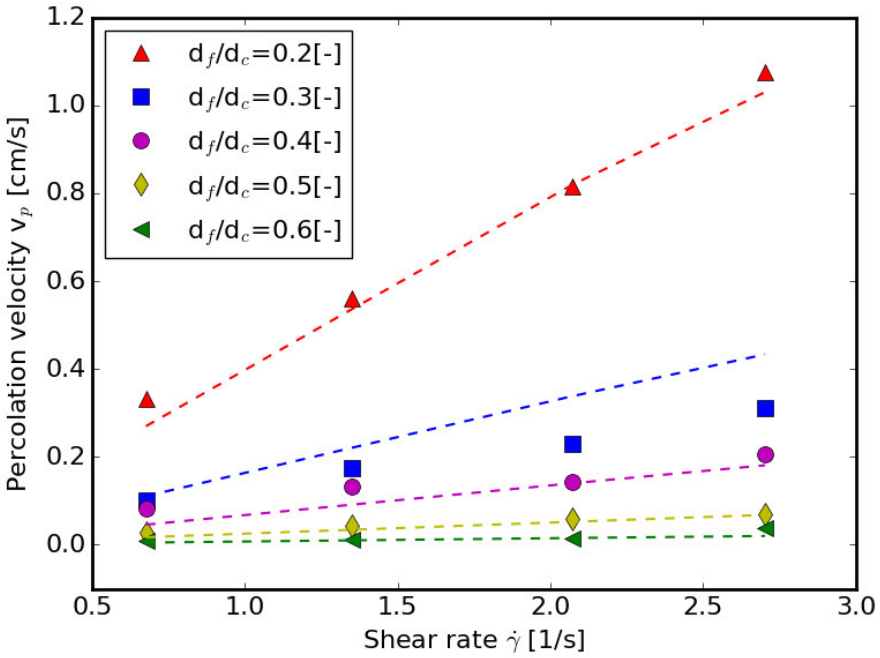

FIGURE 6.13: Percolation velocity corrected at high d^* for a range of shear rates.

6.5 Conclusions

In this Chapter both experimental and a theoretical approaches have been used to study the percolation phenomena in a bi-dispersed mixture of cohesionless, spherical particles. It was decided to study the simplest flow of the granular material, aware that this type of slow is an approximation of what happens normally in local scale in larger flow. The experiments were performed in a shear cell, apparatus that allowed to measure the percolation speed of a small particle over a range of particle size ratio, shear rate and varying the shape of the particles. From experimental data empirical correlations were proposed. From the visualization of the experiments, it was also possible to better understand how the percolation mechanism worked and conjectured a theoretical model to describe the segregation. For glass spheres, the comparison between the theoretical relation and the experiments gave a good agreement. The relation found could be used in a continuum model, as that reported in Chapter 5 to simulate the segregation in more

complex granular flows.

Nomenclature

Symbol	Units	Description
L	m	length of the shear cell
f	1/s	frequency
H	m	total height of material
v_p	m/s	percolation velocity
$\|\dot{\gamma}\|$	1/s	shear rate
$\mathbf{g}$	m/s^2	gravity acceleration vector
t	s	percolation time
$\bar{h}$	m	average chord length
ε	-	porosity
P	-	probability to find a hole
t_f	s	free fall time
v_f	m/s	free fall velocity
t_s	s	stop time

Chapter 7

A discrete approach to percolation

7.1 Introduction

In the previous work reported in Chapter 5, the segregating flow of a binary mixture of granular material has been studied using continuum models. At a macroscopic scale, the granular material can see as a continuum medium, ignoring the fact that it is composed of grains and ignoring the description of their interaction. As said in Chapter 1, an alternative approach to model the flow of the granular material is the discrete element method (DEM) or molecular dynamics (MD)(Cundall and Strack, 1979) that is used for probing local particle variables, i.e particle positions and velocities, contact force (Radjaï and Dubois, 2011). This method is a numerical technique that treats the granular material as a collection of discrete particles describing their motion and updates any contact with neighboring elements by using a constitutive contact law. This method numerically integrate Newton's equation of motion simultaneously for all the particles in the system, by considering the contact forces and the external forces acting on the particles (Radjaï and Dubois, 2011). The overlap between particles is considered as a displacement variable for the calculation of the repulsive forces.

There exists other discrete methods, for example the contact dynamics (CD) that considers the particles as perfectly rigid and suppresses phenomena caused by particle deformation. It represents the deformation of the granular medium by particle rearrangements. In the limit of the dense state a quasi static method

(QS), that describes the evolution of the system as consecutive state of mechanical equilibrium, is to prefer. Dilute systems, i.e granular gases, are governed by event-driven (ED) dynamics in which the evolution of the state are described by binary collision between the particles.

These numerical techniques allow to study a system at a microscale level and provides useful indication to connect a microscopic phenomenon with a macroscopic description. DEM technique results an efficient technique to provide details about flow and mixing, but it is limited to relative small system and and simulations can be carried out for only a small period of the flow (Khakhar *et al.*, 2001). The number of particles that can be simulated is no more than about 10^5, while practical mixing devices and in general a typical bulk solid consists of 10^9 particles (Schulze, 2007). Notwithstanding this limit, DEM is an important technique that allow to obtain information on the behavior of granular cases in limited case difficult to reproduce experimentally. The simulations reported in this Chapter were done using MD method, in particular soft-particle technique, that generally models the interactions between the particles as a spring. The soft sphere technique describes the contact between the particles assuming an overlap. To describe the dissipation behavior of the granular material, a viscous dashpot is put in parallel with the spring (Campbell, 1990). DEM simulation, here, was used to describe the behavior of a bi-disperse granular material in dense state in a shear cell. This system is simple and the flow condition can be controlled; at the same time, this flow allow to understand ,starting from micro scale, what happens in more complex macro particle flow. Recently, Khola and Wassgren (2016) use the same geometry to investigate the percolation speed and the diffusion coefficient in a steady shear flow of bi-dispersed mixture of cohesionless, spherical particles varying the size ratio, the shear rate and the volume concentration of smaller particles. Different boundary conditions were used (Khola and Wassgren, 2016); they imposed periodic boundary in the direction perpendicular to the shear and fixed boundary in the other direction. Our simulations are similar,

but fully periodic boundary conditions and different range of parameters were used.

The simulations reported in this Chapter were done with the help and assistance of Stefan Radl, Assistant Professor at Institute of Process and Particle Engineering (TU Graz). This study are devoted to study situations difficult to replicate with experiments. In particular, we will show how the percolation velocity is influenced by the concentration of fines and on the direction of the gravity vector.

7.2 Contact model in DEM simulations

The discrete element method, also often referred to as molecular dynamics (MD) (Luding, 2008), uses Newton's second law to describe the interaction between the grains:

$$m_i \frac{d\mathbf{v}_i}{dt} = \mathbf{F}_i, i = 1, ..., N \tag{7.1}$$

where N is the number of the grains in the simulation, m_i is the mass of the grain i, v_i is the velocity of each grain and $\mathbf{F}_i$ is the force exerted on that grain. This method calculates the force $\mathbf{F}_i$ and then the differential equation 7.1 is solved. This method is largely flexible because the force $\mathbf{F}_i$ can be described in different manner. Usually, it is a combination of repulsion and friction forces as internal force and gravity or confining forces due to walls of a container. Thus, the force $\mathbf{F}_i$ can be written as the sum of the force exerted by grain j on grain i, $\mathbf{F}_{ij}$ and an external force $\mathbf{F}_{ext,i}$:

$$\mathbf{F}_i = \sum_{j \neq i} \mathbf{F}_{ij} + \mathbf{F}_{ext,i} \tag{7.2}$$

The external forces $\mathbf{F}_{ext,i}$ is often the gravity force:

$$\mathbf{F}_{ext,i} = m_i \mathbf{g}_i \tag{7.3}$$

The way of calculating the interaction forces $\mathbf{F}_{ij}$ depends on the numerical method chosen. The DEM method considers the contact force between two particles composed by two components:

$$\mathbf{F}_{ij,n} = F_n\mathbf{n} + F_t\mathbf{t} \tag{7.4}$$

where F_t and F_n are the normal and the tangential component, and **n** and **t** are the unit vectors, pointing in the normal and the tangential directions. An interaction force is accounted only when two grains touch and each one causes deformation in the other. The deformation produces an interaction force. The shape of grains does not change, but they can overlap and the force becomes a function of the overlap. The overlap δ_n is:

$$\delta_n = |\mathbf{x}_i - \mathbf{x}_j| - r_i - r_j \tag{7.5}$$

where x_i and x_j are the centers of the grains and r_i and r_j are they radii. When the overlap is greater than 0 the two grains are not in contact; when the overlap is smaller than 0, the two grains are in contact and the force that describe it is a repulsive contact force that pushes the two grains apart. The simplest force with the desired properties is the damped harmonic oscillator force:

$$\boldsymbol{F_{ij,n}} = \begin{cases} f\left(\frac{\delta}{d}\right)\left(-k_n\delta_n - \gamma_n\frac{d\delta_n}{dt}\right) & \delta_n < 0 \\ 0 & \delta_n > 0 \end{cases} \tag{7.6}$$

where k_n is the stiffness of the grains that it has to be chosen large so that the overlap between grains remains small and γ_n is a viscous damping constant. The damping force is necessary to describe the dissipation at contacts that is an intrinsic characteristic of granular materials. The relative velocity in normal direction $\frac{d\delta_n}{dt}$ is defines as:

$$\frac{d\delta_n}{dt} = (\mathbf{v}_i - \mathbf{v_j}) \cdot n \tag{7.7}$$

where $\mathbf{v}_i$ and $\mathbf{v}_j$ are respectively the velocity of grain i and of the grain j. The tangential force, that describes how friction is considered in the model, is treated in the same way of the normal force and it results equal to:

$$\boldsymbol{F_{ij,t}} = \begin{cases} f\left(\frac{\delta}{d}\right)\left(-k_t\delta_t - \gamma_t\frac{d\delta_t}{dt}\right) & \delta_t < 0 \\ 0 & \delta_t > 0 \end{cases} \tag{7.8}$$

where k_t is the elastic constant for the tangential contact and γ_t is the viscoelastic damping constants the tangential contact. The relative velocity is obtained in analogy with equation 7.7:

$$\frac{d\delta_t}{dt} = (\mathbf{v}_i - \mathbf{v_j}) \cdot t \tag{7.9}$$

The Coulomb's friction law governs the tangential force:

$$|\boldsymbol{F_t}| \leq \mu \boldsymbol{F_n} \tag{7.10}$$

where μ is the coefficient of friction. $m_{eff} = m_i m_j/(m_i+m_j)$ is the effective mass of spheres with masses m_i and m_j, $\mathbf{v}_{nij}$ and $\mathbf{v}_{tij}$ are the normal and tangential components of relative particle velocity. Setting $f\left(\frac{\delta}{d}\right)$=1 we obtain the linear spring-dashpot model(Cundall and Strack, 1979), model that we used in our simulations. This model has the advantage that its analytic solution (with appropriate initial conditions) allows the calculation of important quantities, for example the coefficient of restitution or the time of collision. This model assumes a constant coefficient of restitution defined as:

$$\varepsilon = exp\left(\frac{-\gamma_n}{2m_{eff}}t_c\right) \tag{7.11}$$

where

$$t_c = \pi\left(\frac{k_n}{m_{eff}} - \left(\frac{\gamma_n}{2m_{eff}}\right)^2\right)^{-0.5} \tag{7.12}$$

represents the duration of collision.

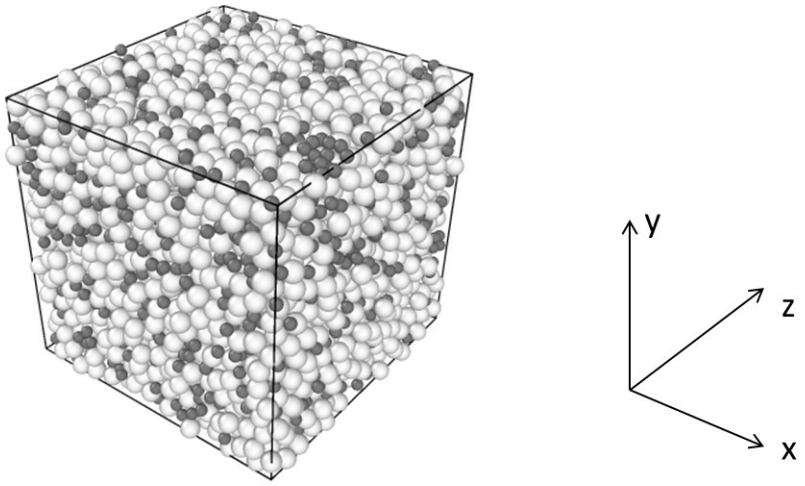

FIGURE 7.1: Snapshot of the shear box during the simulations

7.3 Geometry and simulations conditions

The segregation of fine material was investigated in homogeneous, simple shear flow of soft, frictional, non-cohesive binary mixture of spheres. The simulations were done with the open source DEM software LIGGGHTS-TUG (v.3.3.1). Using the contact model described in 7.2, bi-dispersed mixture of spheres were confined in a cubic periodic box and subjected to homogeneous steady simple shear at a shear rate $\dot{\gamma}$. The geometry of the simulations is sketched in 7.1. We used a coordinate system where x indicated the direction of the mean motion, y is the direction of the velocity gradient, hence the shear rate $\dot{\gamma} = \frac{dv_x}{dy}$ and z represented the coordinate out of the shear plane. The box size, and hence the solid volume fraction ϕ, were kept constant for each simulation. At the beginning, the particles were inserted in a control volume with each linear dimension doubled and then the control volume were compressed to the desire volume fraction. This technique is similar to insert the particles in the box in a random position at one-half their desired radius and then, when the shear flow was set in motion, the particles were grown to their final diameter (Campbell, 1990). The particle parameters used in the simulations are resumed in Table 7.1. The coarse particles had diameter d_c and

TABLE 7.1: Fixed DEM particles parameter.

Parameter	Value
$\rho_f, \rho_c,$	1 [kg/m^3]
μ	0.1 [-]

density ρ_c; the fine particles had a diameter d_f and density ρ_f. The fine-fine, the coarse-coarse and fine-coarse friction coefficients were the same and kept equal to 0.1 during the simulations. A previous study (Aarons and Sundaresan, 2006) has shown that in the absence of cohesive forces, sheared granular assemblies exist in the quasistatic-dense regime only at the high particle solid volume fractions that depend on the friction coefficient. Also the critical volume fraction, ϕ_c, that determines the transition between the three different regimes, i.e quasi-static, intermediate and collisional, is a function of the friction coefficient. From Aarons and Sundaresan (2006) and Chialvo *et al.* (2012) we know that to simulate a dense-quasi static regime, $\phi \geqslant 0.613$ when $\mu = 0.1$. Also the normal stiffness of the materials play an important role in the determination of the correct regime of flow. To guarantee the dense flow, this parameter was put equal to 10^5. The ratio k_t/k_n was set equal to 2/7 and γ_t equal to 0; γ_n was imposed equal to 139 kg/s to ensure a restitution coefficient equal to 0.4. In every simulations the effective mass is calculated in terms of mass of coarser particle. The contact duration reported in 7.12 is of practical technical importance; the integration of the equations of motion results stable only if the integration time-step, Δt_{DEM} is much smaller than t_c (Luding, 2008). Thus, the integration time-step was imposed fifty times smaller. The number of particles inside the box varied, changing the fine volume fraction and the diameter of fine particles that ranged between 0.3 and 0.7. The macroscopic stress tensor $\boldsymbol{\sigma}$ was calculated as the sum of contact stress due to particle collisions $\boldsymbol{\sigma}_{coll}$ and the kinetic stress due to velocity fluctuations of the particles $\boldsymbol{\sigma}_{kin}$:

$$\boldsymbol{\sigma} = \frac{1}{V} \sum_i \left[\sum_{j \neq i} \frac{1}{2} \bar{\boldsymbol{r}}_{ij} \mathbf{F}_{ij} + m_i (\mathbf{v}_i')(\boldsymbol{v}_i') \right] \tag{7.13}$$

where V is the volume of the box, $\boldsymbol{r}_{ij}$ is the vector pointing from the center of particle j to the center of particle i, $\boldsymbol{F}_{ij}$ is the contact force acting on particle i by particle j, $\boldsymbol{v}_i'$ is the fluctuating velocity (the particle velocity relative to its mean streaming velocity). The principal diagonal elements of the stress tensor is composed by the normal stress that, through the following relation:

$$p = \frac{\sigma_{xx} + \sigma_{yy} + \sigma_{zz}}{3} \tag{7.14}$$

gives an ensemble-averaged pressure. The non-diagonal elements of the stress tensor represent the shear stresses. The segregating velocity of the fine particles was calculated as the difference between the average velocity of the mixture and the average velocity of the fines in the direction of percolation. The data displayed in the following consists of the time-averaged percolation velocity at the steady state. All macroscopic quantities will be presented in dimensionless form, scaled by some combination of the particles diameters, shear rate, percolation velocity, gravitational acceleration and fines volume fraction. The dimensionless approach guarantees that the material properties depend only on dimensionless combinations of the parameters of the problem (Radjaï and Dubois, 2011).

7.3.1 Lees-Edward boundary conditions

Two different types of boundary conditions can be used in the perpendicular direction to shear. The first option plans to bound the material between rough and parallel walls and to control the shear rate, one of the walls is fixed while the other moves with an imposed velocity. The second possibility, used in our simulations, is to use periodic conditions that eliminate the undesired effects of wall boundary condition. In fact, using wall boundary conditions, the distortion of the box caused by the shearing creates arching effect at the corner of the box, that generate stress gradient inside the material, also far from the limit of the

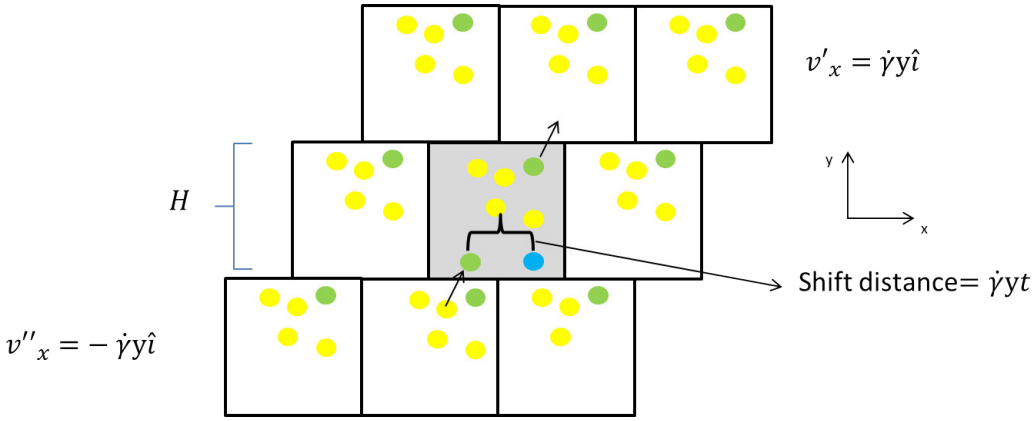

FIGURE 7.2: A schematic explanation of the behavior of the LEbc

box (Thornton and Zhang, 2001). In particular, in the simulations, we used Lees-Edward boundary conditions (LEbc) (Lees and Edwards, 1972), that represent an extension of the boundary condition for the simple shear flow. Implementing this type of boundary conditions in DEM simulation it is possible to obtain a system with uniform shear velocity profile. The original Lees-Edward boundary condition (LEbc) were implemented in a box with dimensions (H_x, H_y, H_z) in which the particles are in positions (r_x, r_y, r_z) and they move with a velocity (v_x, v_y, v_z). The center of the simulation box is (x,y)=(0,0). It is surrounded by images of itself in the x, y and z directions and its central images are stationary. An image of the function of the LEbc is reported in Figure 7.2. Boxes in the layer above the simulation box move with a velocity speed equal to $v'_x = \dot{\gamma} y \hat{\imath}$ where $\hat{\imath}$ is the vector unit in the x direction; boxes in the layer below move at speed $v''_x = -\dot{\gamma} y \hat{\imath}$. In the other layer, boxes are moving proportionally faster relative to the central one. The periodic boundary conditions are imposed on particles that leave the domain in the direction perpendicular to the velocity gradient. When the particles reappear in the box above the simulation cell will be reinserted with the velocity incremented of the shear rate multiply for the width of the cell. The origin of the coordinates being immaterial, the dynamics of the particles is invariant by translation and therefore necessarily homogeneous.

7.4 Results and discussion

The first set of simulations showed in the following were performed for a range of size ratio and dimensionless shear rate. Here, the results were showed in dimensionless quantities, using the relations reported in Eq. 6.6, to allow the comparison with Literature results and with the experimental results showed in the previous Chapter. Table 7.2 shows the details of the dimensionless parameter ranges investigated in the simulations.

7.4.1 Influence of size ratio on percolation velocity

It is already known from previous experiments (Chapter 6) and from the works of Bridgwater (1994) and Scott and Bridgwater (1975) that the ratio of the diameters is one of the most important variable that affect the percolation. Both the diameters are crucial in the determination of the percolation speed because as seen in 6.4, they play an important role in the determination of the percolation rate. Some explorative simulation were done to see if the percolation velocity profiles could be in agreement with the experimental data. The simulations were computed using different dimensional variables with respect to the experiments, but the same in terms of dimensionless variables. Figure 7.3 plots the dimensionless percolation velocity of fine against size ratio for dimensionless shear rate equal to 0.04. Similar trend is obtained from experiments and simulation. The simulation predict that for d_f/d_c greater that 0.5 the dimensionless percolation velocity tends to 0. In the simulation, the dimensionless percolation speed resulted slightly higher with respect to the experimental data for the size ratio 0.3. For lower size ratio, the simulations were not performed, because very long time could be requested.

TABLE 7.2: Dimensionless parameters ranges used in the simulations

Parameter	Value
Dimensionless shear rate	0.04, 0.06, 0.08, 0.12
Size ratio	0.3-0.7 in increments of 0.05
Fines volume fraction	0.04-0.7

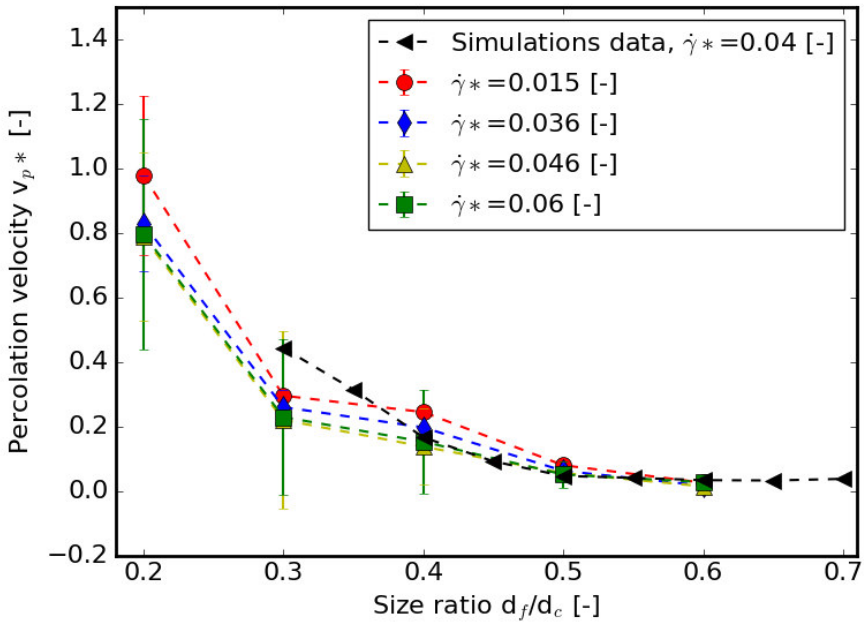

FIGURE 7.3: Comparison between dimensionless percolation velocity against the size ratio varying the shear rate obtained from experiments and from simulations.

7.4.2 Influence of the shear rate on percolation velocity

The values of dimensionless shear rate considered in this work range between 0.04 and 0.12. Since that simulations have given consistent results with experiments (see Figure7.3), we explored how the percolation velocity changed using dimensionless shear rate greater than those used in the experiments.

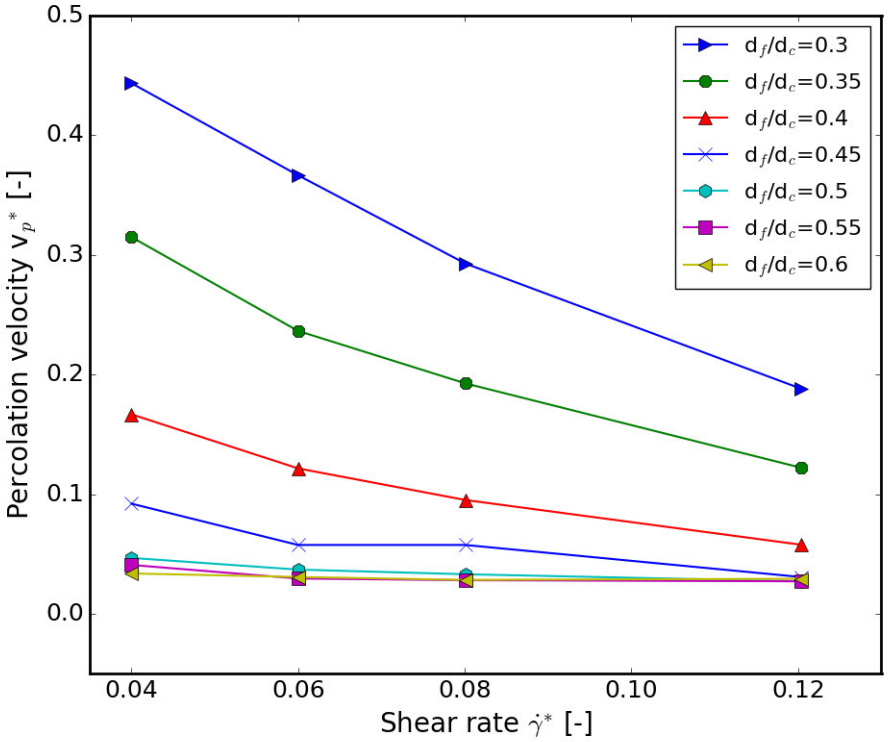

FIGURE 7.4: Dimensionless percolation velocity displayed as a function of the dimensionless shear rate for several size ratio.

Figure 7.4 displayed the dimensionless percolation velocity against the dimensionless shear rate, showing a decreasing trend of v_{p*} increasing $\dot{\gamma}^*$. The dimensionless percolation velocity was inversely proportional to the dimensionless shear rate as already seen in relation 6.15. Increasing the size ratio, this dependence decreases until, for size ratio greater than 0.5, the dimensionless percolation velocity resulted independent on the dimensionless shear rate.

7.4.3 Influence of the fines concentration on percolation velocity

Simulations allowed to explore also the situation where the fines concentration is large so that to become an important factor that influences the percolation. The simulations were done varying the fines volume fraction between 0.004 and 0.7. In the previous experiments, we use only four different small particles inside the bed and thus the system could be considered as infinitely diluted. Experimentally the dependence of the percolation velocity on the concentration of fines in the

mixture is difficult to explore because it should devise a system in which the fines particles, after leaving the shear box, are recirculated to the top to ensure a steady state. This study is important also because the percolation model used in Chapter 5 includes a dependence of fines fraction, expressed as $1-\omega_{p,f}$ that represents the fraction of coarse particles. In Figure **??** the dimensionless percolation velocity is plotted against the volume fraction of coarse materials.

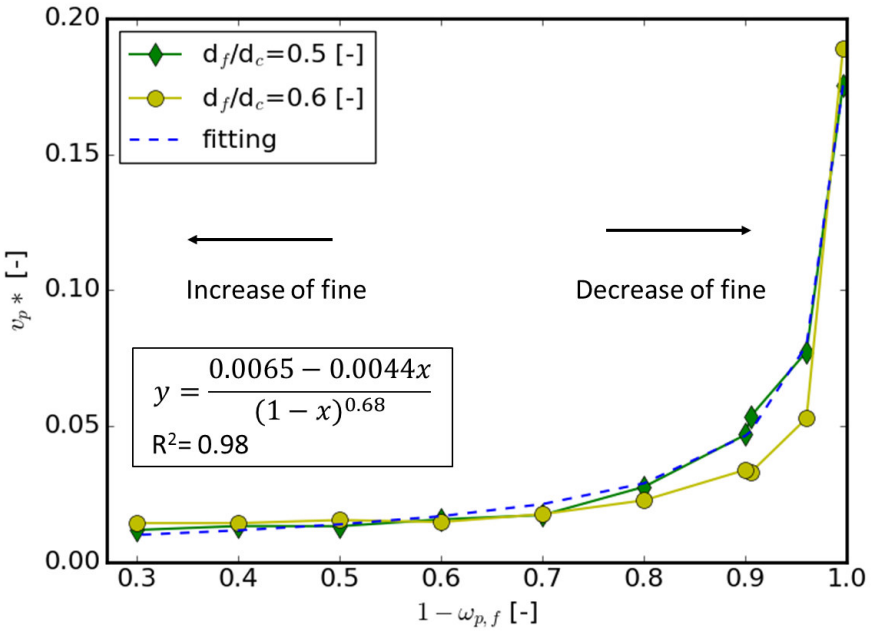

FIGURE 7.5: Comparison between dimensionless percolation velocity against the volume fraction od fines particles at different size ratio and dimensionless shear rate equal to 0.04.

We expected that increasing the number of fine particles in the system, fines particles segregate slower because the competition for space through which fines can move increases. This expectation is consistent with observation, as shown in Figure 7.5.

In the Figure 7.5 it is reported the fitting done for the size ratio equal to 0.5. The trend found here resulted different with respect to the trend used in Eq. 2.12 which provided a percolation velocity proportional to $1-\omega_f$, thus linear with the fraction of coarse particles. Anyway, also this relation can be considered correct if the percolation velocity is measured far from critical cases, i.e when $1-\omega_f$ tends

to 1 or to 0. The proportion of the percolation velocity to $1-\omega_f$ also expected that the percolation was zero only when $1-\omega_f$ was equal to zero, that happened when the volume fraction of coarse was equal to one. From Figure7.5 it can be seen that the percolation velocity tends to zero for value of $1-\omega_f$ larger than 0. (Artega and Tüzün, 1990) found a critical fine volume fraction value, at which the percolation velocity tends to zero, that depends on the ratio of the diameters:

$$\omega_{p,f}^{c} = \frac{4}{4+\frac{d_c}{d_f}} \tag{7.15}$$

According to 7.15, the percolation velocity in the simulation should go to zero for volume fraction of coarse material equal to 0.3 and 0.33 in the case of size ratios, respectively equal to 0.6 and 0.5, that is coherent with the profiles shown in **??**.

7.4.4 Influence of the direction of gravity

Up to now, the influence of the direction of gravity with respect to the shear rate was not taken in consideration. In simulated shear box, the direction of gravity was perpendicular to the shear rate, as it is possible to see in 7.6. In more complex granular flow, the gradient of velocity can change according to the geometrical configuration of the industrial device and different cases can occur as shown in Figure7.8.

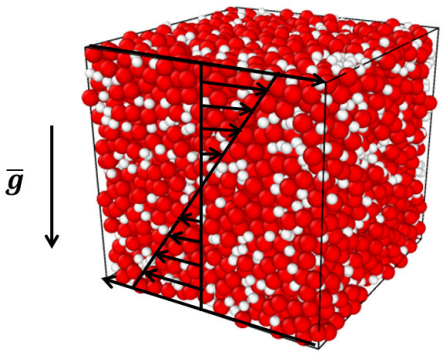

FIGURE 7.6: Image of the shear cell simulated with the indication of the shear rate and the acceleration of gravity.

In a silo the direction of gravity is parallel to the gradient of x-velocity; in the tumbler and in the hopper an intermediate case is verified, since the gravity and the shear form an angle between 0 and 90 degrees. From the analyses done until now, we identified several variables that influenced the segregation, between which there is the gravity and the shear rate. In Chapter 5 we affirmed that the segregation velocity acted in the direction of the gravity, but the magnitude of this were not present in the percolation relation. After an experimental analysis, we included in the percolation velocity also the magnitude of the acceleration of gravity.

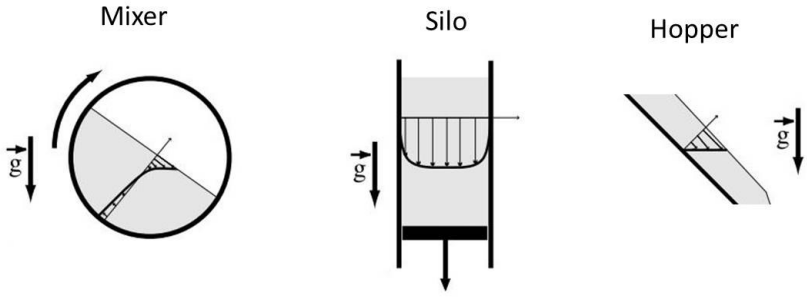

FIGURE 7.7: Comparison between different flow of granular material: Image takes from (MiDi, 2004).

Figure 7.8 show the dimensionless percolation velocity against the size ratio evaluated at a dimensionless shear rate equal to 0.04. Three different curves are

reported in different case: (1) the angle between the gravity vector and the shear rate is equal to zero, as for example in the case of silo; (2) the angle is equal to 90 degrees as happens in the shear box; (3) the angle is between 0 and 90°, as happens in a hopper and in a tumbler. The percolation velocity results slightly higher in the case in which the gravity had the same direction of the velocity gradient. This result seemed to confirm that both the variables, shear and gravity, played an important role in the determination of the segregation velocity, however it is not enough to consider their magnitude and it is also necessary to consider how they acted in respect to each other.

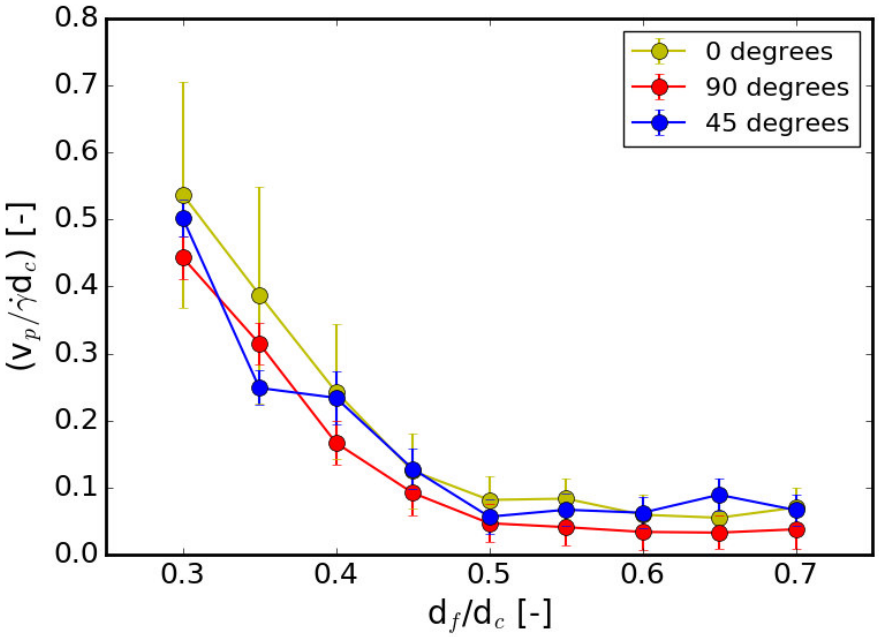

FIGURE 7.8: Dimensionless percolation velocity against the size ratio varying the direction of gravity with respect to the velocity gradient.

The intermediate case (45 degrees) did not give clear numerical results. We expected that the velocity profile could be in an intermediate position with respect to the other two cases. Anyway, these results are just preliminary and are reported here because they suggests the possibility for further development in the future.

7.5 Conclusions

In this Chapter, DEM simulation were used to investigate the effect of size ratio, dimensionless shear rate, fines volume fraction and direction of gravity on percolation velocity. DEM simulations allowed to study some conditions difficult to obtain experimentally. As already said in Chapter 5, the variables that affect the percolation velocity were the size ratio, the shear rate and volume fraction of fines inside the mixture of granular material. As expected, DEM simulations confirmed that the size ratio played an important role on the percolation speed as already seen in the experimental data reported in Chapter 7. Also in Chapter 4, studying the mixing inside double cone mixture, we discovered that in a PSD of the material the distance between the diameter of the fine material from the average diameter of the mixture play a fundamental role in the determination of the mixing degree. The velocity profile found was in agreement with the experimental data reported in the previous Chapter. The dimensionless percolation velocity resulted inversely proportional to the dimensionless shear rate independent from the shear rate. The increase of fine fraction inside the mixture, decrease the percolation speed because reduce the voids available to the percolating small particles. DEM was also used to investigate the relation between the direction of gravity with respect to the gradient of shear velocity. The study done is only preliminary, but it confirm that the dimensionless percolation speed is influenced also by this variable.

Nomenclature

Symbol	Units	Description
N	-	number of the grains
m	kg	mass of the grain
v	cm	total height of material
$\boldsymbol{v_p}$	m/s	velocity of the grain
$\|\dot{\gamma}\|$	1/s	shear rate
F	N	force exerted on the grain
$\mathbf{F}_{ext}$	N	external force
δ	m	overlap
k	N/m	stiffness of the grain
γ	kg/s	viscous damping
μ	-	coefficient of friction
ε	-	coefficient of restitution
t_c	s	time of collision

Chapter 8

Conclusions and perspectives

8.1 Summary

This work was focused on the segregation and mixing in granular materials, two phenomena strictly connected with their flow. In this thesis' work different approaches were used to investigate the segregation. As a first and preliminary step, an hydrodynamic model developed by Artoni *et al.* (2009) for dense granular flow was customized used to simulate the flow inside different types of mixers and devices of industrial interest. To describe the transient phenomena that occurs in flowing granular materials and to describe a bi-phasic system composed by the two species, air and granular material, the hydrodinamic model was coupled with a transport equation able to track the free surface between the two species. This study, carried out by a kinematic point of view, has allowed to indicate which type of flow, and thus which type of mixer geometries, reaches a best mixing potential. Aware of the fact that real mixture are typically polydisperse, to bind the characteristics of the granular flow to the homogeneity of the mixture, an experimental study was conducted. Thus, we performed experiments in mixers, similar to those used in the simulations, to understand how the PSD affected the mixture homogeneity after the discharge. In fact, from an industrial point of view, the important thing is not the level of the homogeneity after mixing, but the degree of mixture homogeneity discharged from the mixer. During the discharge, powder creates new flow pattern completely different from those occurring in the

previous mixing stage. The experiments showed that the distance between the diameter of the particles of interest (for example the API in the pharmaceutical industries) from the average value of the particle distribution influenced the homogeneity of the mixture after the discharge. This results were confirmed from the continuum simulations done in silos, with different operating hopper. The simulations were done using the hydrodynamic model presented above coupled with a segregation model. Among different segregation mechanism, the percolation was identified as the main segregating mechanism during the discharge. The segregation was modeled using a transport equation to describe the changes in granular material composition due to segregation. The segregation velocity model, obtained combining two independent Literature approaches, was based on the fact that it is proportional to the difference between the diameter of particle of interest and the average diameter of the mixture, as found from experiments on mixers. Simulations, conducted in two types of flow regimes, were compared with experimental data found in Literature (Artega and Tüzün, 1990; Ketterhagen *et al.*, 2007). The simulations were done varying the size ratio of the binary mixture and the initial fines concentration. The model resulted predictive for spatial distribution of the mass fraction of fines. To better understand how the percolation mechanism affect segregation, an experimental study conducted on a shear box was carried out. The results allowed to better understand what happen in a simple shear flow, and allowed to developing relationships for find a theoretical model for quantitative prediction of percolation velocity. In the final Chapter, DEM simulations were done to explore how the percolation velocity was affected by other variables difficult to be studied experimentally, such as the effect of fine volume fraction or the orientation of the gravity field with respect to shear direction.

8.1.1 Perspectives

The thesis' work opens different future investigations and developments. Different works can be done both using an experimental or numerical approaches. From a numerical point of view, it could be possible improve the segregation model used for the continuum simulations. The segregation model is flexible and allows the inclusion of other mechanisms of segregation or a combination of different mechanisms. Furthermore, this model can be applied to different device, for example in mixers, to also find a relation between the kinematic of the flow of poly-dispersed mixture and the segregation.

DEM simulations allow several types of investigations. Surely, they can deepen the effect of gravity on the percolation. It also possible to extend the study on cohesive granular material to better asses the contrasting effect of cohesion on segregation. It could be interesting to find what is the critical value of this cohesion force able to avoid the segregation. From the experimental point of view, a more detailed study on how the shape of the particles affects the segregation must be done. Satisfactory results have been obtained with the percolation theory, also in this case further studies to refine the model could be made.

Bibliography

Aarons, L. and S. Sundaresan (2006). "Shear flow of assemblies of cohesive and non-cohesive granular materials". *Powder Technology* 169, pp. 10–21.

Allen, T. (2013). *Particle size measurement*. Springer.

Andreotti, B., Y. Forterre, and O. Pouliquen (2013). *Granular media: between fluid and solid*, p. 469.

Aranson, I.S. and L.S. Tsimring (2001). "Continuum description of avalanches in granular media". *Physical Review E* 64, p. 020301.

Artega, P. and U. Tüzün (1990). "Flow of binary mixtures of equal-density granules in hoppers-size segregation, flowing density and discharge rates". *Chemical engineering science* 45, pp. 205–223.

Artoni, R. and P. Richard (2015). "Average balance equations, scale dependence, and energy cascade for granular materials". *Physical Review E* 91.3, p. 032202.

Artoni, R., A. Santomaso, and P. Canu (2009). "Simulation of dense granular flows: Dynamics of wall stress in silos". *Chemical Engineering Science* 64, pp. 4040–4050.

Artoni, R., A. Zugliano, A. Primavera, P. Canu, and A. Santomaso (2011). "Simulation of dense granular flows: Comparison with experiments". *Chemical engineering science* 66, pp. 548–557.

Barker, G.C. and A. Mehta (1993). "Transient phenomena, self-diffusion, and orientational effects in vibrated powders". *Physical Review E* 47, p. 184.

Bertuola, D., S. Volpato, P. Canu, and A.C. Santomaso (2016). "Prediction of segregation in funnel and mass flow discharge". *Chemical Engineering Science* 150, pp. 16–25.

Boateng, A.A. (1998). "Boundary layer modeling of granular flow in the transverse plane of a partially filled rotating cylinder". *International Journal of Multiphase Flow* 24, pp. 499–521.

Boateng, A.A. and P. V. Barr (1997). "Granular flow behaviour in the transverse plane of a partially filled rotating cylinder". *Journal of Fluid Mechanics* 330, pp. 233–249.

Boateng, A.A. and P.V. Barr (1996). "Modelling of particle mixing and segregation in the transverse plane of a rotary kiln". *Chemical Engineering Science* 51, pp. 4167–4181.

Bocquet, L., W. Losert, D. Schalk, T.C. Lubensky, and J.P. Gollub (2001). "Granular shear flow dynamics and forces: Experiment and continuum theory". *Physical review E* 65, p. 011307.

Bonamy, D., F. Daviaud, and L. Laurent (2002). "Experimental study of granular surface flows via a fast camera: a continuous description". *Physics of Fluids* 14, pp. 1666–1673.

Bridgwater, J. (1994). "Mixing and segregation mechanisms in particle flow". In: *Granular Matter*. Springer, pp. 161–193.

Brown, R.L. (1939). "The fundamental principles of segregation". *The Institute of Fuel* 13, pp. 15–19.

Campbell, C.S. (1990). "Rapid granular flows". *Annual Review of Fluid Mechanics* 22, pp. 57–90.

Cantelaube, F. and D. Bideau (1995). "Radial segregation in a 2d drum: an experimental analysis". *EPL (Europhysics Letters)* 30, p. 133.

Chialvo, S., J. Sun, and Sankaran S. (2012). "Bridging the rheology of granular flows in three regimes". *Physical review E* 85, p. 021305.

Chou, H.T. and C.F. Lee (2009). "Cross-sectional and axial flow characteristics of dry granular material in rotating drums". *Granular Matter* 11, pp. 13–32.

Chou, S.H., C.C. Liao, and S.S. Hsiau (2011). "The effect of interstitial fluid viscosity on particle segregation in a slurry rotating drum". *Physics of Fluids* 23, p. 083301.

Christakis, N., M.K. Patel, M. Cross, J. Baxter, H. Abou-Chakra, and U. Tüzün (2002). "Predictions of segregation of granular material with the aid of PHYSICA, a 3-D unstructured finite-volume modelling framework". *International journal for numerical methods in fluids* 40, pp. 281–291.

Christakis, N., P. Chapelle, N. Strusevich, I. Bridle, J. Baxter, M.K Patel, M. Cross, U. Tüzün, A.R. Reed, and M.S.A. Bradley (2006). "A hybrid numerical model for predicting segregation during core flow discharge". *Advanced Powder Technology* 17, pp. 641–662.

Cooke, M.H. and J. Bridgewater (1979). "Interparticle percolation: a statistical mechanical interpretation". *Industrial & Engineering Chemistry Fundamentals* 18, pp. 25–27.

Cooke, M.H., J. Bridgwater, and A.M. Scott (1978). "Interparticle percolation: lateral and axial diffusion coefficients". *Powder Technology* 21, pp. 183–193.

Cundall, P.A. and O.D.L. Strack (1979). "A discrete numerical model for granular assemblies". *Geotechnique* 29, pp. 47–65.

Da Cruz, F., S. Emam, M. Prochnow, J. Roux, and F. Chevoir (2005). "Rheophysics of dense granular materials: Discrete simulation of plane shear flows". *Physical Review E* 72, p. 021309.

De Gennes, P. (1999). "Granular matter: a tentative view". *Reviews of Modern Physics* 71, S374–S382.

De Silva, S.R., A. Dyrøy, and G.G. Enstad (2000). "Segregation mechanisms and their quantification using segregation testers". In: *IUTAM Symposium on Segregation in Granular Flows*. Springer, pp. 11–29.

Ding, Y.L., J.P.K. Seville, R. Forster, and D.J. Parker (2001). "Solids motion in rolling mode rotating drums operated at low to medium rotational speeds". *Chemical Engineering Science* 56, pp. 1769–1780.

Dolgunin, V.N. and A.A. Ukolov (1995). "Segregation modeling of particle rapid gravity flow". *Powder Technology* 83, pp. 95–103.

Doolittle, A.K (1951). "Studies in Newtonian flow. I. The dependence of the viscosity of liquids on temperature". *Journal of Applied Physics* 22, pp. 1031–1035.

Fan, Y., C.P. Schlick, P.B. Umbanhowar, J.M. Ottino, and R.M. Lueptow (2014). "Modelling size segregation of granular materials: the roles of segregation, advection and diffusion". *Journal of Fluid Mechanics* 741, pp. 252–279.

Felix, G., V. Falk, and U. D'Ortona (2007). "Granular flows in a rotating drum: the scaling law between velocity and thickness of the flow". *The European Physical Journal E* 22, pp. 25–31.

Forterre, Y. and O. Pouliquen (2008). "Flows of dense granular media". *Annu. Rev. Fluid Mech.* 40, pp. 1–24.

Ginzburg, V.L. (1955). "On the theory of superconductivity". *Il Nuovo Cimento (1955-1965)* 2, pp. 1234–1250.

Goldhirsch, I. (2003). "Rapid granular flows". *Annual review of fluid mechanics* 35, pp. 267–293.

Gray, J. M. N. T. and C. Ancey (2011). "Multi-component particle-size segregation in shallow granular avalanches". *Journal of Fluid Mechanics* 678, pp. 535–588.

Gray, J. M. N. T., P. Gajjar, and P. Kokelaar (2015). "Particle-size segregation in dense granular avalanches". *Comptes Rendus Physique* 16, pp. 73–85.

Hajra, S.K., D. Shi, and J.J. McCarthy (2012). "Granular mixing and segregation in zigzag chute flow". *Physical Review E* 86, p. 061318.

Henein, H. and R.G. Brimacombe J.K. Watkinson (1983). "Experimental study of transverse bed motion in rotary kilns". *Metallurgical transactions B* 14, pp. 191–205.

Hersey, J.A. (1975). "Ordered mixing: a new concept in powder mixing practice". *Powder Technology* 11, pp. 41–44.

Hill, K. M., A. Caprihan, J. Kakalios, other, other, and other (1997). "Bulk Segregation in Rotated Granular Material Measured by Magnetic Resonance Imaging". *Phys. Rev. Lett.* 78 (1), pp. 50–53.

Hogg, R. (2009). "Mixing and segregation in powders: evaluation, mechanisms and processes". *KONA Powder and Particle Journal* 27, pp. 3–17.

Hsiau, S.S. and M.L. Hunt (1996). "Granular thermal diffusion in flows of binary-sized mixtures". *Acta Mechanica* 114, pp. 121–137.

Ingram, A., J.P.K. Seville, D.J. Parker, X. Fan, and R.G. Forster (2005). "Axial and radial dispersion in rolling mode rotating drums". *Powder technology* 158, pp. 76–91.

Jaeger, H.M., S.R. Nagel, and R.P. Behringer (1996). "Granular solids, liquids, and gases". *Reviews of modern physics* 68, p. 1259.

Jain, N., J.M. Ottino, and R.M. Lueptow (2002). "An experimental study of the flowing granular layer in a rotating tumbler". *Physics of Fluids (1994-present)* 14, pp. 572–582.

Kamrin, K. and G. Koval (2012). "Nonlocal constitutive relation for steady granular flow". *Physical Review Letters* 108, p. 178301.

Ketterhagen, W.R., J.S. Curtis, C.R Wassgren, A. Kong, P.J. Narayan, and B.C Hancock (2007). "Granular segregation in discharging cylindrical hoppers: a discrete element and experimental study". *Chemical Engineering Science* 62, pp. 6423–6439.

Khakhar, D.V., A.V. Orpe, and J.M. Ottino (2001). "Continuum model of mixing and size segregation in a rotating cylinder: concentration-flow coupling and streak formation". *Powder Technology* 116, pp. 232–245.

Khola, N. and C. Wassgren (2016). "Correlations for shear-induced percolation segregation in granular shear flows". *Powder Technology* 288, pp. 441–452.

Knight, J.B., H.M. Jaeger, and S.R. Nagel (1993). "Vibration-induced size separation in granular media: the convection connection". *Physical review letters* 70, p. 3728.

Lees, A.W. and S.F. Edwards (1972). "The computer study of transport processes under extreme conditions". *Journal of Physics C: Solid State Physics* 5, p. 1921.

Losert, W., L. Bocquet, T.C. Lubensky, and J.P. Gollub (2000). "Particle dynamics in sheared granular matter". *Physical review letters* 85, p. 1428.

Luding, S. (2008). "Introduction to discrete element methods: basic of contact force models and how to perform the micro-macro transition to continuum theory". *European Journal of Environmental and Civil Engineering* 12, pp. 785–826.

McCarthy, J.J. (2009). "Turning the corner in segregation". *Powder Technology* 192, pp. 137–142.

Mellmann, J. (2001). "The transverse motion of solids in rotating cylinders forms of motion and transition behavior". *Powder Technology* 118, pp. 251–270.

MiDi, GdR (2004). "On dense granular flows". *The European Physical Journal E* 14, pp. 341–365.

Mills, P., D. Loggia, and M. Tixier (1999). "Model for a stationary dense granular flow along an inclined wall". *EPL (Europhysics Letters)* 45, p. 733.

Nakagawa, M., S.A. Altobelli, A. Caprihan, E. Fukushima, and E.-K. Jeong (1993). "Non-invasive measurements of granular flows by magnetic resonance imaging". *Experiments in fluids* 16, pp. 54–60.

Nedderman, R.M. (2005). *Statics and kinematics of granular materials*. Cambridge University Press.

Nienow, A.W., M. F. Edwards, and N. Harnby (1997). *Mixing in the process industries*. Butterworth-Heinemann.

Olsson, E. and G. Kreiss (2005). "A conservative level set method for two phase flow". *Journal of computational physics* 210, pp. 225–246.

Orpe, A.V. and D.V. Khakhar (2001). "Scaling relations for granular flow in quasi-two-dimensional rotating cylinders". *Physical review E* 64, p. 031302.

Pavlovitch, A., R. Jullien, and P. Meakin (1991). "Geometrical properties of a random packing of hard spheres". *Physica A: Statistical Mechanics and its Applications* 176, pp. 206–219.

Pignatel, F., C. Asselin, L. Krieger, I.C. Christov, J.M. Ottino, and R.M. Lueptow (2012). "Parameters and scalings for dry and immersed granular flowing layers in rotating tumblers". *Physical Review E* 86, p. 011304.

Poole, K.R., R.F. Taylor, and G.P. Wall (1964). "Mixing powders to fine-scale homogeneity: studies of batch mixing".

Pouliquen, O. and F. Chevoir (2002). "Dense flows of dry granular material". *Comptes Rendus Physique* 3, pp. 163–175.

Pouliquen, O., Y. Forterre, and S. Ledizes (2001). "Dense granular flows down incline as a self activated process". *Advances in Complex systems* 4, pp. 441–450.

Radjaï, F. and F. Dubois (2011). *Discrete-element modeling of granular materials*. Wiley-Iste.

Rajchenbach, J. (2000). "Granular flows". *Advances in physics* 49, pp. 229–256.

Richard, P., M. Nicodemi, R. Delannay, P. Ribiere, and D. Bideau (2005). "Slow relaxation and compaction of granular systems". *Nature materials* 4, pp. 121–128.

Santomaso, A.C., L. Petenò, and P. Canu (2006). "Radial segregation driven by axial convection". *EPL (Europhysics Letters)* 75, p. 576.

Santomaso, A.C., R. Artoni, and P. Canu (2013). "Controlling axial segregation in drum mixers through wall friction: Cellular automata simulations and experiments". *Chemical Engineering Science* 90, pp. 151–160.

Santos, D.A., I.J. Petri, C.R. Duarte, and M.A.S. Barrozo (2013). "Experimental and CFD study of the hydrodynamic behavior in a rotating drum". *Powder technology* 250, pp. 52–62.

Savage, S.B. and C.K.K. Lun (1988). "Particle size segregation in inclined chute flow of dry cohesionless granular solids". *Journal of Fluid Mechanics* 189, pp. 311–335.

Scanferla, L. (2015). "Studio sperimentale sulla miscelazione di polveri scorrevoli in miscelatori biconici". MA thesis. Department of Industrial Engineering, University of PAdova.

Schaeffer, D.G. (1987). "Instability in the evolution equations describing incompressible granular flow". *Journal of differential equations* 66.1, pp. 19–50.

Schulze, D. (2007). *Powders and bulk solids: behavior, characterization, storage and flow*. Springer Science & Business Media.

Scott, A.M. and J. Bridgwater (1975). "Interparticle percolation: a fundamental solids mixing mechanism". *Industrial & Engineering Chemistry Fundamentals* 14, pp. 22–27.

Thornton, A., T. Weinhart, S. Luding, and O. Bokhove (2012). "Modeling of particle size segregation: calibration using the discrete particle method". *International Journal of Modern Physics C* 23, p. 1240014.

Thornton, C. and L. Zhang (2001). "A DEM comparison of different shear testing devices".

Volpato, S., R. Artoni, A.C. Santomaso, and other (2014). "Numerical study on the behavior of funnel flow silos with and without inserts through a continuum hydrodynamic approach". *Chemical Engineering Research and Design* 92, pp. 256–263.

Wightman, C., M. Moakher, F.J. Muzzio, and O. Walton (1998). "Simulation of flow and mixing of particles in a rotating and rocking cylinder". *AIChE Journal* 44, pp. 1266–1276.

Williams, J. (1963). "The segregation of powders and granular materials". *Fuel Soc. J* 14, pp. 29–34.

Zik, O., D. Levine, S.G. Lipson, S. Shtrikman, and J. Stavans (1994). "Rotationally induced segregation of granular materials". *Physical review letters* 73, p. 644.